AD NUMBER

**AD917517**

LIMITATION CHANGES

TO:

**Approved for public release; distribution is unlimited.**

FROM:

**Distribution authorized to U.S. Gov't. agencies only; Test and Evaluation; DEC 1973. Other requests shall be referred to Army Air Mobility Research and Development Lab., Fort Eustis, VA.**

AUTHORITY

**USAAMRDL ltr 30 Mar 1976**

AD

# USAAMRDL TECHNICAL REPORT 73-31

# IMPINGEMENT-FILM HEAT TRANSFER INVESTIGATION



By

T. Chew
R. S. Fatyol
B. F. Shattuck

December 1973



EUSTIS DIRECTORATE
U. S. ARMY AIR MOBILITY RESEARCH AND DEVELOPMENT LABORATORY
FORT EUSTIS, VIRGINIA

CONTRACT DAAJ02-72-C-0094
GENERAL ELECTRIC COMPANY
AIRCRAFT ENGINE GROUP
CINCINNATI, OHIO / LYNN, MASSACHUSETTS

## DISCLAIMERS

The findings in this report are not to be construed as an official Department of the Army position unless so designated by other authorized documents.

When Government drawings, specifications, or other data are used for any purpose other than in connection with a definitely related Government procurement operation, the United States Government thereby incurs no responsibility nor any obligation whatsoever; and the fact that the Government may have formulated, furnished, or in any way supplied the said drawings, specifications, or other data is not to be regarded by implication or otherwise as in any manner licensing the holder or any other person or corporation, or conveying any rights or permission, to manufacture, use, or sell any patented invention that may in any way be related thereto.

Trade names cited in this report do not constitute an official endorsement or approval of the use of such commercial hardware or software.

## DISPOSITION INSTRUCTIONS

Destroy this report when no longer needed. Do not return it to the originator.

DEPARTMENT OF THE ARMY
U. S. ARMY AIR MOBILITY RESEARCH & DEVELOPMENT LABORATORY
EUSTIS DIRECTORATE
FORT EUSTIS, VIRGINIA 23604

This report covers the experimental investigation of an impingement-film cooling system designed to cool the exhaust ducts of turboshaft engines and thereby reduce the IR radiation levels.

The objectives of this contractual effort were to search the current literature for data on the impingement-film cooling concept, to evaluate the data, and to establish a test program to experimentally evaluate the important parameters as required by the contract.

Film cooling test results were in good agreement with the correlations and results quoted in the literature. The cooling effectiveness with impingement-film cooling was consistently superior to that with film cooling only. The conclusions contained in this report are concurred in by this Directorate.

The technical monitor for this contract was Dr. Cecil C Gentry, Military Operations Technology Division.

Task 1F162205AA5202
Contract DAAJ02-72-C-0094
USAAMRDL Technical Report 73-31
December 1973

# IMPINGEMENT-FILM HEAT TRANSFER INVESTIGATION

Final Report

By

T. Chew
R.S. Fatyol
B.F. Shattuck

Prepared by

General Electric Company
Aircraft Engine Group
Cincinnati, Ohio/Lynn, Massachusetts

for

EUSTIS DIRECTORATE
U. S. ARMY AIR MOBILITY RESEARCH AND DEVELOPMENT LABORATORY
FORT EUSTIS, VIRGINIA

## ABSTRACT

This report covers the investigation of an impingement-film cooling system designed to cool the exhaust ducts of turboshaft engines. The program was initiated with a literature search which indicated the useful range of impingement hole size, spacing, and distance from impingement hole to cooled panel. It provided similar information for the cooling slot design. Test hardware incorporating these features was fabricated for testing. Seventeen configurations, four of which had no impingement (film cooling only), were tested. The remaining 13 configurations were tested with different combinations of impingement hole size, spacing, and distance to cooled panel.

Film cooling test results were in good agreement with the correlations and results quoted in the literature. The cooling effectiveness with impingement-film cooling was consistently superior to that with film cooling only. The highest effectiveness was achieved with the configuration having the largest impingement hole diameter, D = 0.070 in. and spacing $X_n/D = 12$. The optimum impingement distance $Z_n$ was in the neighborhood of 4 impingement hole diameters. While the largest hole spacing tested gave the highest cooling effectiveness, it also required a relatively large pressure drop across the cooling system. Under the most difficult cooling conditions of hot gas Mach number equal to 0.4, the highest cooling effectiveness ($\eta$) achieved within a specified impingement system pressure drop of 100 in. of water was 0.93.

# TABLE OF CONTENTS

TABLE OF CONTENTS - Continued

## LIST OF ILLUSTRATIONS

## LIST OF ILLUSTRATIONS - Continued

LIST OF ILLUSTRATIONS - Continued

LIST OF ILLUSTRATIONS - Continued

LIST OF ILLUSTRATIONS - Continued

LIST OF ILLUSTRATIONS - Continued

LIST OF ILLUSTRATIONS - Continued

## LIST OF TABLES

## LIST OF SYMBOLS

$A_m$ metering hole area, in.$^2$

$A_c$ total slot area, in.$^2$

$A_s$ cooled panel surface area, in.$^2$

$B_{es}$ width of equivalent area slot jet, in.

$C_f$ metering hole and slot flow coefficient.

$C_{fI}$ impingement baffle flow coefficient.

$C_{pc}$ specific heat for coolant air, Btu/lb-°F

D impingement hole diameter, in.

d injection hole diameter, in.

G (X, I) airflow rate per unit crossflow area downstream of local plate (I), lb/sec/in.$^2$

G (H, I) airflow rate per unit area of total impingement holes over local heater plate (I), lb/sec/in.$^2$

$\bar{h}$ average heat transfer coefficient on cool side of test panel, Btu/hr ft$^2$ °F =

$$\left[\left(\frac{1}{A}\sum_{n=1}^{10} T_{wn} \quad A_n\right) - T_{ci}\right] A$$

where $A = \sum_{n=1}^{10} A_n$

k heat conduction coefficient of air, Btu/hr ft °F

L lip length, in.

$l_n$ length of heat transfer region downstream from a single row of impingement holes, in.

M mass flow ratio (secondary to mainstream mass flow ratio)

M* cross jet-flow mass flow ratio ($m_c/m_j$)

| | |
|---|---|
| $M_g$ | hot gas Mach number |
| $m_c$ | crossflow mass rate, lb/hr |
| $m_j$ | total jet mass flow rate, lb/hr |
| m | Reynolds number exponent (see Figure 2) |
| $N_r$ | number of rows of impingement holes |
| Nu | Nusselt number, Dh/k |
| n | number of impingement holes |
| P | pitch (center-to-center spacing distance between orifice holes), in. |
| Pr | Prandtl number, $C_p \mu / k$ |
| Re | Reynolds number, $\frac{4}{n\pi} \times \frac{W_c}{\mu D}$ |
| $Re_{es}$ | equivalent slot width Reynolds number, $2 B_{es} Re/D$ |
| St | average Stanton number, Nu/(Pr x Re) |
| S | slot height, in. |
| t | thickness, in. |
| Tw | wall temperature, $^oF$ |
| $T_{ra}$ | $\left[\frac{1}{n} \sum_{i=1}^{n} T_{wi}^4\right]^{\frac{1}{4}} {}^oF$ |
| $T_c$ | coolant temperature, $^oF$ |
| $T_g$ | main stream gas temperature, $^oF$ |
| $V_c$ | velocity of secondary stream, ft/sec |
| $V_g$ | velocity of main stream, ft/sec |

| | |
|---|---|
| $W_c$ | cooling mass flow rate, lb/sec |
| $X_n$ | center-to-center impingement baffle hole spacing, in. |
| X | distance downstream measured from end of lip overhang, in. |
| $Z_n$ | impingement distance (distance between cooled plate and impingement baffle), in. |
| $\eta$ | cooling effectiveness based on radiation-averaged wall temperature $= \frac{T_g - T_{aw}}{T_g - T_{ci}}$ |
| $\mu$ | absolute viscosity, lb/sec ft |
| $\rho$ | density, $lb/ft^3$ |
| $\rho_c$ | cooling air density, $lb/ft^3$ |
| $\rho_g$ | hot gas density, $lb/ft^3$ |
| $\phi_1$ | function of $X_n/D$ (see Figure 1) |
| $\phi_2$ | function of $Z_n/D$ (see Figure 3) |

## INTRODUCTION

The impingement-film heat transfer program was conducted to determine the performance of an impingement-film cooling system designed to cool exhaust duct walls. The design objective was to cool the exhaust duct with the least expenditure of cooling airflow possible and with a relatively small pressure drop across the cooling system. The impingement-film heat transfer system tested was evaluated on the basis of the performance of similar systems quoted in the literature, General Electric calculated performance, and combustor and turbine airfoil cooling.

The program, carried out over a period of six months, was made up of four tasks:

| | | |
|---|---|---|
| Task I | - | Survey of Impingement-Film Technology |
| Task II | - | Design and Fabrication of Test Apparatus |
| Task III | - | Impingement-Film Experimental Tests |
| Task IV | - | Data Reduction and Analysis |

This report describes the results of efforts applied to these tasks.

# SURVEY OF IMPINGEMENT-FILM HEAT TRANSFER TECHNOLOGY

## APPROACH

A literature search was conducted to determine the present state of the art in impingement-film heat transfer technology. The primary search covered documents currently available in the Lynn Technical Information Center for the time period 1961 through the present. In addition, two report bibliographies on impingement cooling and film cooling for the last 5-year period were obtained from the Defense Documentation Center (DDC).

## IMPINGEMENT COOLING TECHNOLOGY

Documents pertaining to impingement cooling which were reviewed are presented as References 1 through 12. Much of this literature was not useful since it covered single jets or single rows of jets with no air flowing across the jets. However, References 1,2,3,4, and 6 are particularly applicable to this impingement-film heat transfer program since they report the results of testing arrays of circular jets which eject into a crossflow. These results were used in the pretest performance predictions and in the test panel design. Impingement hole diameter, center-to-center spacing, and impingement distance were the geometrical variables found to have the greatest influence on the impingement heat transfer process. Each of these variables is discussed below.

### Impingement Hole Diameter (D)

Kercher[1,2] tested impingement holes having diameters from 0.010 to 0.080 in. He found that decreasing the hole diameter to one-half its initial value and increasing the number of holes, with the important dimensionless design parameters and total cooling flow held constant, improved the heat transfer performance 10 to 15 percent. This result can be obtained from his correlation,

$$Nu = \phi_1 \phi_2 \, Re^m \, Pr^{1/3} (Z_n/D)^{0.091} \qquad (1)$$

where $\phi_1$ and m = functions of the hole spacing to diameter ratio $X_n/D$ (see Figures 1 and 2). $\phi_2$ = correction coefficient for crossflow (see Figure 3).

When the hole diameter is varied while all geometrical, dimensionless parameters remain constant, all quantities on the right side of Equation (1) are constant except

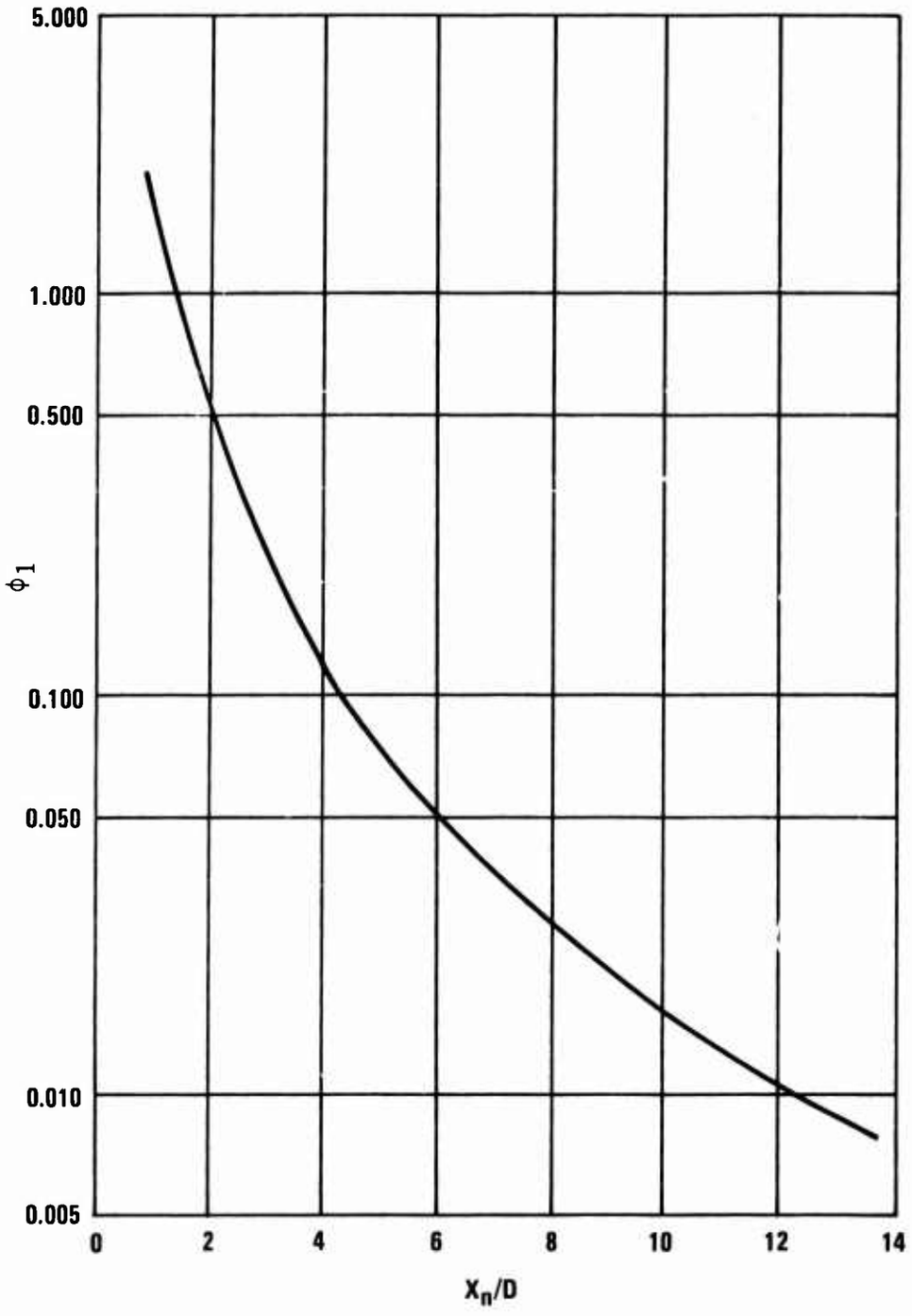


Figure 1. Correlation Constant $\phi_1$ vs $X_n/D$.

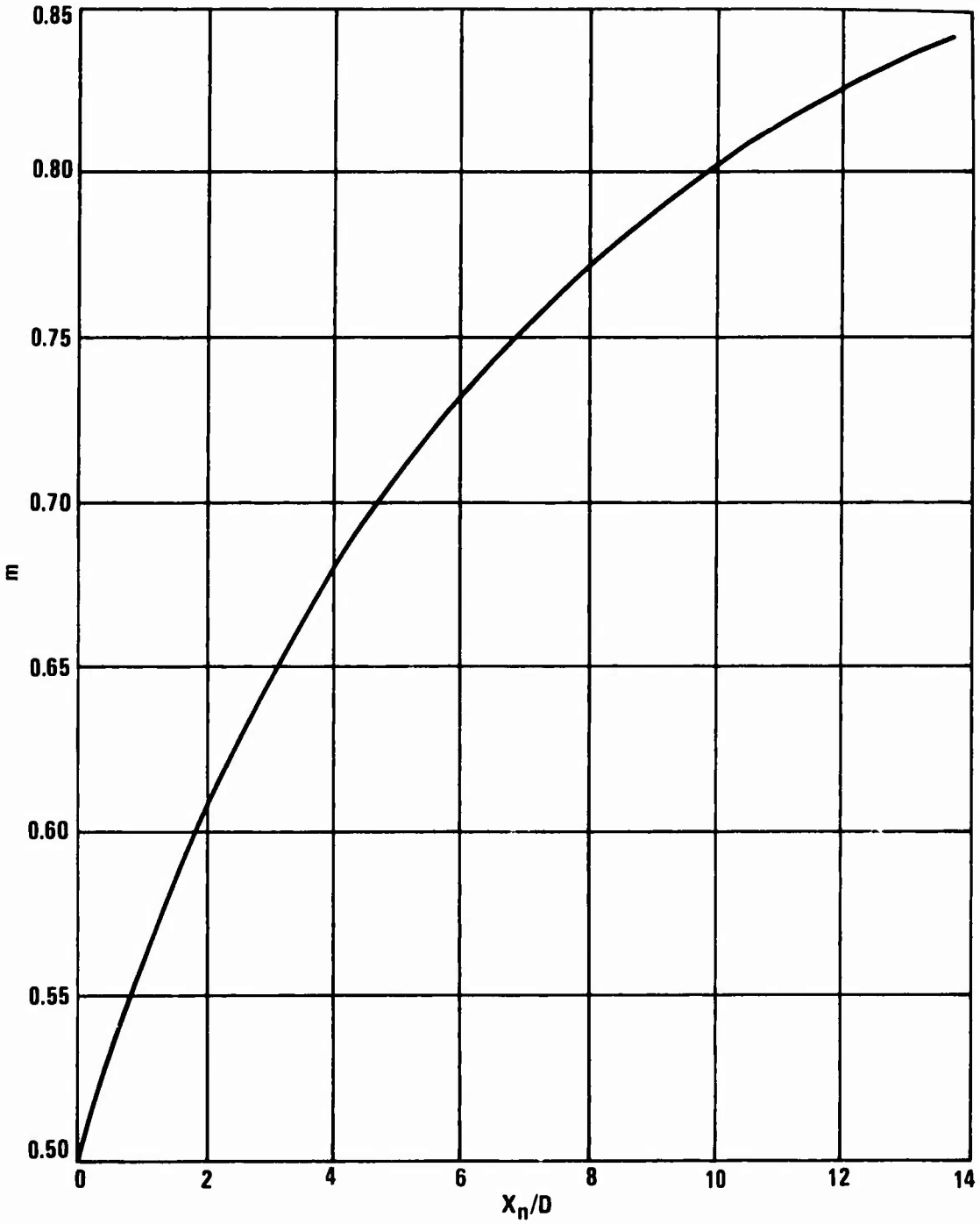


Figure 2. Reynolds Number Exponent.

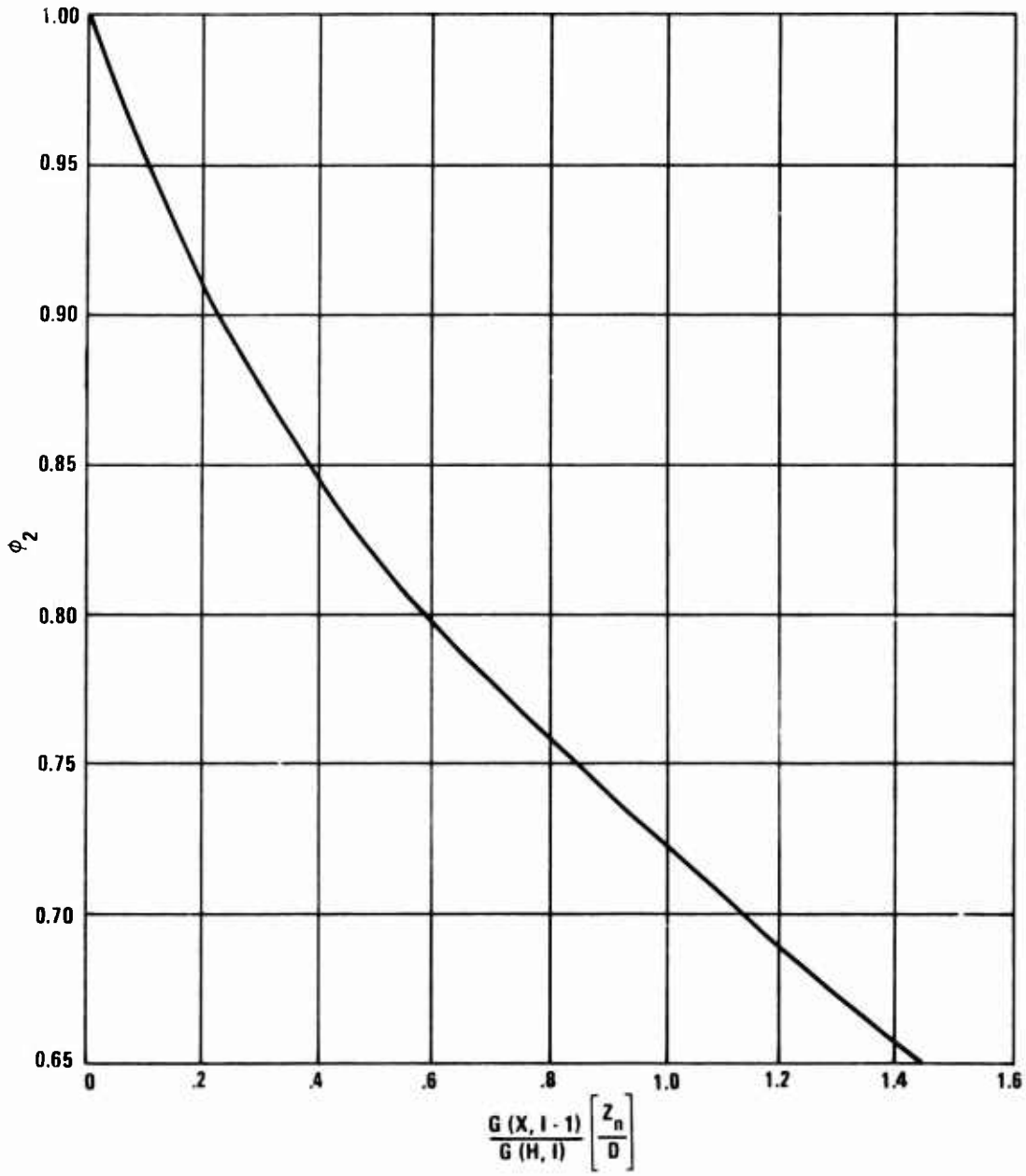


Figure 3. Degradation of Heat Transfer Coefficient vs Crossflow.

Reynolds number and Prandtl number. At constant cooling air temperature, viscosity, specific heat, heat conduction coefficient, and Prandtl number are constant so that Equation (1) can be written

$$\bar{h} = \frac{Nuk}{D} = \text{constant} \times \frac{(\rho VD)^m}{D}$$

When the flow per unit area $\rho V$ remains constant, this becomes

$$\bar{h} = \frac{\text{constant}}{D^{1-m}} \qquad (2)$$

At small Reynolds numbers and relatively large hole spacing, Kercher found m to be about 0.8. In that case Equation (2) indicates that heat transfer is increased by 15% when hole diameter is halved.

Tabakoff and Clevenger[3] also found from their tests (Figure 4) that the array having the smallest hole diameter (D) and the largest spacing ($X_n$) resulted in the highest heat transfer. Thus, the literature indicated general agreement that heat transfer rate increases as impingement hole diameter decreases. The minimum diameter is generally set by the size of environmental contaminant which the impingement baffle must pass without plugging. General Electric experience has shown that the minimum diameter is in the range of 0.02 to 0.03 in. for non-rotating components. Based on this experience, 0.030, 0.050, and 0.070 in. were the impingement hole diamaters used in the test panels for the impingement-film heat transfer program.

Equation 1 was based on maintaining complete geometrical similarity. As the hole diameter is changed, the length and width of the cooled panel and impingement baffle must also be proportionately changed so that the number of impingement holes and their arrangement is not varied. This is not important for a single row of holes where there is no crossflow so that $\phi_2 = 1$ and Equation (2) applies directly. In the impingement-film tests, however, the test apparatus size was fixed. Therefore, as impingement hole diameter was changed the number of holes changed and the geometry of the test apparatus changed. As a result, the crossflow ratio was greater for the configurations which had more and smaller holes. According to Figure 3, the increasing crossflow reduced $\phi_2$ and by Equation (1) the Nusselt Number. The test results in this report indicate that the crossflow effect overcame the scaling effect given by Equation (2) so that heat transfer increased rather than decreased, with increasing impingement hole diameter. This discrepancy is discussed further in the Test Results section.

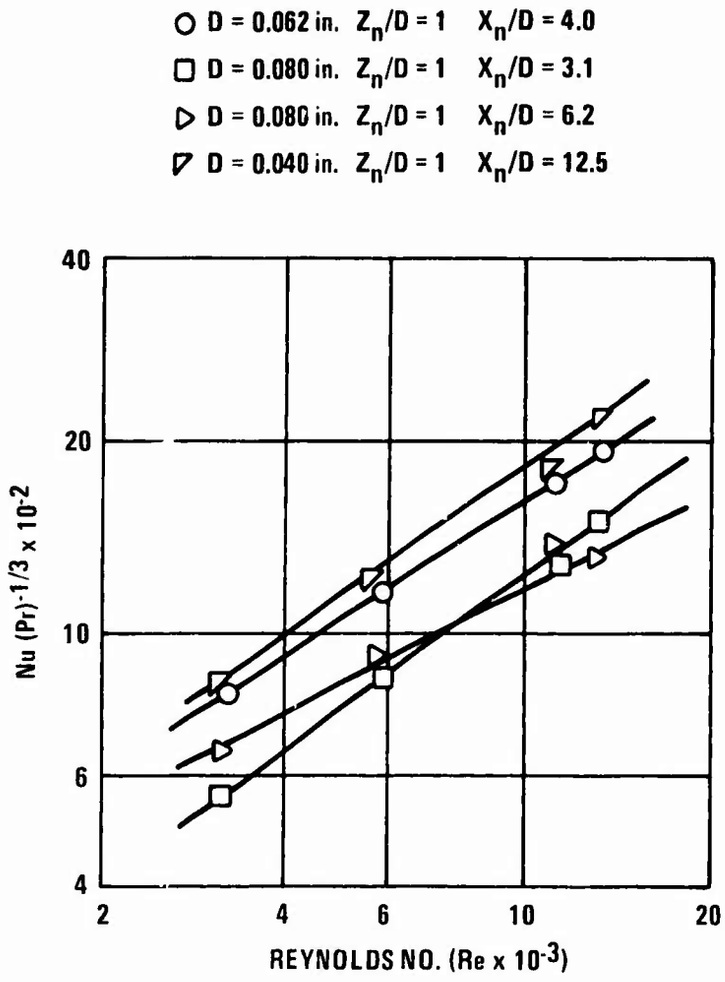


Figure 4. Comparison of Round Jet Arrays Having Different Diameters and Spacing.

Impingement Hole Spacing ($X_n$)

The hole spacing ($X_n$) is defined as the center-to-center spacing of the holes in the impingement array. Kercher[1,2] investigated the effect of hole spacing without crossflow for values of $X_n/D$ in the range 3.1 to 12.5. He found that decreasing the hole spacing, at a constant hole diameter, increases the heat transfer performance of the array. However, the total airflow required by the array increased with decreasing hole spacing. An examination of his correlations reveals the opposite conclusion if a given area is cooled at a constant value of total cooling airflow. For that case, the larger the hole spacing, the greater the

heat transfer performance of the array. This effect is shown by the following example in which Kercher's correlation, Equation (1), is used.

Consider a square array 3.6 in. x 3.6 in. containing twenty 0.030-in.-diameter holes per row. There is no crossflow.

Let

$W = 0.0315$ lb/sec

$Z_n/D = 4$

$\mu = 12.5 \times 10^{-6}$ lb/sec ft

$Pr = 0.705$

For these conditions

$Re = 3.06 \times 10^3$

$X_n/D = 6$

$m = 0.73$

$\phi_1 = 0.05$

$\phi_2 = 1$

$Nu = (0.05)\ (1)\ (3.06 \times 10^3)^{0.73}\ (0.705)^{1/3}\ (4)^{0.091}$

$Nu = 17.7$

Reducing the number of holes/row to 10 with constant flow gives

$Re = 12.24 \times 10^3$

$X_n/D = 12$

$m = 0.965$

$\phi_1 = 0.0035$

$\phi_2 = 1$

$Nu = 37.4$

This calculation indicates that the increased Reynolds number and m associated with increased spacing and constant hole diameter are responsible for the improved heat transfer. Figure 4 shows that the Reynolds number effect is predominant.

Metzger and Korstad[4] tested the effect of hole spacing $X_n/D$ in the range 2.5 to 5.0. The tests were conducted with impingement hole diameter and total impingement airflow held constant and with crossflow. Within that range of spacing ratio, the heat transfer performance also improved as the hole spacing was increased. The above quoted references agree that for constant impingement hole diameter, impingement distance, and total cooling airflow, within the ranges of $X_n/D$ values investigated, heat transfer to a given area is greatest for an array with the largest hole spacing. Spacing ratios used in the impingement-film test vehicle design were 4, 8 and 12. The Test Results section shows the same trend. As the spacing ratio increased, the heat transfer coefficient increased.

Impingement Distance ($Z_n$)

The distance between the impingement plate and the surface to be cooled is defined as the impingement distance ($Z_n$). The "Heat Transfer Design Data Book"[5] states that for values of ($Z_n/D$) well above 5.3, the "arrival" velocity of the jet on the plate and the corresponding average heat transfer coefficient decrease with increasing $Z_n/D$ for a constant impingement hole Reynolds number. This effect is indicated in Figure 5. The region of a jet where the velocity remains constant and equal to the velocity at the hole exit is defined as the potential core. It is generally accepted that the peaks of the curves in Figure 5 occur at $Z_n/D$ corresponding to this core length. Gauntner et al[6] indicate that various investigators have measured potential core lengths for turbulent jets which vary from 4.7 to 7.7 hole diameters. They recommend the use of 6.1 hole diameters as the potential core length if the actual length for a particular configuration is not known.

Kercher[1,2] tested the effect of impingement distance on heat transfer for $Z_n/D$ in the range 1.0 to 4.8. In this range, increasing $Z_n/D$ increases heat transfer without crossflow (see Equation (1) and Figure 5) but tends to decrease heat transfer with crossflow. Metzger and Korstad[4] ran similar tests for values of $Z_n/D$ in the range 2 to 6.7. Their data in Figure 6 shows the importance of crossflow. It indicates that heat transfer with large crossflow decreases rapidly as $Z_n/D$ increases.

In summary, the impingement cooling literature does not point out a single optimum impingement distance for heat transfer with crossflow. However, it indicates that the range of interest should be limited to values of $Z_n/D$ less than six. The values used in the impingement-film test vehicle design were 2, 4, and

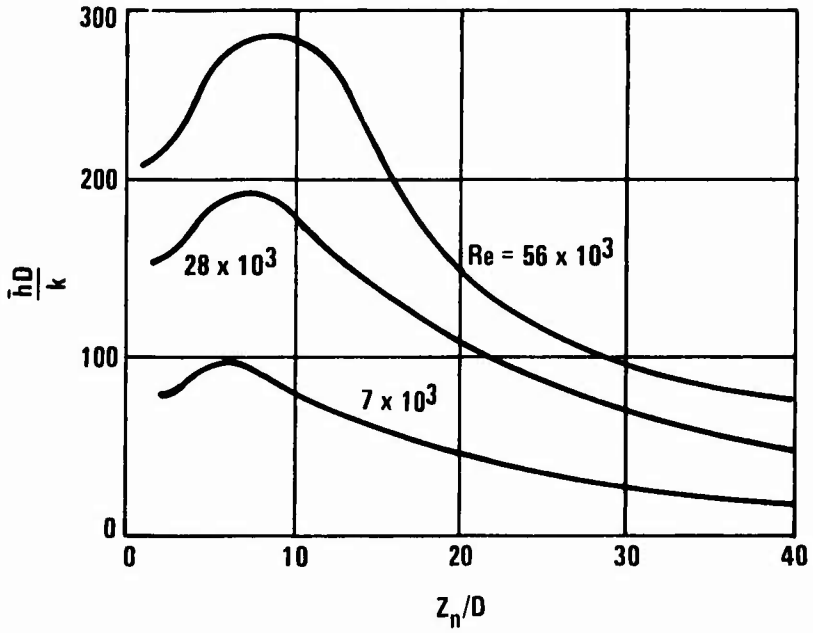


Figure 5. Typical Effects of $Z_n/D$ on Heat Transfer Performance Without Crossflow.

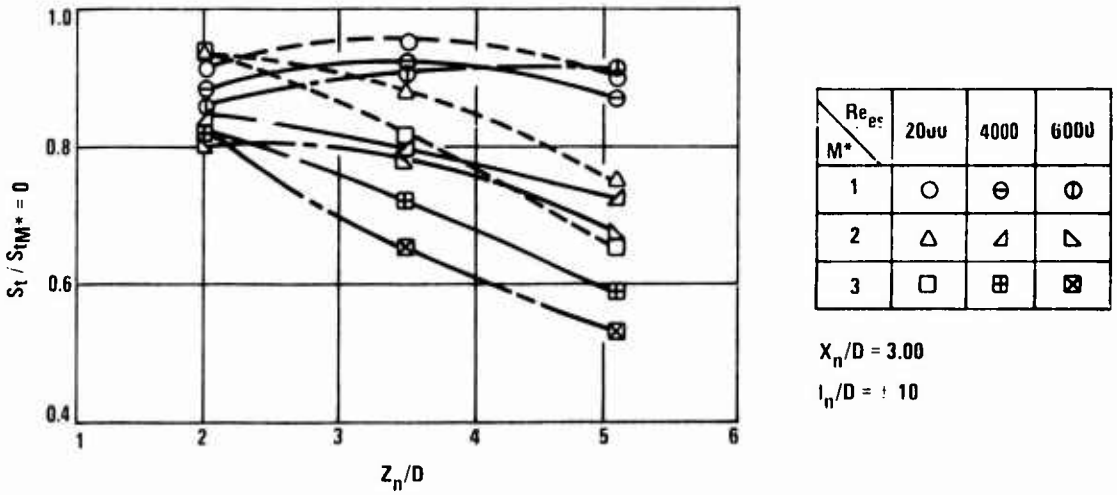


Figure 6. Average Effect of $Z_n/D$.

6. The Test Results, in this report, show a small effect of $Z_n/D$. A maximum heat transfer occurred in the neighborhood of $Z_n/D = 4$. The cooling effectiveness was less at $Z_n/D = 2$ and 6.

## FILM COOLING TECHNOLOGY

Documents reviewed in the field of film cooling technology are References 13 through 28. No references were found which treated impervious wall film effectiveness ($\eta$) in nonuniform density flows with an imposed adverse pressure gradient and nonideal slot geometries. References were found which treated the effects of these items and other variables, such as coolant to hot gas velocity rates, lip thickness, lip length and slot height on an individual basis and in combinations of two or three variables. This information is summarized in the text which follows.

### Slot Configuration

Nina and Whitelaw [13] investigated two types of three-dimensional slot configurations--tangential injection and splash cooling impingement injection--which are shown schematically as Configurations 1 and 2 of Figure 7. They found that for a given open area ratio (the ratio of metering hole area to slot area), higher film effectiveness can be achieved with tangential injection than with splash cooling injection. However, fabrication of either of these configurations for a high-temperature environment is impractical. Configuration 3 of Figure 7 (practical splash cooling injection), which is currently utilized for combustor liner cooling, is the design which was adopted for the impingement-film investigation tests. The metering hole configurations could be made in several ways, as shown in Figure 7: facing downstream (front impingement), facing upstream (back impingement), tangential as in Configuration 1, or normal as in Configuration 2. Tangential injection holes were not suitable for the test panel because film effectiveness of the upstream slot is lowest at the downstream lip. Therefore, impingement cooling of the lip was necessary to achieve a low lip temperature and a low overall radiation-averaged temperature. Figure 8 contains data from Proctor[14], which shows that slot designs similar to Configuration 3 of Figure 7 have greater effectiveness with back impingement holes than with front impingement. Since the requirement of a low radiation-averaged temperature makes it desirable to provide impingement cooling as close as possible to the end of the lip, front impingement holes will be used in this design at some sacrifice in effectiveness. Based on the results of Nina and Whitelaw[13] shown in Figure 9, it was assumed that the front impingement holes introducing air between tangential and normal directions have an effectiveness falling between those achieved with tangential and normal injection. Some useful data on nonideal slot geometries, in uniform density flows ($\rho_c/\rho_g \approx 1.0$) without pressure gradients, can be found in References 13 through 17.

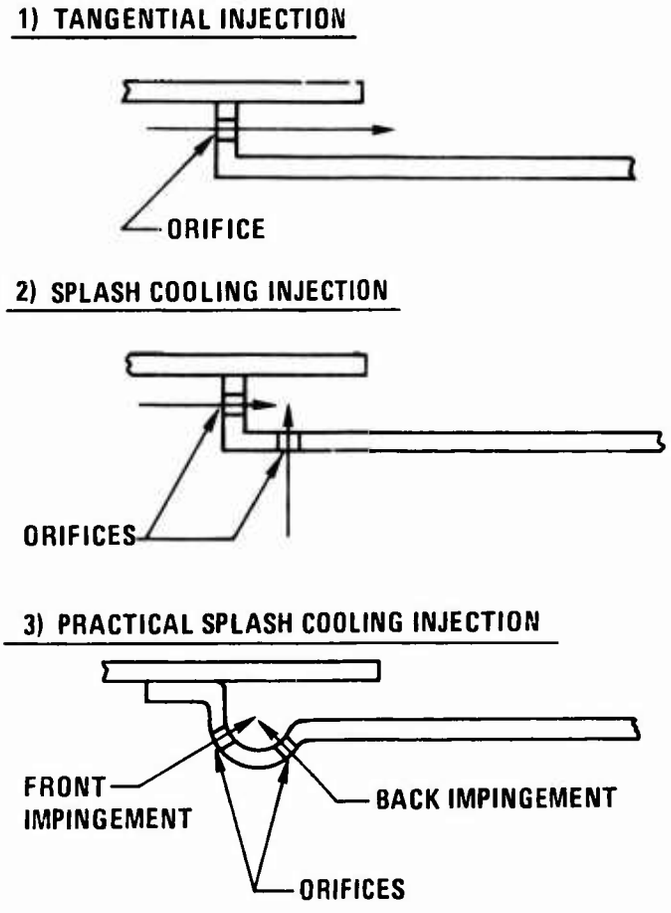


Figure 7. Slot Configurations .

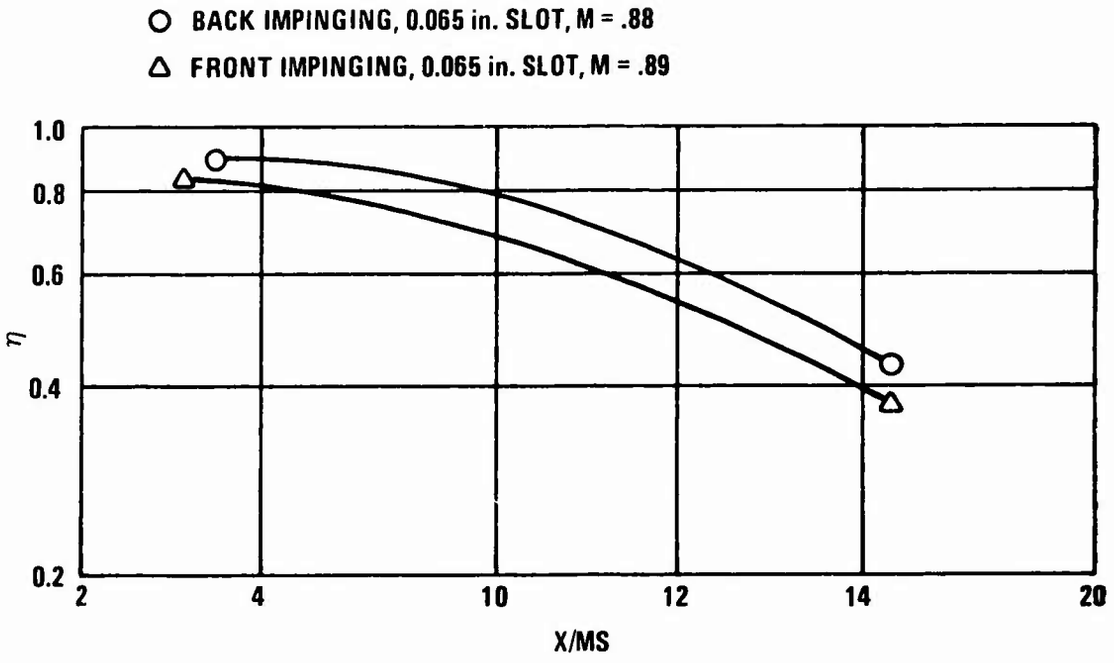


Figure 8. Effect of Backward Impingement and Forward Impingement on Film Effectiveness.

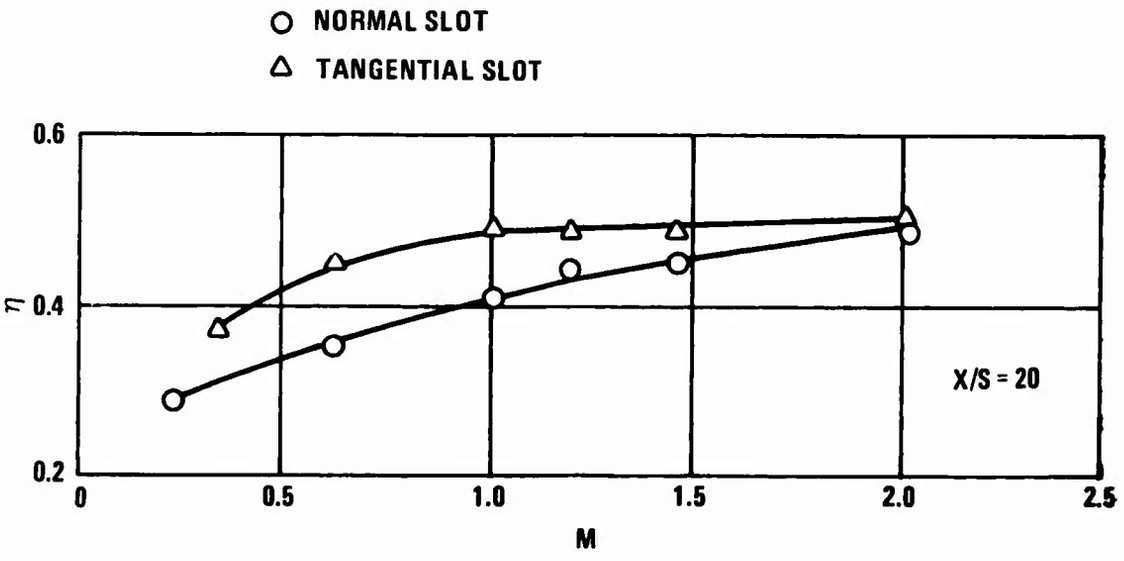


Figure 9. Comparison of Film Cooling With Normal and Tangential Injection.

Metering Holes

Nina and Whitelaw[13] determined the influence of open area ratio (the ratio of metering hole area to slot area) on film effectiveness for the tangential injection slot configuration shown in Figure 7. Two different hole diameters, 0.290 and 0.410 in. at a hole spacing of 0.50 in., were tested. They had open area ratios of 0.264 and 0.528, respectively.

It was found (Figure 10) that the large open area ratios resulted in higher film effectiveness. Nina and Whitelaw[13] also determined the influence of a change in hole spacing with the open area held constant. Two different hole diameters, 0.290 and 0.410 in. at an open area ratio of 0.264, were tested with spacings of 0.5 and 1.0 in. Their results, found in Figure 11, show that at a point 40 slot heights downstream, effectiveness for a given open area ratio increases as spacing increases; but at a point 10 slot heights downstream, it decreases with increasing spacing. Sturgess[18] recommends, for good mixing and uniform films, that the spacing to diameter ratio should be small and that ratios in the range 2.0 to 2.5 are desirable. The spacing ratio used in the impingement-film test vehicle design was 1.83.

Lip Thickness and Length

Sivasegaram and Whitelaw[19] tested the influence of slot lip thickness on film effectiveness for an ideal, two-dimensional, unobstructed slot. A constant 0.032 in. lip thickness was used with 0.074-, 0.132-, 0.25-, and 0.50-in. slot heights, which correspond to lip thickness to slot height ratios (t/S) of 0.432, 0.242, 0.128, and 0.064. They found (Figure 12) that for given values of mass flow rate through the slot and given free-stream velocities, the effect of an increase in the lip thickness to slot height ratio is in general to decrease the effectiveness, especially if thickness to slot height ratio is greater than approximately 0.25. Sturgess[20] studied the effect of slot lip thickness for a slot configuration similar to that of Configuration 3 in Figure 7 and recommends that the ratio t/S should not exceed 0.30. Nina and Whitelaw[3] ran tests on a tangential injection slot, as shown in Configuration 1 in Figure 7, using lip thickness ratios t/S 0.5 and 0.125. They found (Figure 13) that smaller values of t/S result in higher effectiveness. Proctor [14] tested the effect of lip thickness on the performance of a practical impingement slot configuration, as shown in Configuration 3 in Figure 7. He used a fixed 0.26-in. slot height and lip thickness of 0.12, 0.224 and 0.36 in., which correspond to lip thickness to slot height ratios of 0.46, 0.86, and 1.38. He found that with a configuration of this type, the lip thickness does not have a strong effect on film effectiveness.

Proctor's data was for a slot configuration similar to the configuration which will be used in the test panel design and was better controlled than that of the other experimenters since the lip thickness, rather than the slot height, was varied to

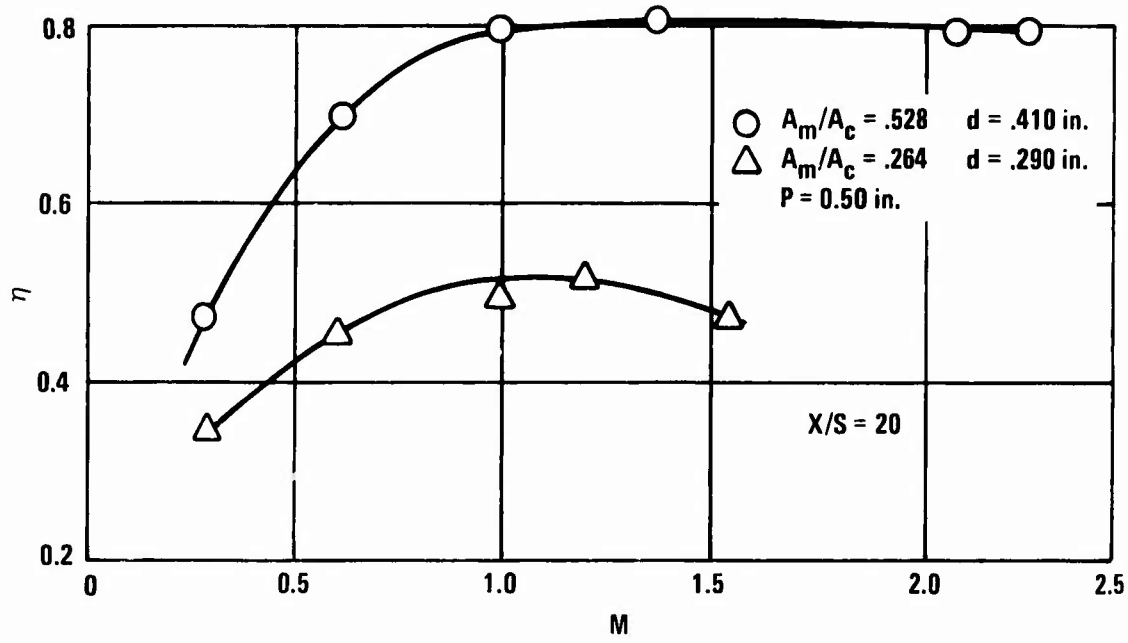


Figure 10. Influence of Open Area Ratio.

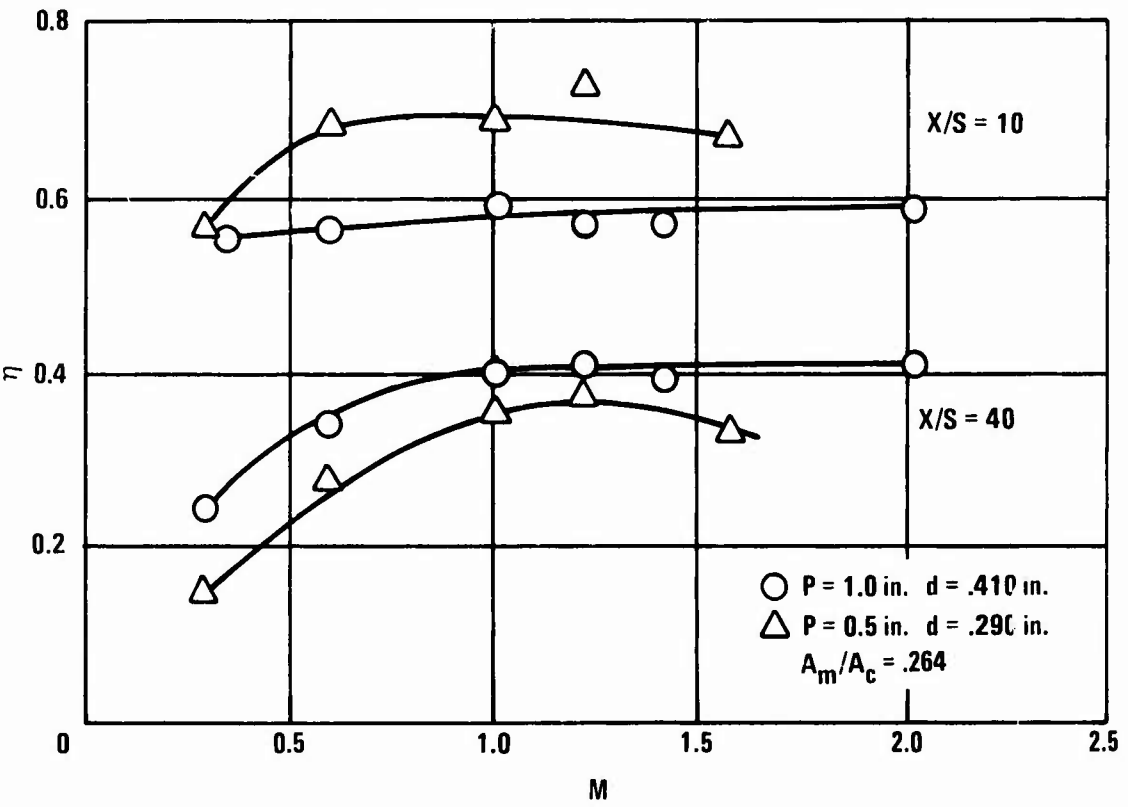


Figure 11. Influence of Pitch (Spacing).

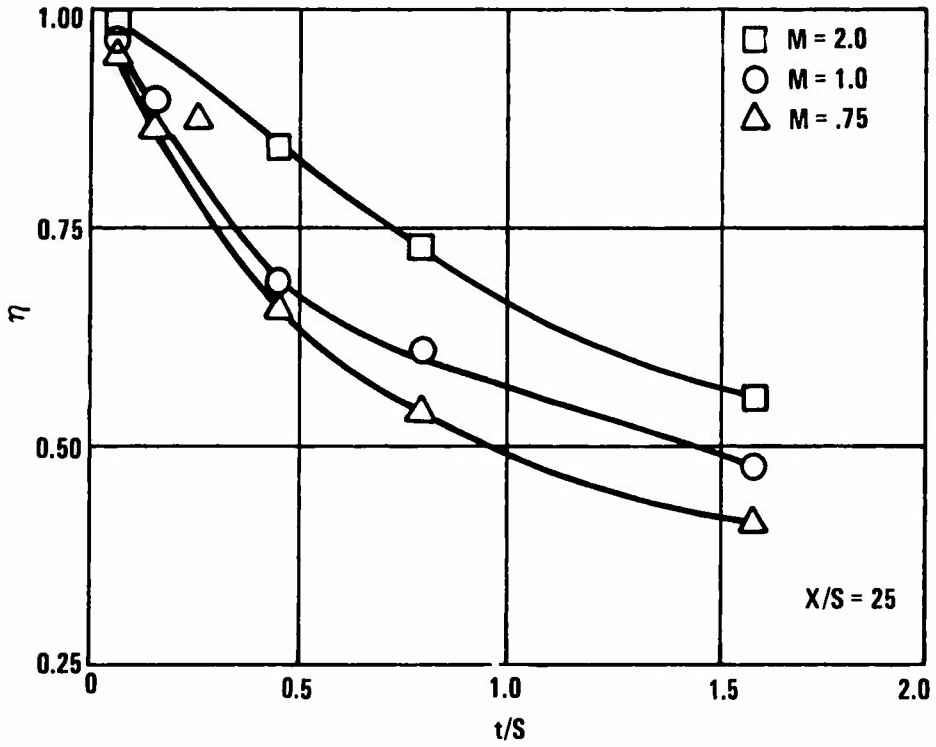


Figure 12. Influence of Lip Thickness for Ideal Two-Dimensional Unobstructed Slot.

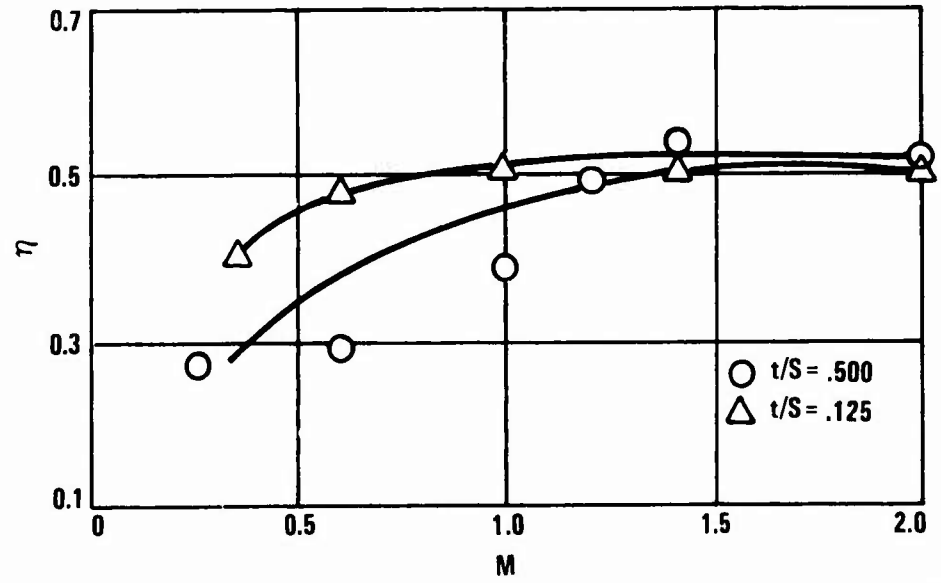


Figure 13. Influence of Lip Thickness for Tangential Injection Slot.

change the t/S ratio. Therefore, it is concluded that for the practical impingement slot configuration, the lip thickness does not have a strong influence on the film effectiveness. However, since no adverse effects have been shown for thin lips with any configuration, lip thicknesses for the test panels were set at 0.044 in., which is sufficient for the requirement to embed thermocouples.

The effect of lip length on the performance of a tangential injection slot (Configuration 1, Figure 7) was investigated by Nina and Whitelaw[13] for lip length to slot height ratios (L/S) of 0, 2.36 and 4.0. Their data (Figure 14) shows that a zero length slot has a low effectiveness but that slot lips with L/S ratios of 2.36 and 4.00 have nearly equal film effectiveness. They also tested a splash cooling injection slot configuration for values of L/S of 2.36 and 4.00. Their data (Figure 15) shows that longer lip length for this configuration resulted in somewhat higher effectiveness near the slot exit but slightly lower effectiveness at a distance of 30 slot heights downstream. Their results indicate that film effectiveness increases as the lip length to slot height ratio increases. In the impingement-film test vehicle the lip length is 1.05 in., which corresponds to L/S of 10.5 and 7.2 for slot heights of 0.100 and 0.145 in. respectively.

Slot Heights

Sturgess [20] recommends that for most efficient use of available cooling air, slot heights should not fall outside the range 0.125 to 0.175 in. Proctor [14] tested the influence of slot heights on film effectiveness for slots in the range 0.040 to 0.100 in. for both front impingement (Figure 16) and back impingement (Figure 17) holes. He concluded that no significant change in film effectiveness occurred with varying slot height and constant cooling airflow. The impingement-film heat transfer program included film cooling tests with 0.100- and 0.145-in. slot heights. Since the film effectiveness was higher at the most severe heating condition, 0.4 Mach number with a 0.100-in. slot, the impingement-film tests were run with a 0.100-in. slot height.

Injection Velocity Ratio ($V_c/V_g$)

Sturgess[20] recommends that coolant to mainstream velocity ratio ($V_c/V_g$) fall within the range 0.5 to 1.1 for maximum film effectiveness. Pai and Whitelaw[21] tested the effect of the injection velocity ratio in the range 0.322 to 3.33 for nonuniform density flows ($\rho_c/\rho_g > 1$). For that case, they found that optimum film effectiveness is obtained when $V_c/V_g$ is about unity. Their data, replotted in Figure 18, shows this effect. There is general agreement that injection velocity ratio near unity is optimum for film effectiveness. This was generally confirmed by the impingement-film test results in which film effectiveness was greater for velocity ratios below one than above one.

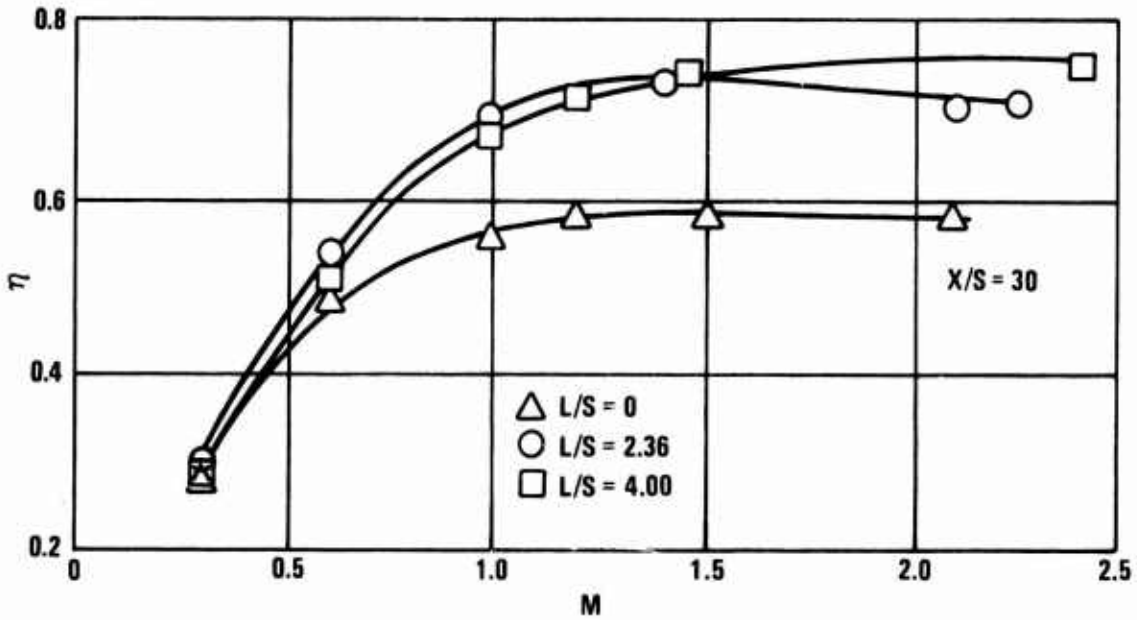


Figure 14. Influence of Lip Length for Tangential Injection Slot.

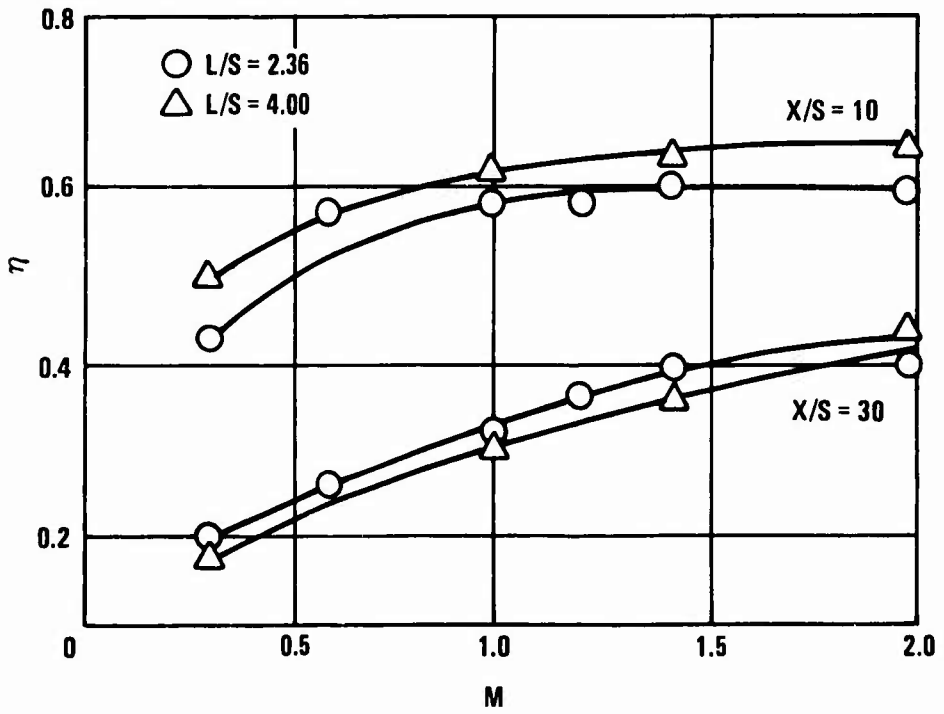


Figure 15. Influence of Lip Length for Splash Cooling Injection Slot.

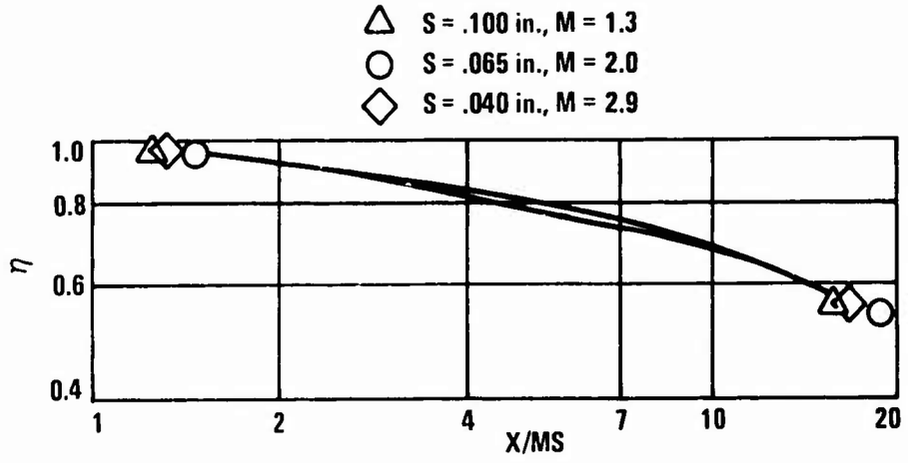


Figure 16. Front Impinging Panel - $W_c$ = 0.26 lb/sec.

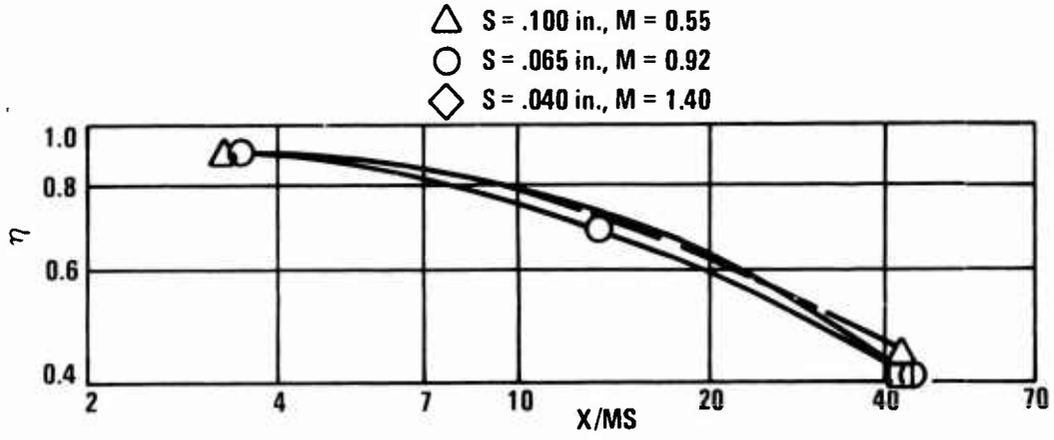


Figure 17. Back Impinging Panel - $W_c$ = 0.11 lb/sec.

Density Ratio ($\rho_c / \rho_g$)

The density ratio is defined as the ratio of the slot coolant density to the mainstream density. Data could not be found which gives film effectiveness for nonuniform density and slot configurations similar to that used in the panel test program. However, the effects of nonuniform density flows for an ideal, two-dimensional slot were obtained by Pai and Whitelaw[21]. They found (Figure 18) that for a given value of ($V_c/V_g$), an increase in the density ratio, $\rho_c/\rho_g$, increased the film effectiveness. The density ratio for the impingement-film tests was determined by the specified hot gas conditions and was in the range 2.5 to 3.0.

Pressure Gradient

Pai and Whitelaw[22] ran tests with nonuniform density flows $\rho_c/\rho_g = 4.17$ in an adverse pressure gradient (Figure 19). They found that for distances less than 50 slot heights downstream, the values of effectiveness are the same as for the zero pressure gradient case. For distances greater than 50 slot heights, the effectiveness was somewhat greater with the adverse pressure gradient than without it. Results of the portion of the impingement-film test program which had film cooling only (no impingement) on the test panel agreed well with predictions based on zero pressure gradient. This indicates that there was no measurable effect of the adverse gradient for X/S values up to 55.

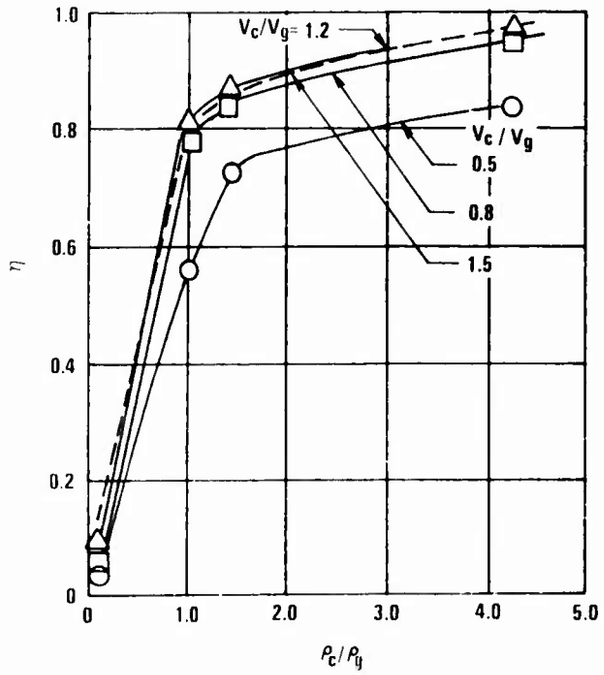


Figure 18. Effect of Density Ratio on Effectiveness for X/S= 32.5.

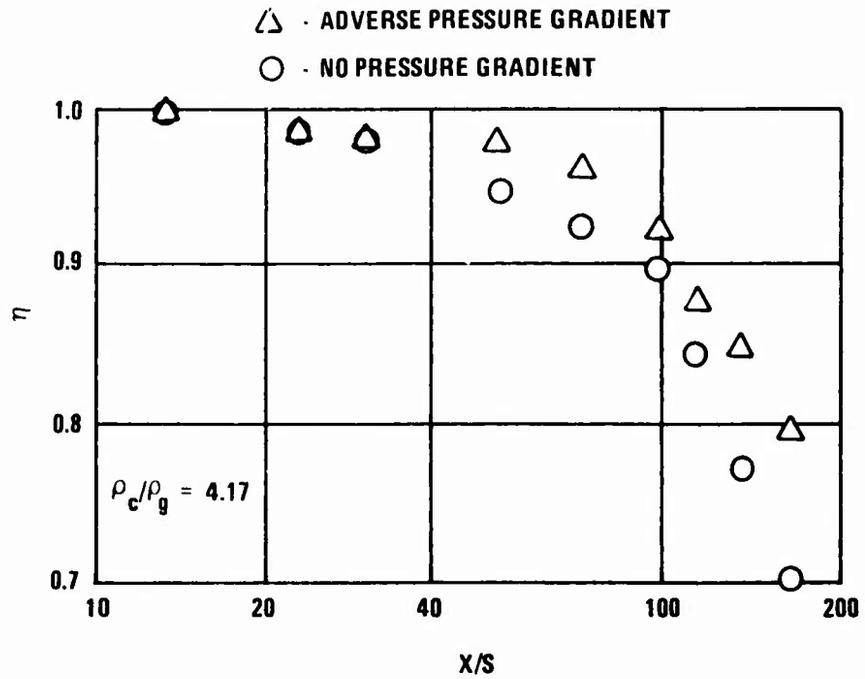


Figure 19. Effect of Pressure Gradient on Effectiveness.

## DESCRIPTION OF TEST APPARATUS

### TEST RIG

The test setup and the test rig are shown in Figures 20 and 21. Figure 22 is a schematic of the test rig. The test rig is a two-dimensional hot gas tunnel consisting of a two-dimensional ASME bellmouth followed by a 15-in.-long constant-area inlet duct, a 14-in.-long cooled diffuser test section on which the inlet and test panels are mounted, and a 9-in.-long constant-area exhaust duct downstream of the diffuser. A flange (see Figure 21) is used to mount the test rig on a 12-in.-diameter high-pressure hot gas supply plenum. The installed test rig is shown in Figure 20.

#### Inlet Section

The ASME bellmouth (see Figure 21) has an elliptic contour with the major axis equal to three-halves of the minor axis. To ensure turbulent flow through the test sections, a 15-in. constant-area inlet duct is incorporated upstream of the diffusing test section and screens are installed upstream of the bellmouth in the inlet plenum duct.

#### Test Section

The diffuser duct test section of the test rig is 14 in. long with a 2 x 7 in. cross section at the inlet and a 3 x 7 in. cross section at the exit. Figure 23 is a top view of the test rig which shows where the inlet and test panels are mounted on the diffuser. The test panels are cooled and form one side of the diffuser duct. The other three sides of the diffuser duct are impingement cooled by shop air so that the radiation-averaged temperature of the three diffuser walls can be controlled and held at the radiation-averaged temperature of the test panels. Also, to reduce radiation, the cooled diffuser walls extend about 2.75 in. upstream and downstream of the test panels. Therefore, the inlet test panels are not heated by radiation from the hot diffuser walls but only by convection from the hot gas stream. Figure 24 is a schematic of the diffuser cooling circuit. The connections can be seen on the bottom of the diffuser in Figure 20. The diffuser cooling air enters through the two hoses shown in Figure 20 and exhausts into the test cell from six pipe nipples seen on the bottom of the test rig.

The test panel design and impingement-film cooling system are shown in Figure 25. The total cooled surface area ($A_S$) for both the inlet and test panels is 82.53 in.$^2$. The cooling air sides of the test and inlet panels are shown in Figures 26 and 27. The main part of each panel is 0.062 in. thick. The slot lips, which are extensions of the panels, are 0.044 in. thick. The inlet panel slot lip is shown in Figure 23. The test panel slot lip is on the inlet panel as shown in Figure 27. The panel thickness was determined by a requirement to embed thermocouples in them and to assure small deflections due to bending. The lip thickness was made as small as possible to avoid the reduced film

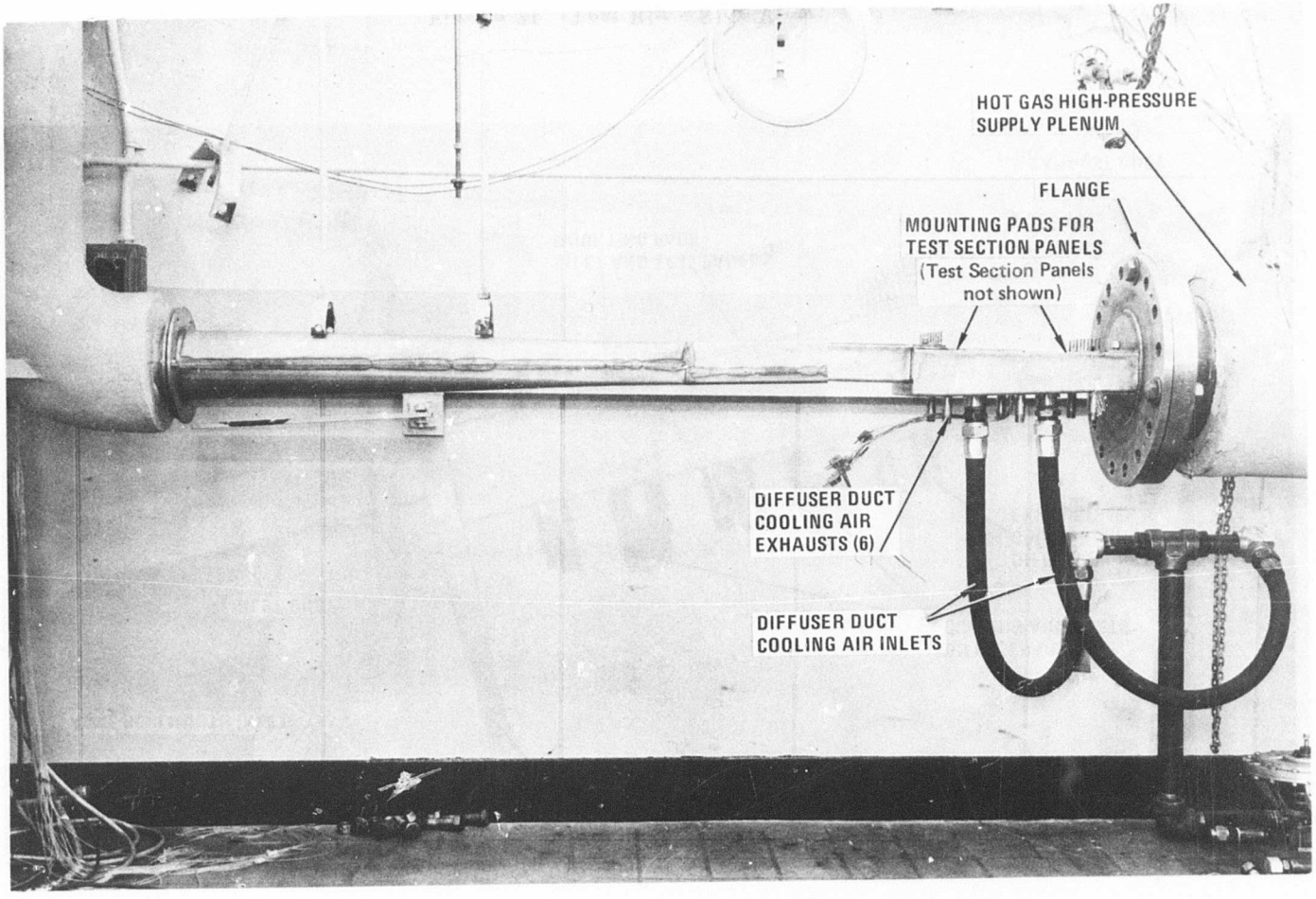


Figure 20. Test Rig Setup.

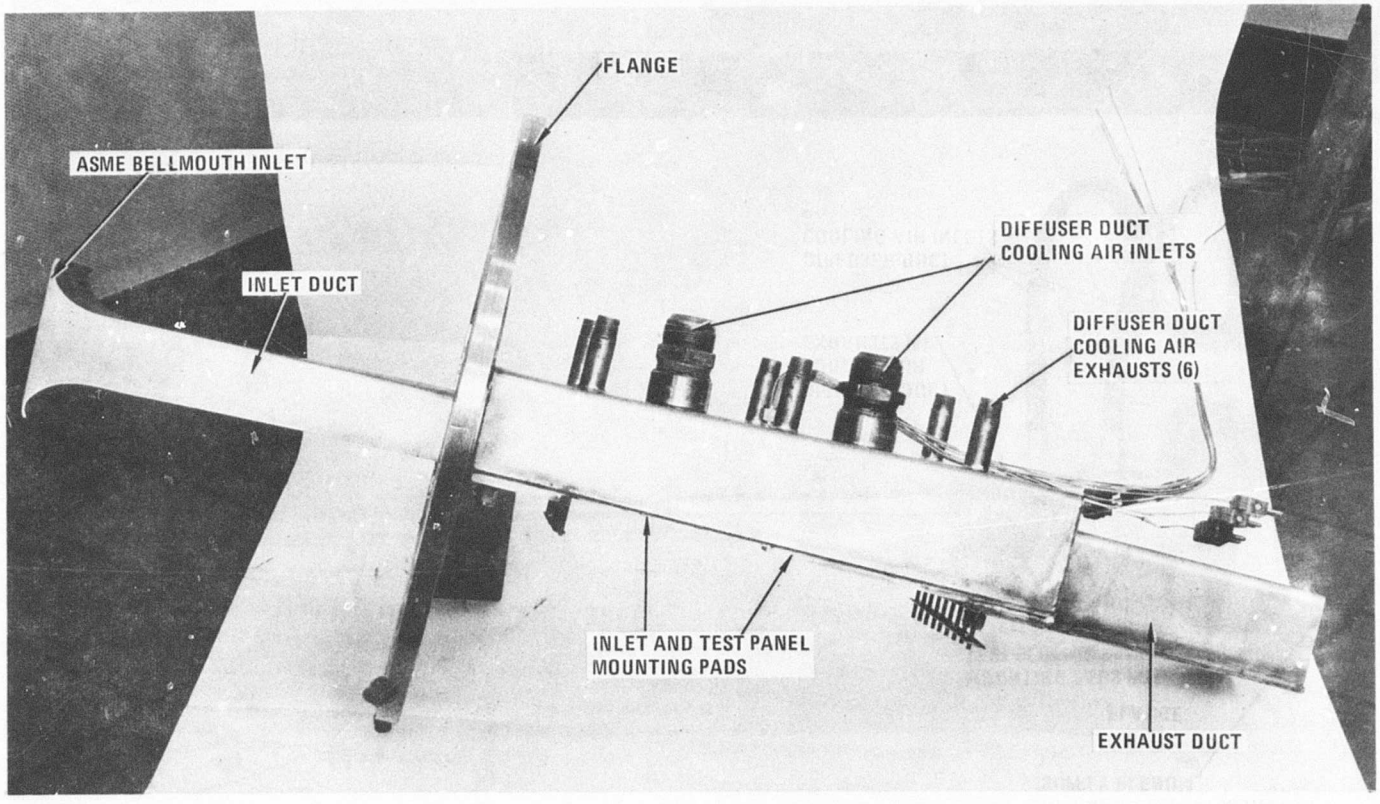


Figure 21. Test Rig - Side View.

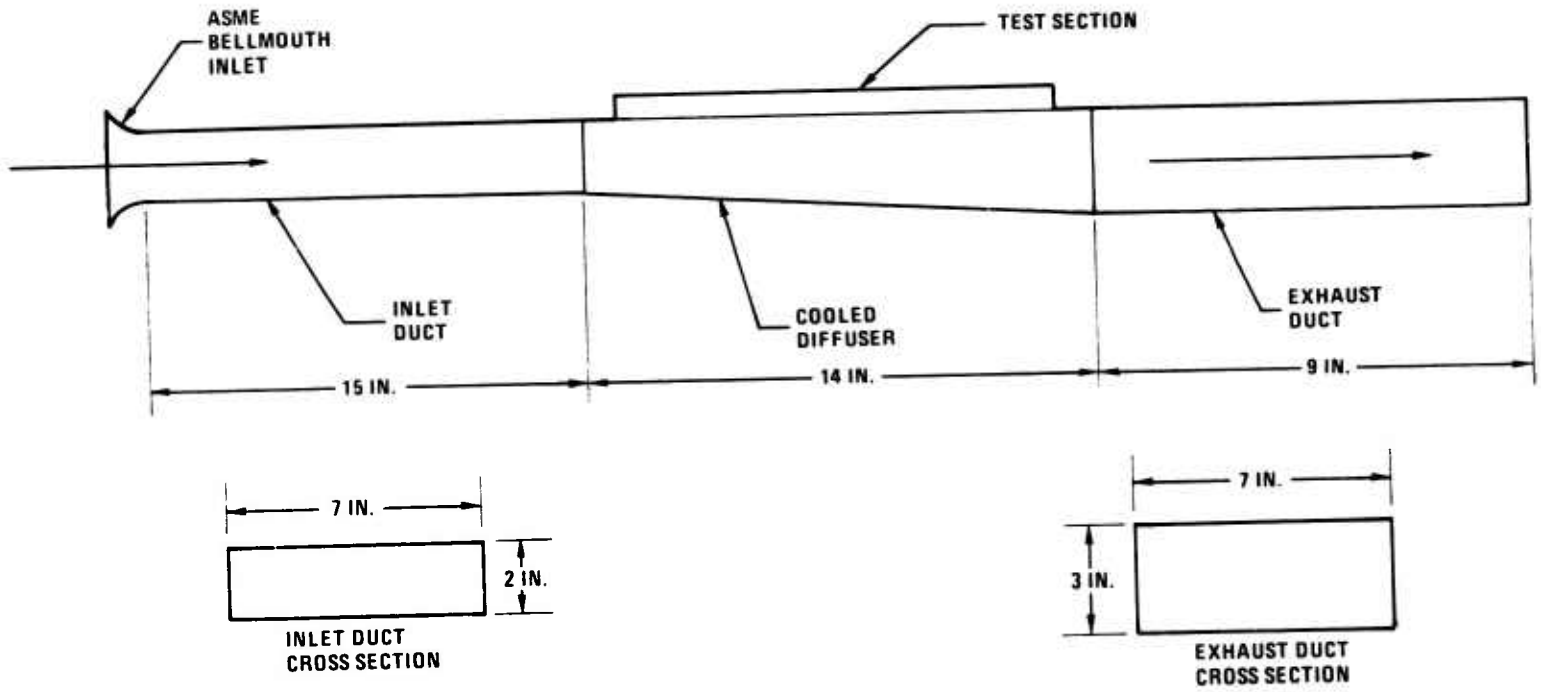


Figure 22. Test Section - Schematic.

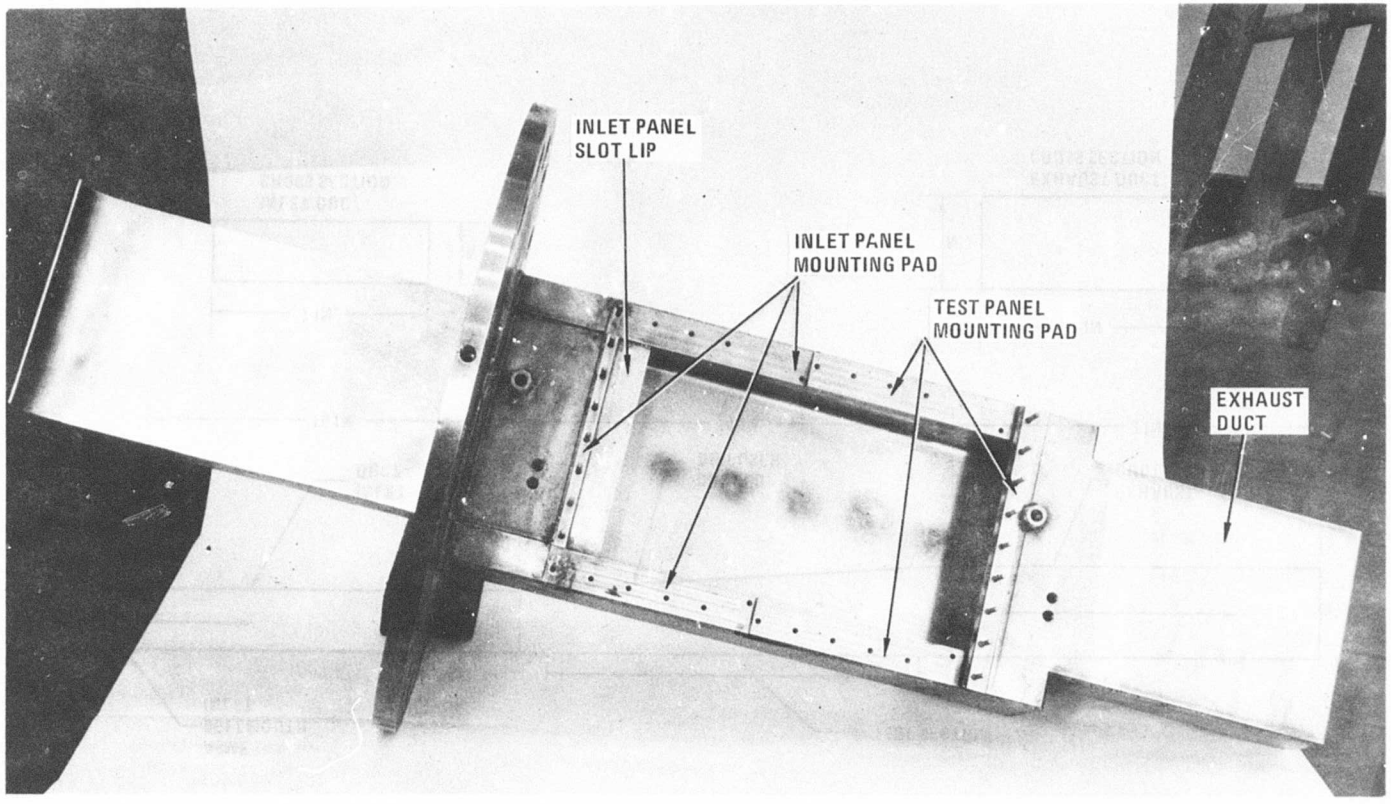


Figure 23. Test Section - Top View.

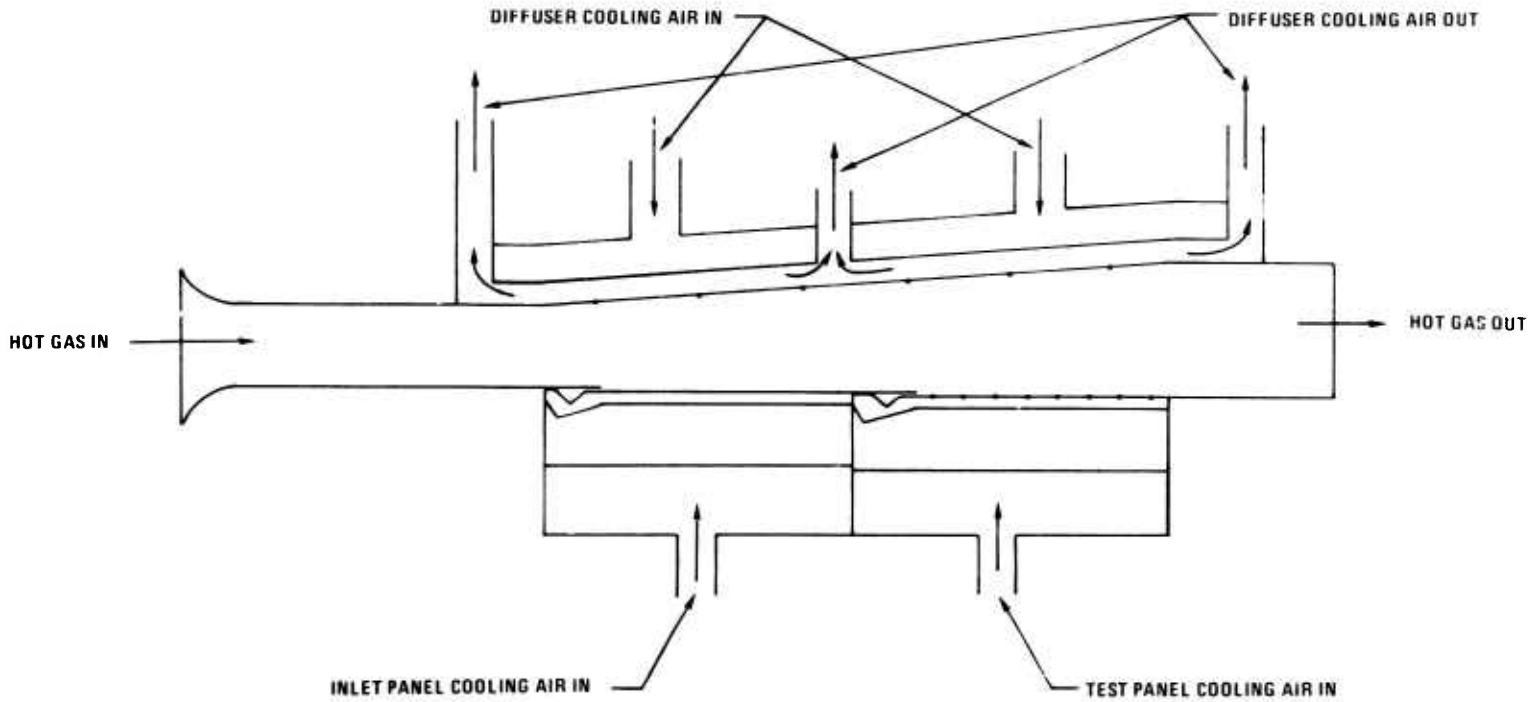


Figure 24. Diffuser Cooling Circuit Schematic.

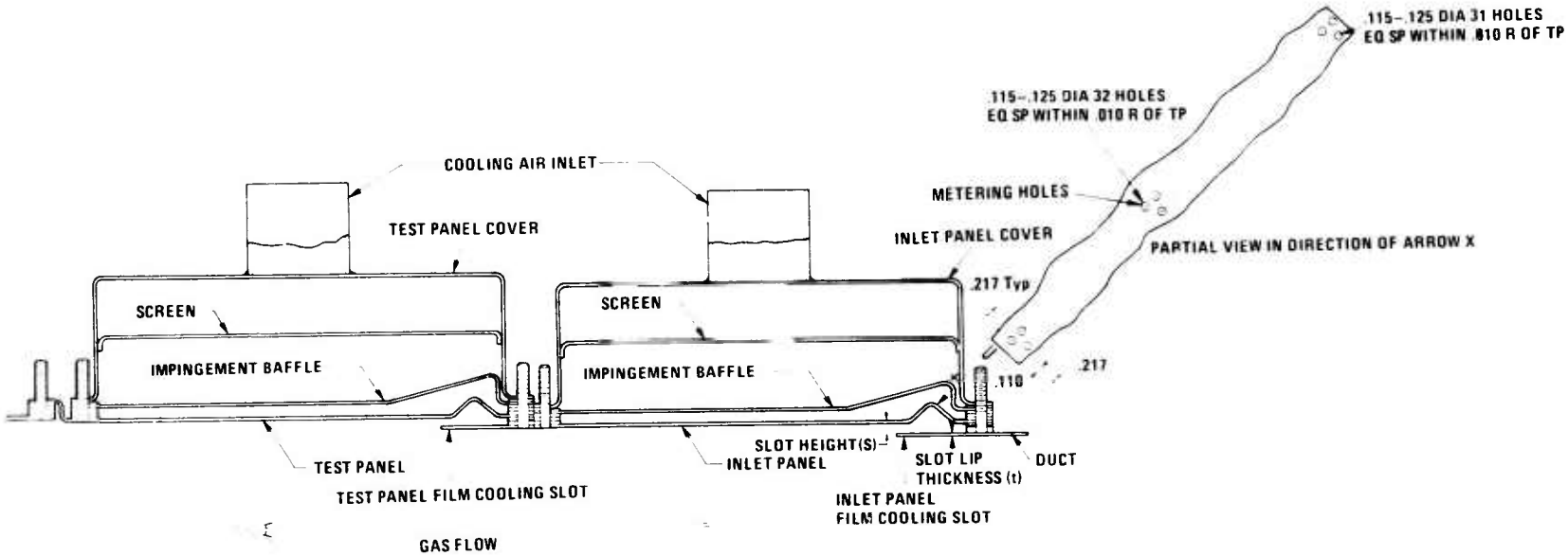


Figure 25. Test Section Schematic .

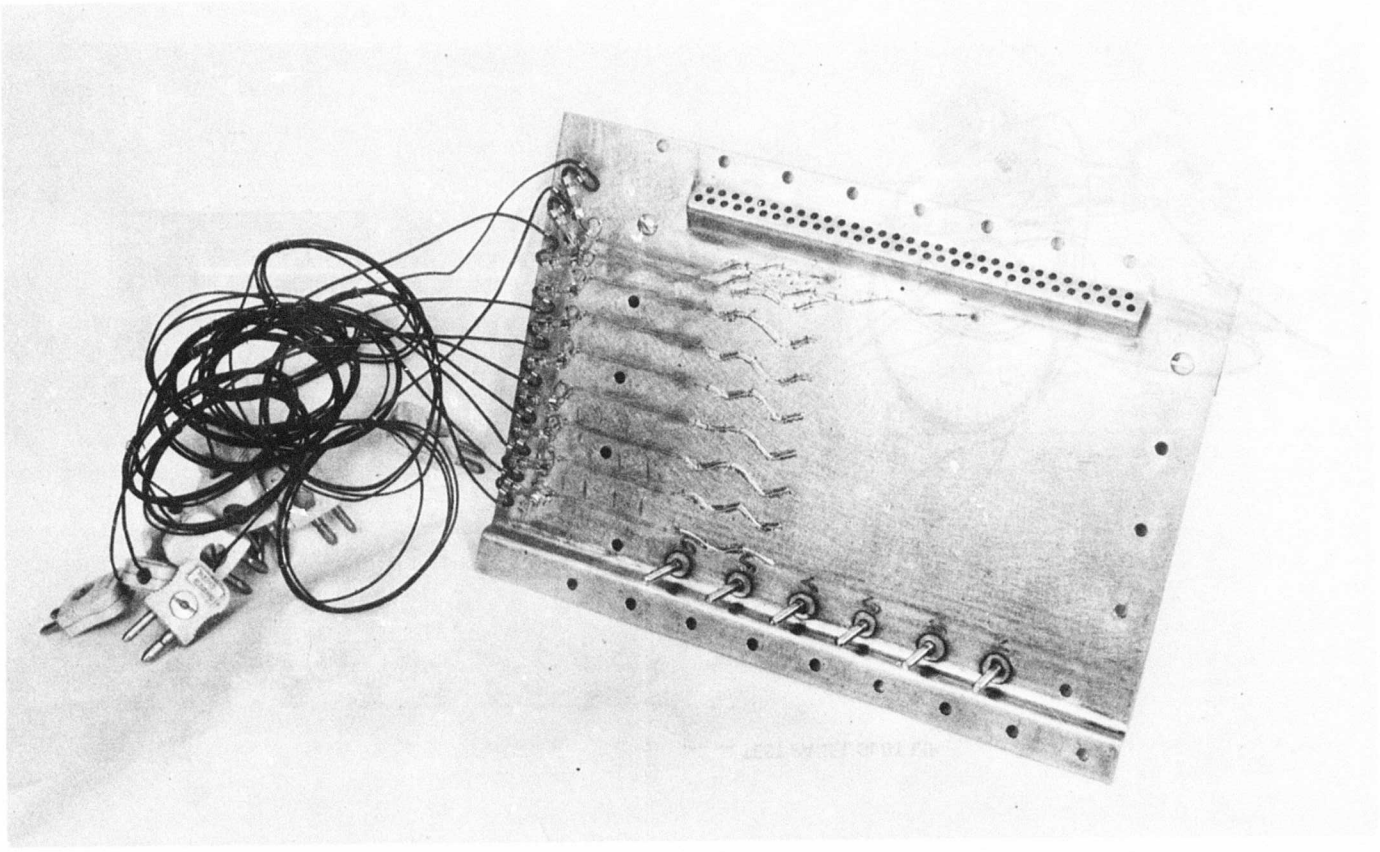

Figure 26. Test Panel - Cooling Air Side.

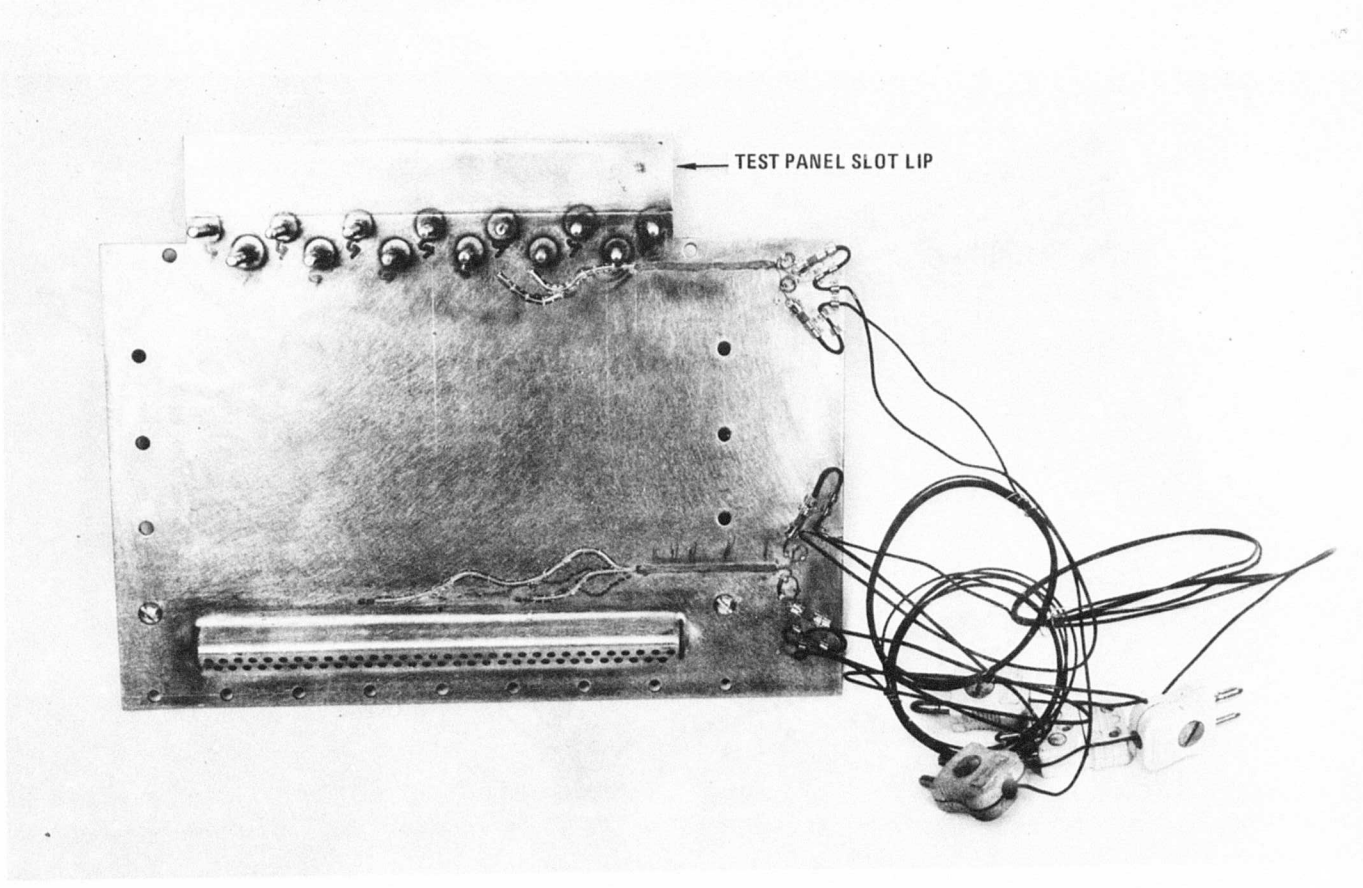


Figure 27. Inlet Panel - Cooling Air Side.

effectiveness, which is indicated in Figure 13, caused by turbulence from the base of the lip. In order to measure temperature distribution in the cooled inlet and test panels, two thermocouples were embedded in the lip region of the inlet panel and eight were embedded in the test panel. They are listed T1 through T10 on the instrumentation list (see page 42) and can be seen in Figures 26 and 27.

Film Slot Design

The film cooling slot design is shown in Figure 25. The pertinent film cooling geometry parameters for the two slot heights, 0.100 and 0.140 in., are:

| | Slot Height (S), in. | |
|---|---|---|
| | 0.100 | 0.140 |
| Cooled panel surface area ($A_s$), in.$^2$ | 82.53 | 82.53 |
| Slot area ($A_c$), in.$^2$ | .70 | .98 |
| Lip thickness (t), in. | .044 | .044 |
| t/S | .44 | .37 |
| Lip length (L), in. | 1.05 | 1.05 |
| L/S | 10.05 | 7.2 |
| Number of metering holes | 63 | 63 |
| Metering hole diameter ($D_m$), in. | .120 | .120 |
| Metering hole pitch ($X_m$), in. | .22 | .22 |
| Metering hole total area ($A_m$), in.$^2$ | .713 | .713 |
| Metering hole pitch/diameter ($X_m/D_m$) | 1.83 | 1.83 |
| Open area ratio ($A_m/A_c$) | 1.019 | .728 |

Impingement Baffle Design

The impingement cooling is accomplished by an array of cooling air jets which impinge on the cool side of the inlet and test panels. The jets are formed by the perforated baffles shown above the inlet and test panels in Figure 25. The two panels have identical impingement baffles which can be changed by removing the two covers shown in Figure 25. The covers also form inlet plenum chambers for

the cooling air. The tests were run with the three pairs of impingement baffles shown in Figures 28, 29 and 30. The baffles have 0.031-, 0.052- and 0.070-in.-diameter impingement holes in a square array. They have a spacing ratio (hole-to-hole centerline distance divided by hole diameter) of 4. Other spacing ratios were obtained by selectively covering rows and columns of holes. In each of Figures 28, 29, and 30 the test panel's baffle is shown untaped and the upstream panel's baffle is shown with its spacing altered by adhesive backed aluminum tape. The impingement distance, from impingement panel to cooled panel, was varied by using different gasket thicknesses between the impingement baffle and the cooled panel. The cooling air systems for the two test panels were completely independent but operated identically to simulate an operational system.

### Exhaust Section

A 12-in. constant-area exhaust duct downstream of the diffuser section was incorporated into the design to prevent the exhaust system from affecting test results.

## TEST FACILITY

The impingement-film heat transfer tests were run in Cell 70, Building 1-70, in Lynn, Massachusetts. The piping system for the cell is shown schematically in Figure 31. It includes a gas-fired indirect heater, which is shown schematically in Figure 32, and uses the 300-psi plant air supply. The system can supply 1200°F air at 2-lb/sec airflow. The impingement-film tests were run at a nominal temperature of 1100°F with a cooling flow range of 0.4 to 1.8 lb/sec. Temperature and pressure were controlled by electropneumatic servo mixing and regulating valves.

Figures 33 and 34 show the instrumented test rig mounted in the facility. Standard cell instrumentation includes multipoint temperature and digital pressure readouts, flow measurement, and deadweight pressure standards for in-place calibration of pressure systems for the impingement-film test program. Cell 70 instrumentation readout capabilities were improved to permit direct input of test panel and diffuser wall temperatures in the time-sharing computer system. The computer prints out temperature and radiation-averaged test panel and diffuser wall temperatures. This information was required so that the radiation-averaged temperatures could be maintained nearly equal to prevent heat transfer by radiation between the test panels and the diffuser walls.

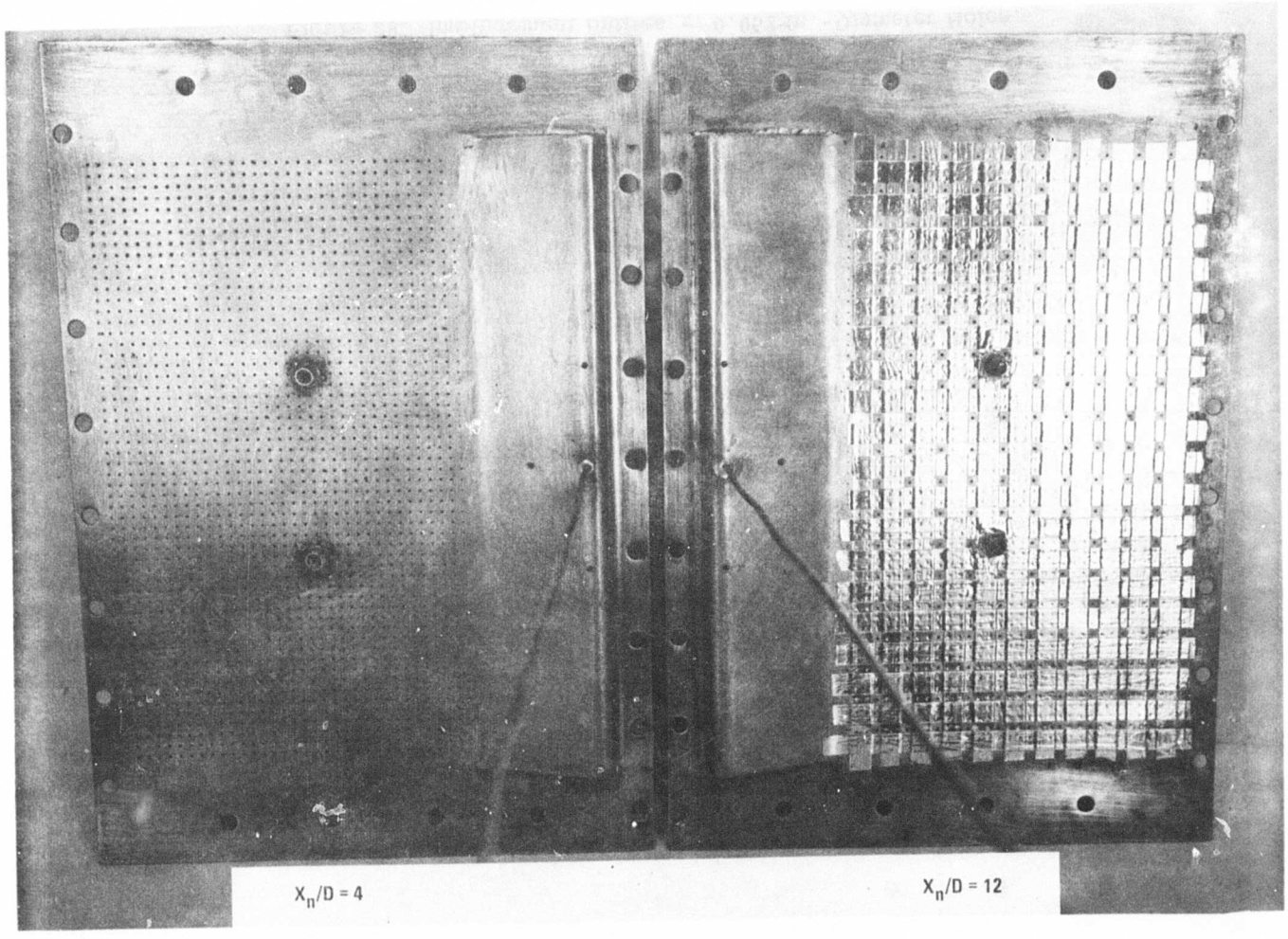


Figure 28. Impingement Baffles - 0.031-In.-Diameter Holes.

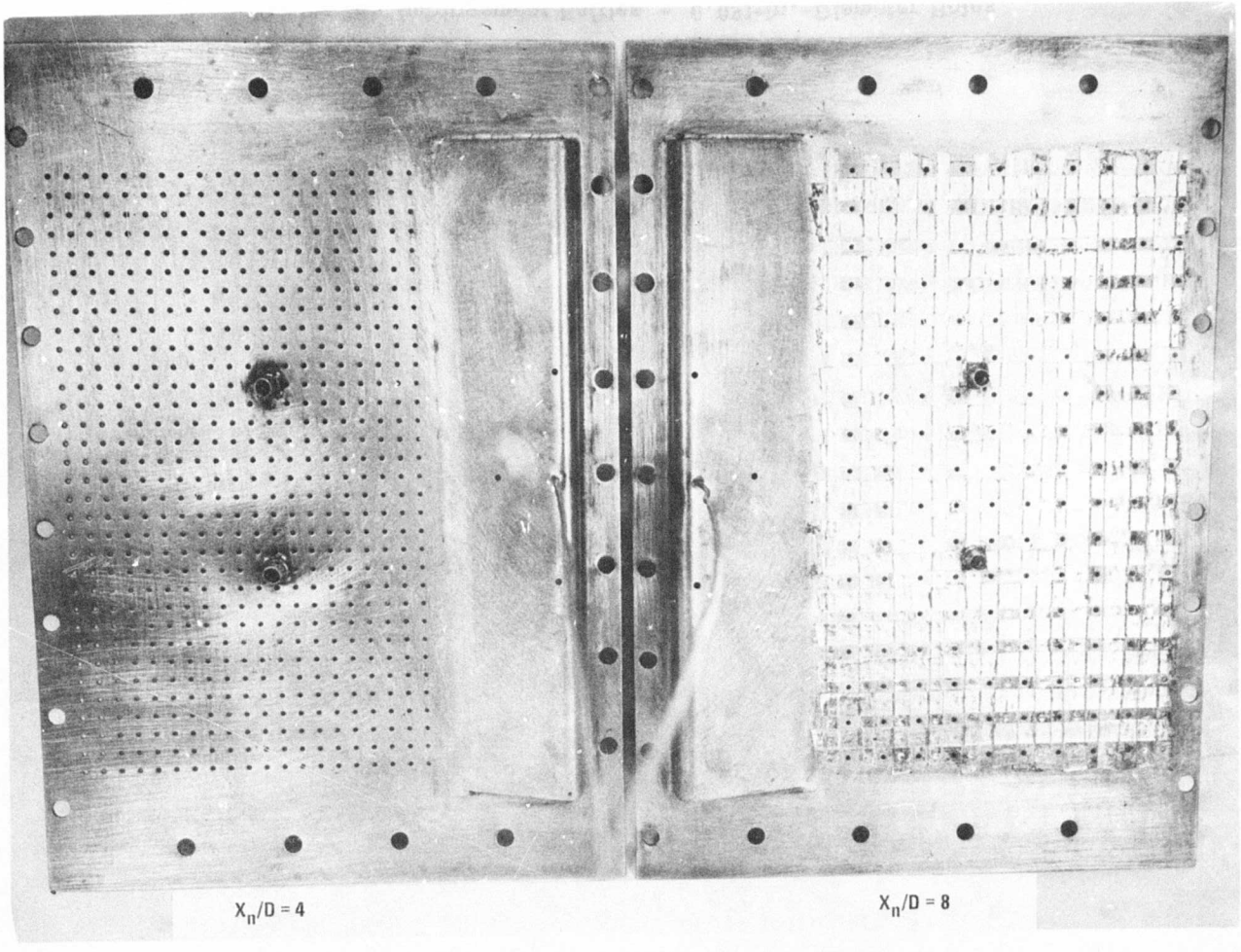


Figure 29. Impingement Baffles - 0.052-In.-Diameter Holes.

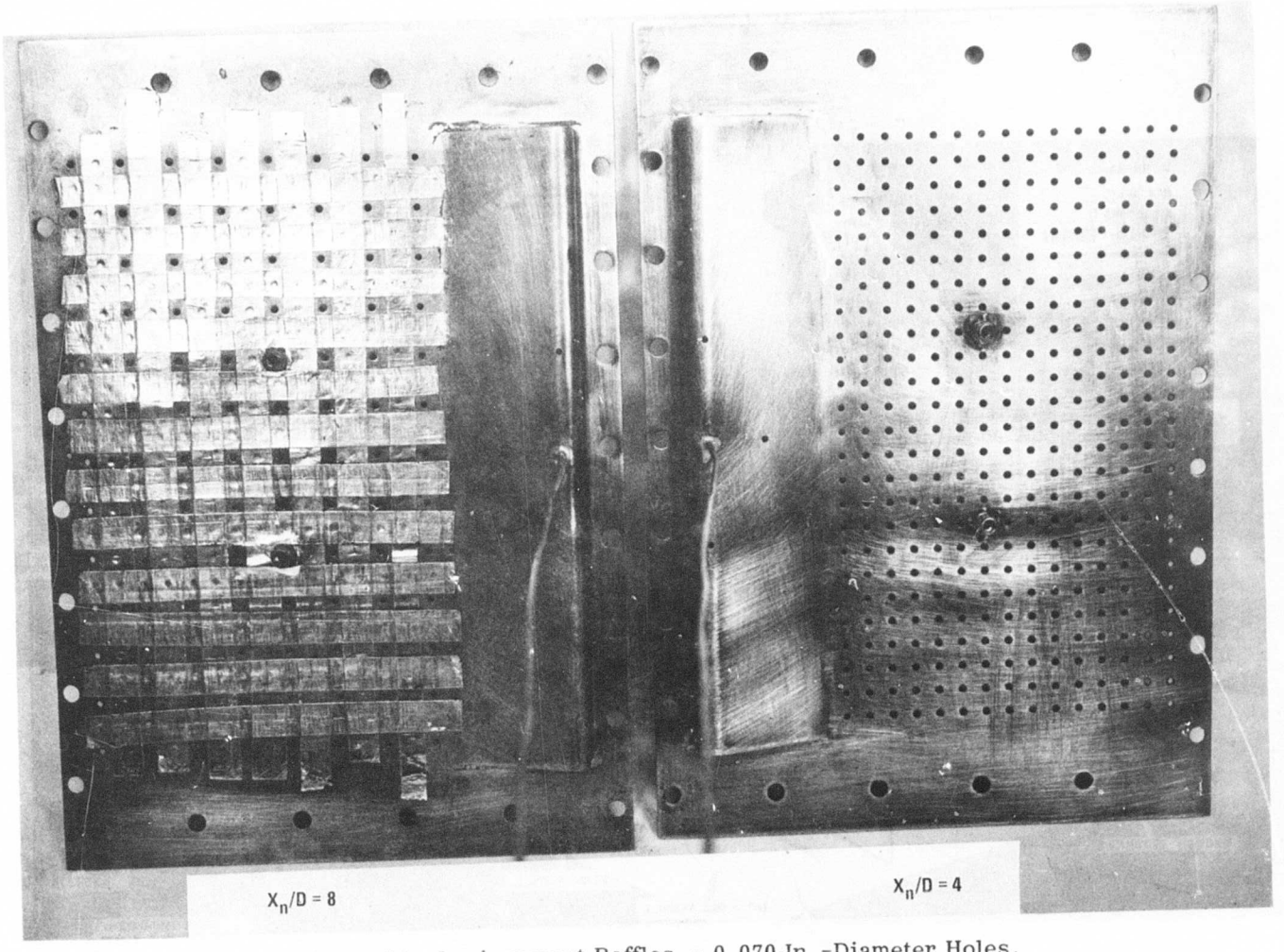


Figure 30. Impingement Baffles - 0.070-In.-Diameter Holes.

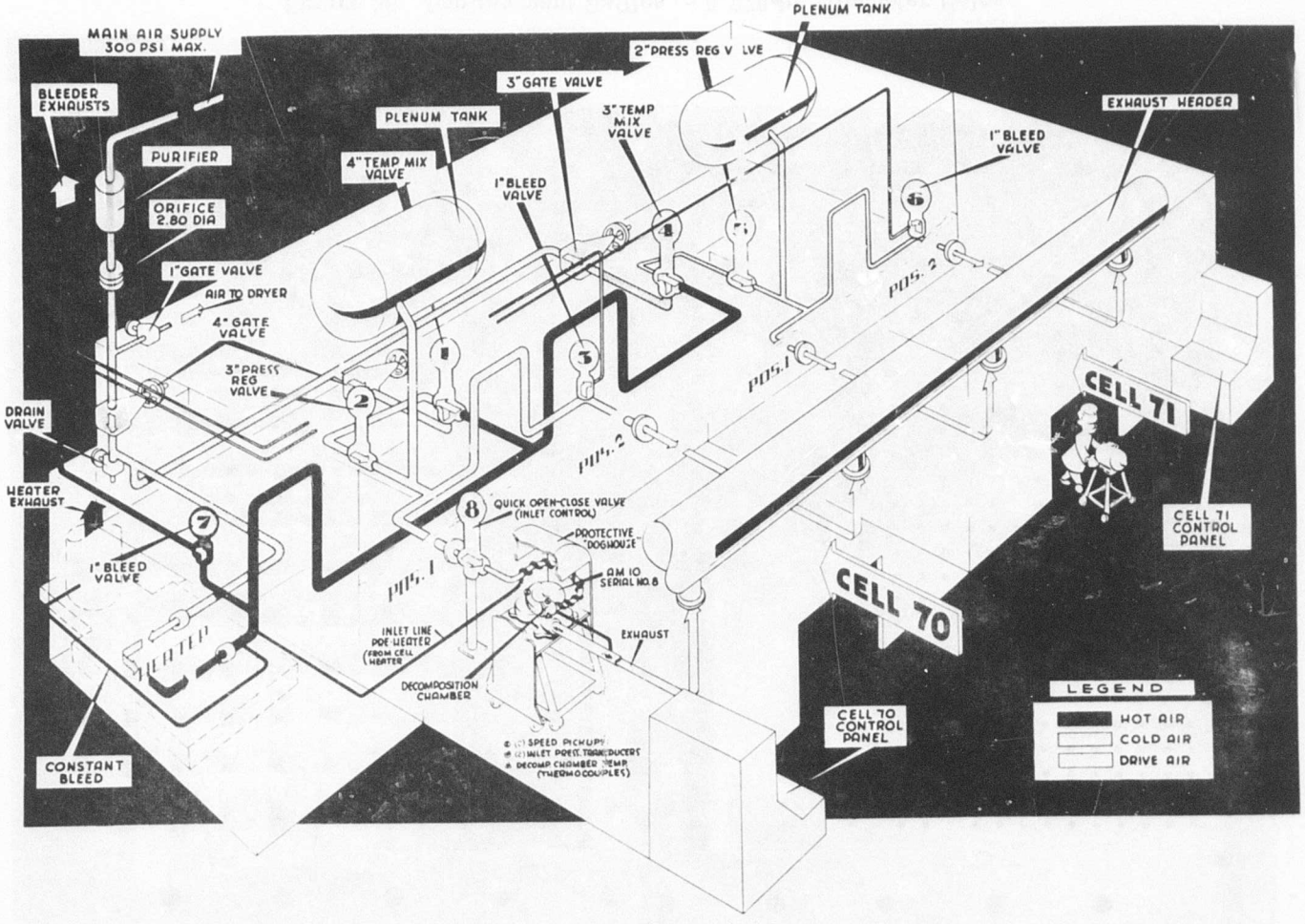


Figure 31. Drive Air Schematic for Cells 70 and 71.

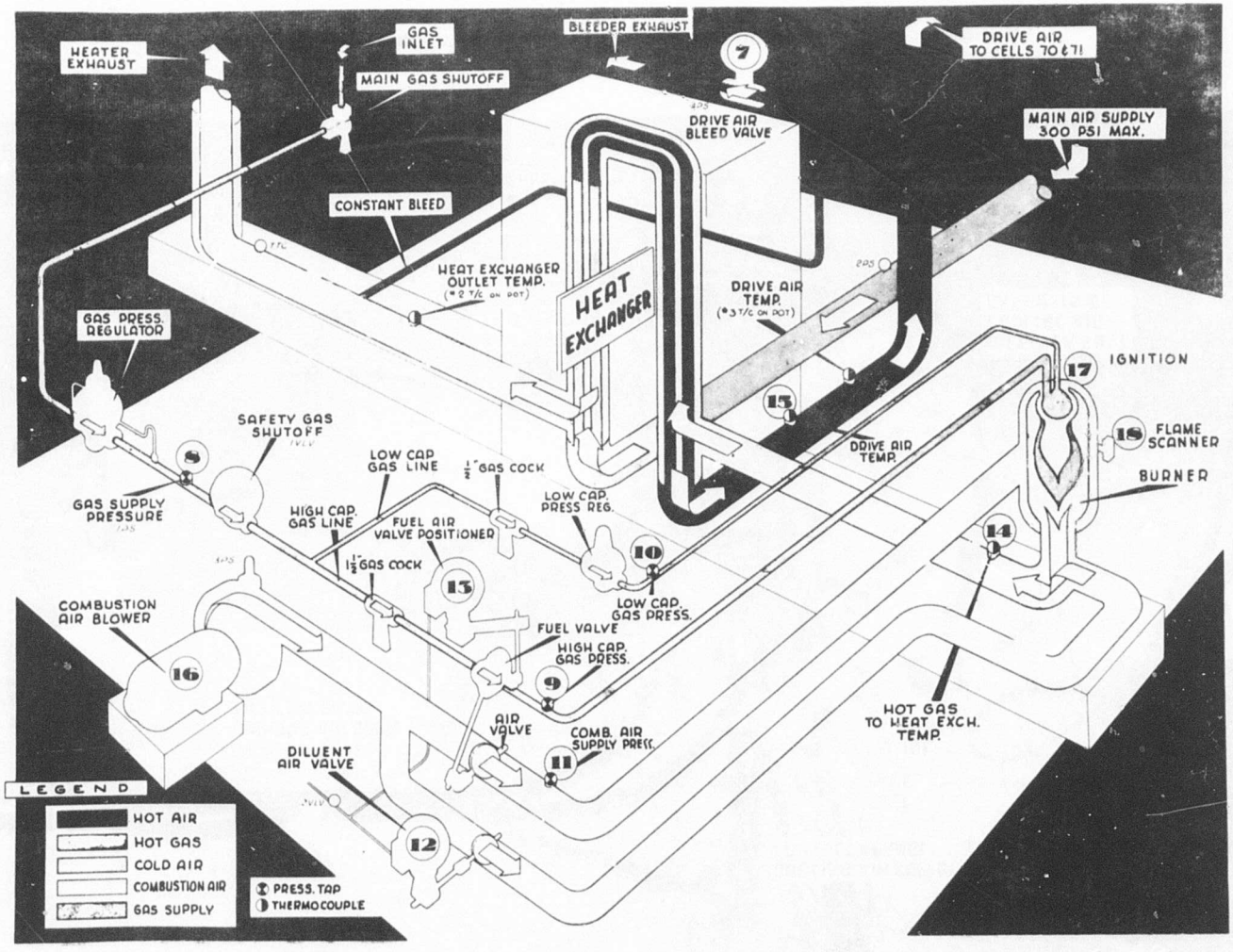


Figure 32. Air Heater Schematic for Cells 70 and 71.

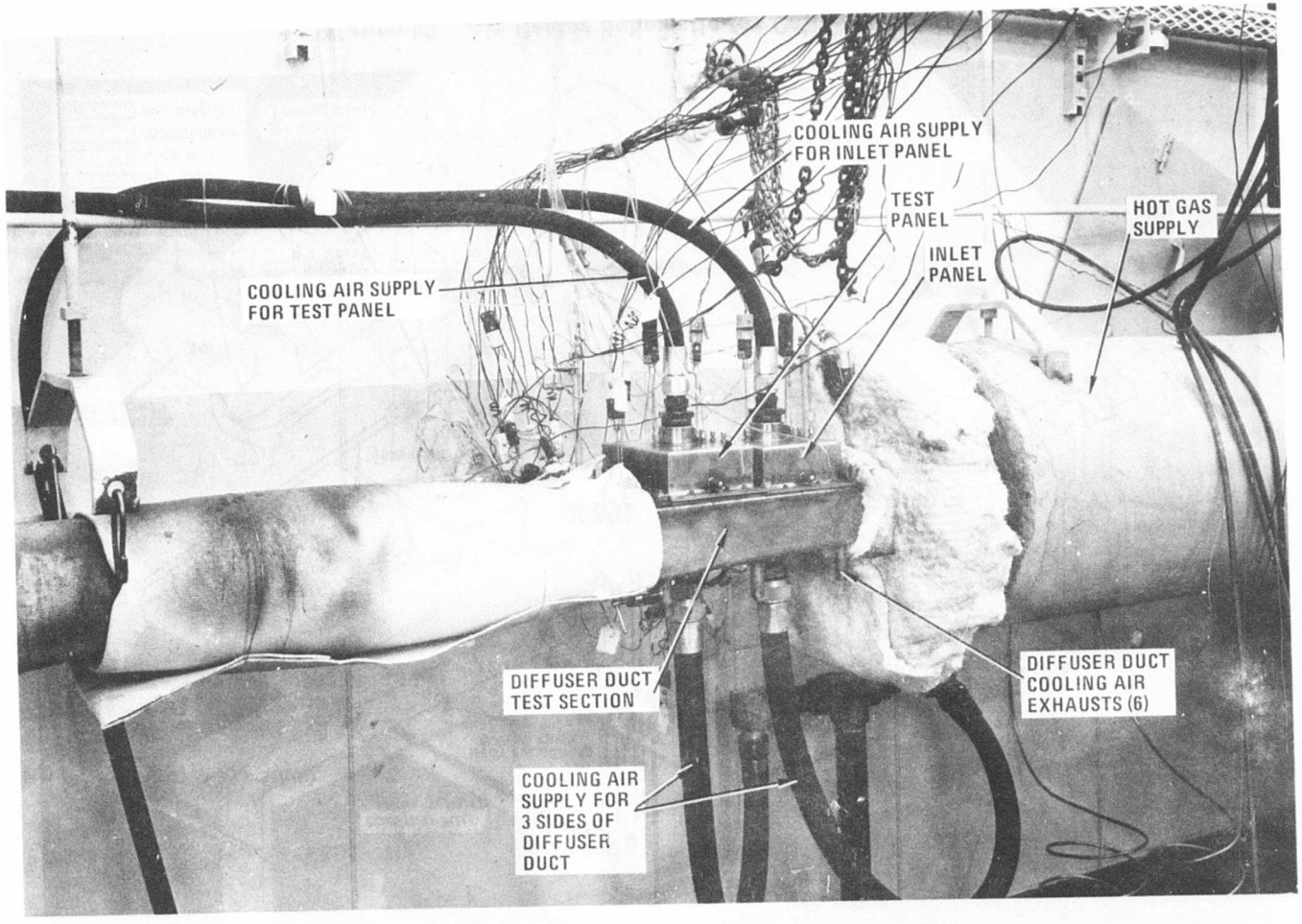


Figure 33. Instrumented Test Rig With Inlet and Test Panels Installed.

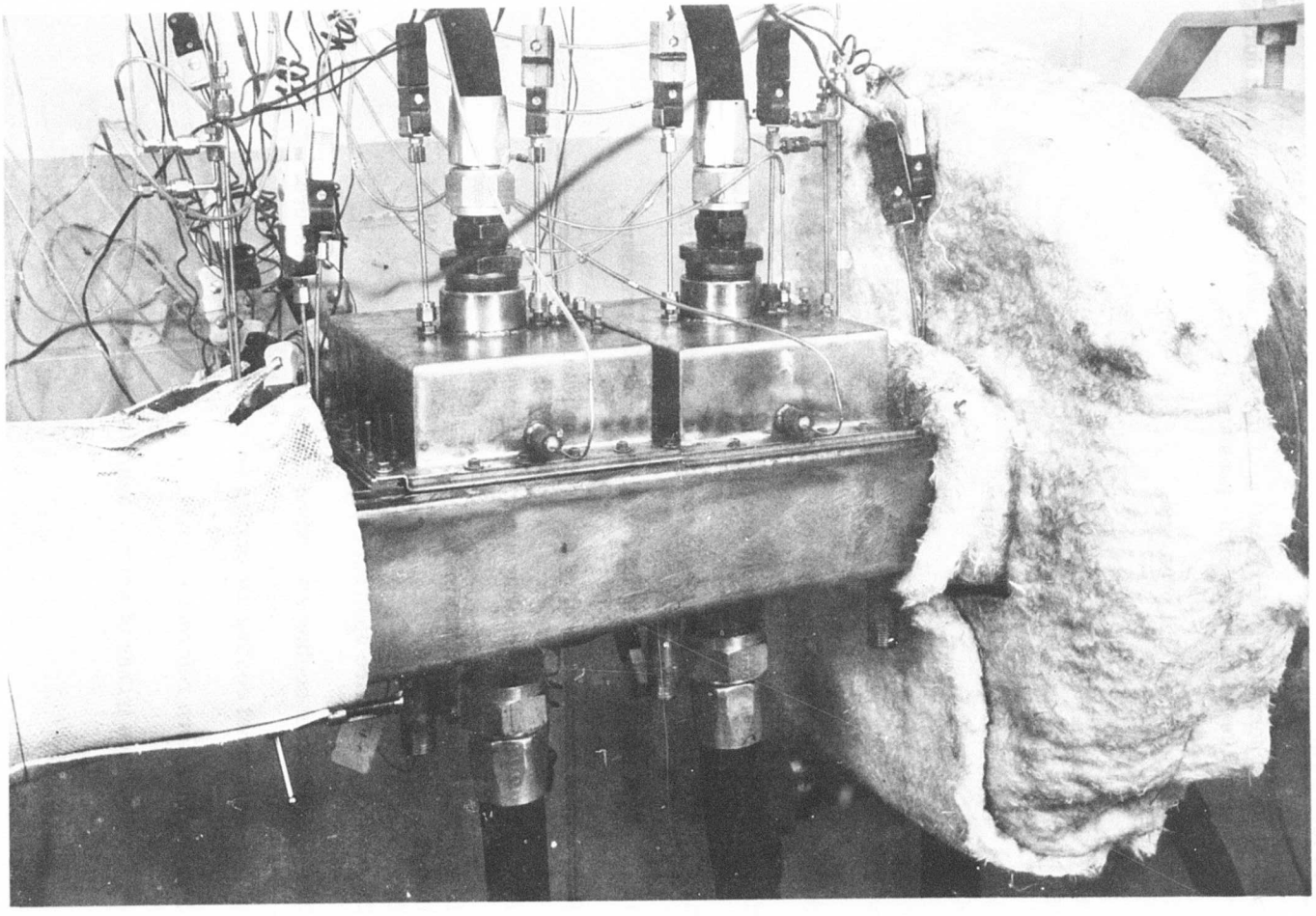

Figure 34. Instrumented Test Rig With Inlet and Test Panels Installed - Close-up.

INSTRUMENTATION

Figure 35 shows schematically the location of pressure instrumentation used during this test to record the following absolute pressures:

P1 Hot gas inlet total pressure.
P2

P3 Hot gas exit total pressure.
P4

P5 Hot gas inlet static pressure.
P6

P7 Hot gas exit static pressure.
P8

P9 Inlet panel impingement cooling air static pressure.

P10 Test panel impingement cooling air static pressure.

P11 Inlet panel metering hole cooling air static pressure.

P12 Test panel metering hole cooling air static pressure.

P13 Inlet panel slot cooling air static pressure.

P14 Test panel slot cooling air static pressure.

P15 Diffuser wall static pressures.
through
P20

P21 Hot gas orifice upstream static pressure.

P22 Inlet panel cooling air orifice upstream static pressure.

P23 Test panel cooling air orifice upstream static pressure.

P26 Vidar zero reference.

P48 Fourteen inches of water - deadweight tester.

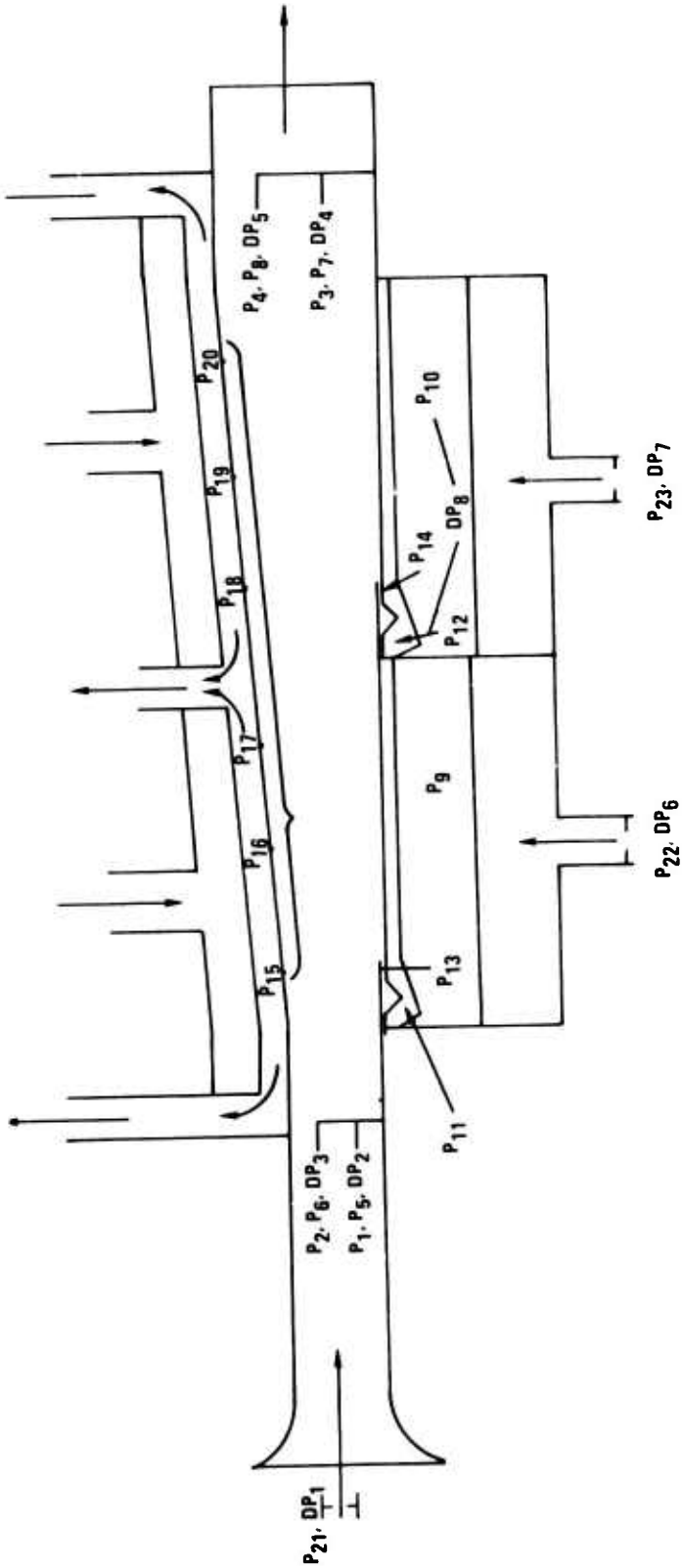


Figure 35. Pressure Instrumentation Schematic.

The following differential pressures were also measured:

DP1 Hot gas orifice differential pressure.

DP2 Hot gas inlet velocity head (P1 - P5) and (P2 - P6).
DP3

DP4 Hot gas exit velocity head (P3 - P7) and (P4 - P8).
DP5

DP6 Inlet panel cooling air orifice differential pressure.

DP7 Test panel cooling air orifice differential pressure.

DP8 Test panel impingement plate differential pressure (P10 - P12).

NOTE: P26 and P48 are used for calibration of the Vidar System.

Figure 36 shows schematically the location of instrumentation used during this test to record the following temperatures:

T1 Test panel slot lip metal temperature.
T2

T3 Test panel metal temperatures.
through
T10

T11 Diffuser wall metal temperatures.
through
T16

T17 Inlet panel impingement cooling air temperature.
T18

T19 Test panel impingement cooling air temperature.
T20

T21 Hot gas inlet temperature.
T22

T23 Hot gas exit temperature.
T24

T25 Test panel metering hole inlet air temperature.
T35

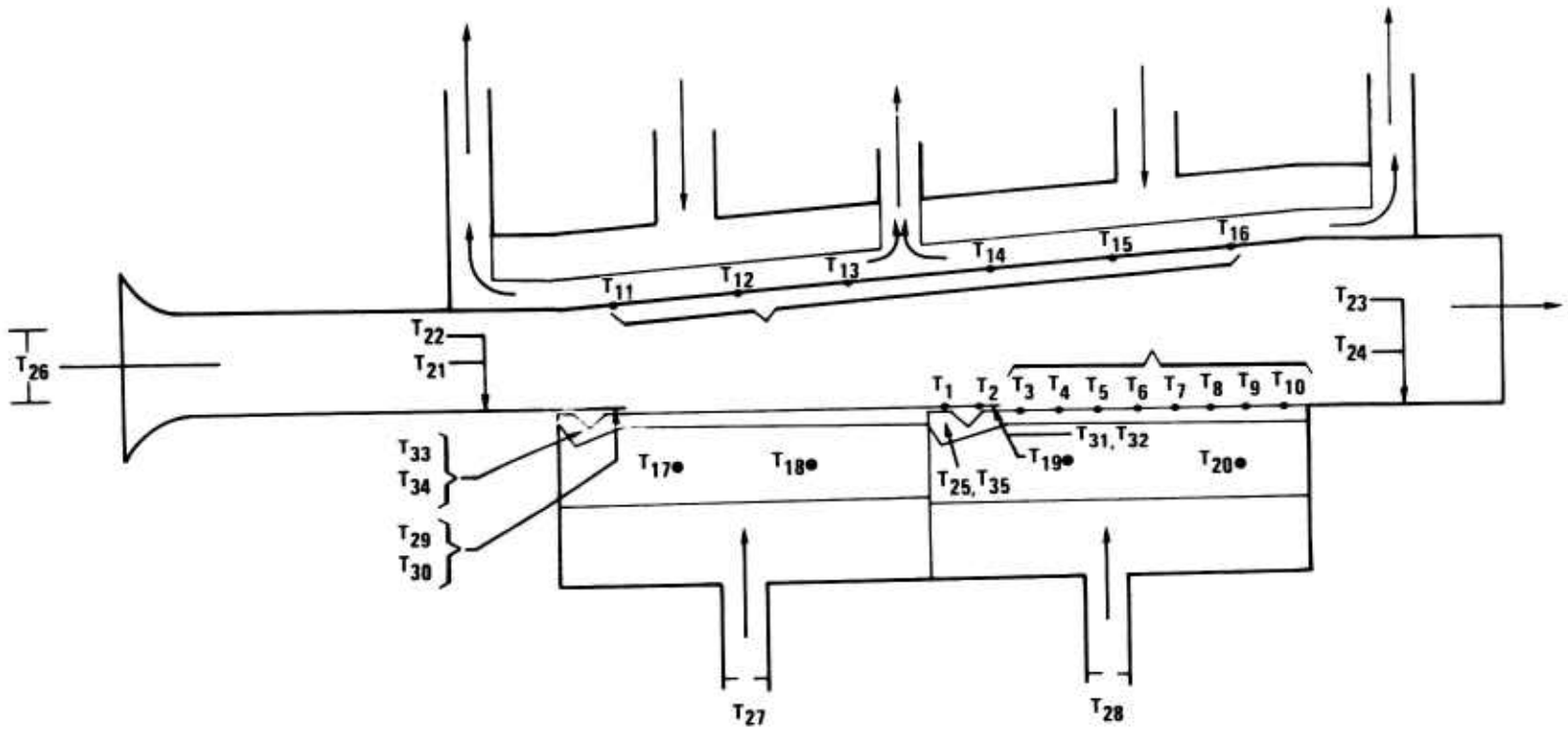


**Figure 36. Temperature Instrumentation Schematic.**

T26 Hot gas orifice upstream temperature.

T27 Inlet panel cooling air orifice upstream temperature.

T28 Test panel cooling air orifice upstream temperature.

T29 Inlet panel slot exit air temperature.
T30

T31 Test panel slot exit air temperature.
T32

T33 Inlet panel metering hole inlet air temperature.
T34

All instrumentation was calibrated against known standards with an allowable instrumentation error of:

Pressure $\pm$ 2%

Temperature $\pm$ 5°F

Flow Rates $\pm$ 2%

$\Delta P \pm 1\%$

Figure 37 shows the control room for the test cell. In the control room can be seen the teletype console of the time-sharing computer (through which temperatures were read out), the digital pressure readout (Vidar System), the water and mercury manometers (on which the differential pressures were measured), the console for controlling the primary hot gas flow and the diffuser and panel cooling flows, and the gas heater control system.

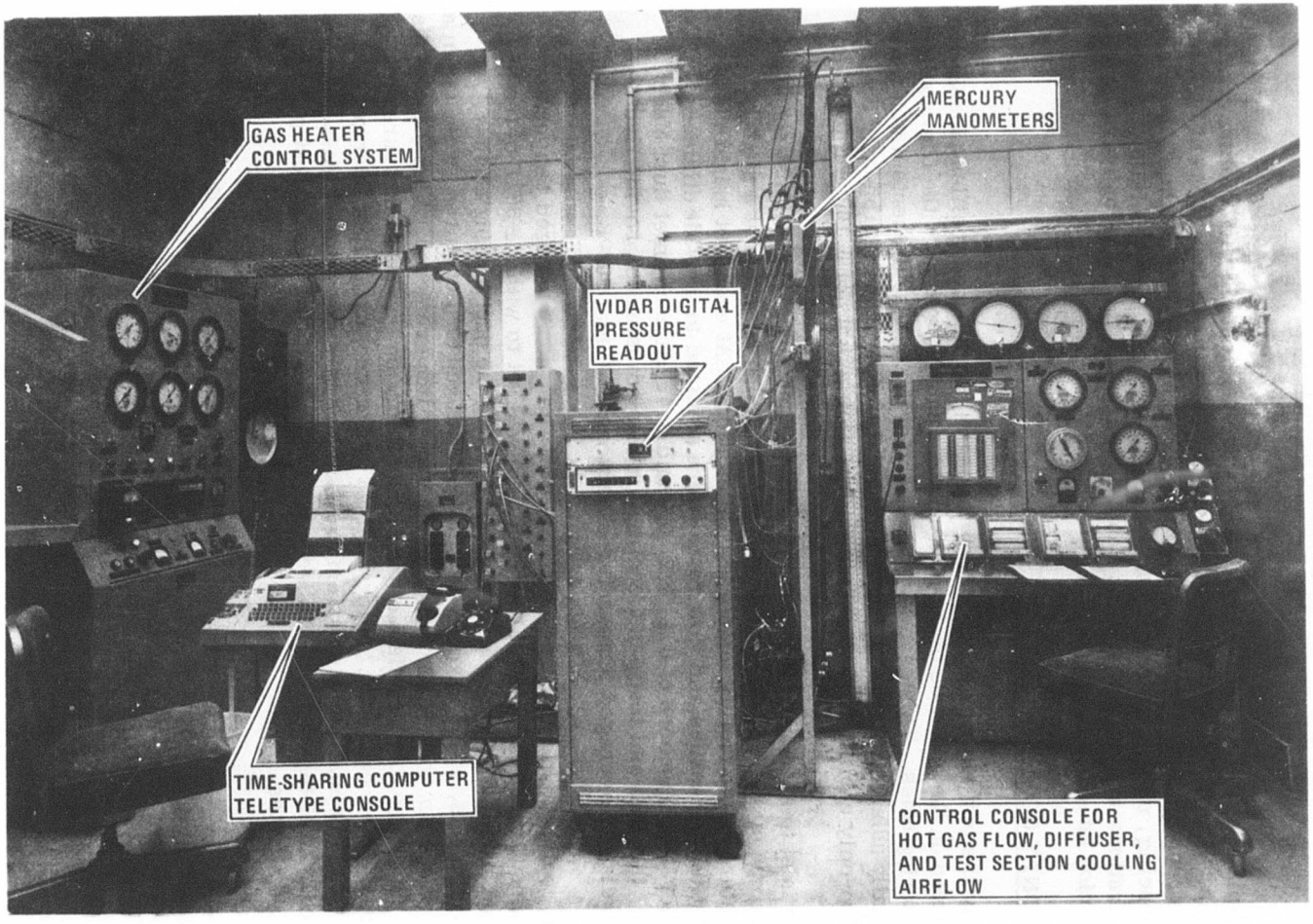


Figure 37. Control Room .

## TEST PROCEDURE

The impingement-film heat transfer tests were conducted on 17 cooling configurations. Four of the configurations were tested without impingement baffles and the remaining 13 with various combinations of impingement hole diameters, hole spacing, and impingement baffle to test panel distance. Details of these configurations are summarized in Table 1. Also see the test configuration description tables in the appendix.

### FILM-ONLY COOLING TESTS

Initially the test rig was assembled without the impingement baffles. Insulation was placed on the cool side of the inlet and test panels, except at the film cooling air metering holes. This gave test panel temperature measurements which were essentially adiabatic for use in determining the effectiveness of film-only cooling. The film-only cooling tests were run at film slot heights of 0.100 and 0.145 in.

Hot gas inlet total temperature was set nominally at 1100°F for all test conditions except some of the 0.1 Mach number conditions,which were run at a slightly lower temperature due to facility temperature limitations. At each slot height the hot gas inlet total pressure and flow rates were adjusted to provide diffuser inlet duct Mach numbers of 0.1, 0.2, 0.3 and 0.4. At each inlet duct Mach number, the inlet and test panel cooling air was adjusted to provide five test panel radiation-averaged temperatures between 200° and 500°F.

At each cooling airflow setting, the duct wall radiation-averaged temperature (determined from six duct wall temperatures) was set to within ± 50°F of the test panel radiation-averaged temperature by adjusting the duct cooling airflow. Additional points, at the same five radiation-averaged temperatures, were taken at 0.2 Mach number with the duct cooling air supply lines removed. This allowed the duct to heat up so that the effect of duct temperature on test panel measured temperature could be evaluated. After each hot gas or cooling airflow change, sufficient time was taken for the system to reach steady-state values before data was recorded. After the system stabilized, the settling-out time for the test panel was about five minutes.

To determine the effect of the upstream (inlet panel) cooling air on the downstream (test) panel, this sequence of testing was repeated at the end of the test program with cooling air to the inlet panel shut off. A total of 100 test points were run during this portion of the test program.

TABLE I. COOLING CONFIGURATIONS TESTED

| Configuration No. | Film Slot Height (in.) | Impingement Hole Diameter (in.) | $X_n/D$ | $Z_n/D$ |
|---|---|---|---|---|
| 1 | 0.100 | * | - | - |
| 2 | 0.145 | * | - | - |
| 3 | 0.100 | 0.070 | 4 | 4 |
| 4 | 0.100 | 0.070 | 8 | 4 |
| 5 | 0.100 | 0.070 | 12 | 4 |
| 6 | 0.100 | 0.052 | 4 | 4 |
| 7 | 0.100 | 0.052 | 8 | 4 |
| 8 | 0.100 | 0.052 | 12 | 4 |
| 9 | 0.100 | 0.052 | 8 | 6 |
| 10 | 0.100 | 0.052 | 8 | 2 |
| 11 | 0.100 | 0.031 | 4 | 4 |
| 12 | 0.100 | 0.031 | 8 | 4 |
| 13 | 0.100 | 0.031 | 12 | 4 |
| 14 | 0.100 | 0.070 | 8 | 2 |
| 15 | 0.100 | 0.070 | 8 | 6 |
| 16 | 0.100** | * | - | - |
| 17 | 0.145** | * | - | - |

*No impingement baffle. Cooling air flowing from both inlet and test panel (i.e., overlapped film cooling on test panel).
**Inlet panel flow shut off to determine single film effect.

IMPINGEMENT-FILM TESTS

Nine impingement arrays were tested to investigate the effect of impingement hole sizes and spacings. The nine arrays were made up from three basic baffles having holes 0.031, 0.052, and 0.070 in. in diameter respectively. The basic baffles had the holes arranged in square arrays spaced 4 diameters on centers. Six additional square arrays with spacings of 8 and 12 diameters were made from the basic baffles by selectively covering the superfluous holes. An impingement distance-to-diameter ratio of 4 was maintained for each of the nine tests.

The impingement-film cooling tests were conducted in the same way as the film-only cooling tests. Again, inlet gas total temperature was held at the same 1100°F for Mach numbers 0.2, 0.3 and 0.4 and somewhat reduced temperatures at 0.1 Mach number because of facility limitations. The 0.2 Mach number point was run both with and without diffuser duct cooling. At each Mach number, five radiation-averaged temperatures, as close as possible to 200°F,

250°F, 300°F, 350°F and 400°F were tested. The difference in temperature range between the film-only and impingement-film tests resulted from an attempt to keep cooling flows in the same general magnitude.

The tests show (Test Results section) that the large 0.070-in.-diameter impingement holes provided the greatest cooling effectiveness. They were superior to both the 0.031- and 0.052-in. holes at an $X_n/D$ of 4 and equal to or better than the smaller holes at $X_n/D$ of 8 and 12. The test also showed that the $X_n/D$ of 12 was better than either 4 or 8 when compared on the basis of cooling effectiveness vs flow per unit area. However, the pressure drop characteristic of the cooling system with $X_n/D$ of 12 restricted the flow and did not allow the desired radiation-averaged panel temperature, within the limit of 100 inches of water pressure drop across the impingement panel. Therefore, for the impingement distance tests, the arrays chosen were those with hole diameters of 0.052 and 0.070 in. having $Z_n/D$ of 8.

## IMPINGEMENT DISTANCE TESTS

At each impingement hole diameter, the selected arrays were tested at impingement distances $Z_n/D$ of 2 and 6. These four configurations were tested at the same inlet gas total temperatures, the same inlet Mach numbers, and the same radiation-averaged temperatures as the previous sequences of impingement-film testing.

## TEST RESULTS

### SINGLE-FILM COOLING

Figures 38 through 47 show the film cooling effectiveness distribution along the test panel with no cooling flow from the upstream slot. Figures 38 through 42 show the cooling effectivness obtained with a slot height of 0.100 in., while Figures 43 through 47 are for a slot height of 0.145 in. Each figure presents the results at a given value of duct inlet Mach number ($M_g$). The cooling effectiveness distribution along the length of the test panel is plotted as a function of X/MS with results for various coolant airflow rates presented on each figure. Each coolant flow rate corresponds to a different value of slot exit velocity ratio, which is the ratio of the coolant air slot exit velocity to the gas velocity at the slot exit ($V_c/V_g$). Also shown in each figure is a curve representing Huffmeier's[16] results, which were run for a similar slot geometry.

The data are presented in terms of cooling effectiveness, which is relatively insensitive to hot gas and cooling air temperature, rather than wall temperature because inlet gas temperature and cooling air temperature could not be held exactly constant from one test point to the next.

However, in all the tests at $M_g = 0.4$, 0.3, and 0.2, hot gas inlet temperature was $1100^oF \pm 25^o$. At $M_g = 0.1$, it was $1050^oF \pm 25^o$. Cooling air temperature was between $80^o$ and $130^oF$ throughout the test.

In general, the results for both slot heights fall in well-defined bands except at a Mach number of 0.10. Figure 42 shows that the cooling effectiveness from test runs 406 and 407 was appreciably lower than that obtained from other runs. The slot exit velocity ratios for runs 406 and 407 were 1.437 and 1.711, respectively. Figure 47 shows that the cooling effectiveness from test run 432, with a slot exit velocity ratio of 1.220, also was appreciably lower than that obtained at the other test points. It is significant that during these tests when the slot exit velocity ratio exceeded a value of one, the film effectiveness decreased rapidly. The results of Pai and Whitelaw shown in Figure 18 also indicated the optimum velocity ratio to be about one. Shown in Figures 40, 41, 45, and 46 are results of film cooling effectiveness with and without duct wall cooling at a Mach number of 0.2 for slot heights of 0.100 in. and 0.145 in. respectively. The figures show that there was no appreciable difference in the level of cooling effectiveness with and without the duct wall radiation.

Comparing the results for the two slot heights indicates that for values of X/MS less than 25, the cooling effectiveness for both slots is essentially the same. At values of X/MS greater than 25, the film from the 0.145-in. slot decays more rapidly than the film from the 0.100-in. slot.

A comparison of the data obtained with the 0.100-in. slot height and the curve representing Huffmeier's results shows good agreement except in the region near the slot exit. In this region, at all Mach numbers, the cooling effectiveness obtained was lower than the Huffmeier curve. The data obtained with the 0.145-in. slot height exhibits similar agreement with Huffmeier's curve up to an X/MS value of 25. Beyond 25, the cooling effectiveness was lower than the curve.

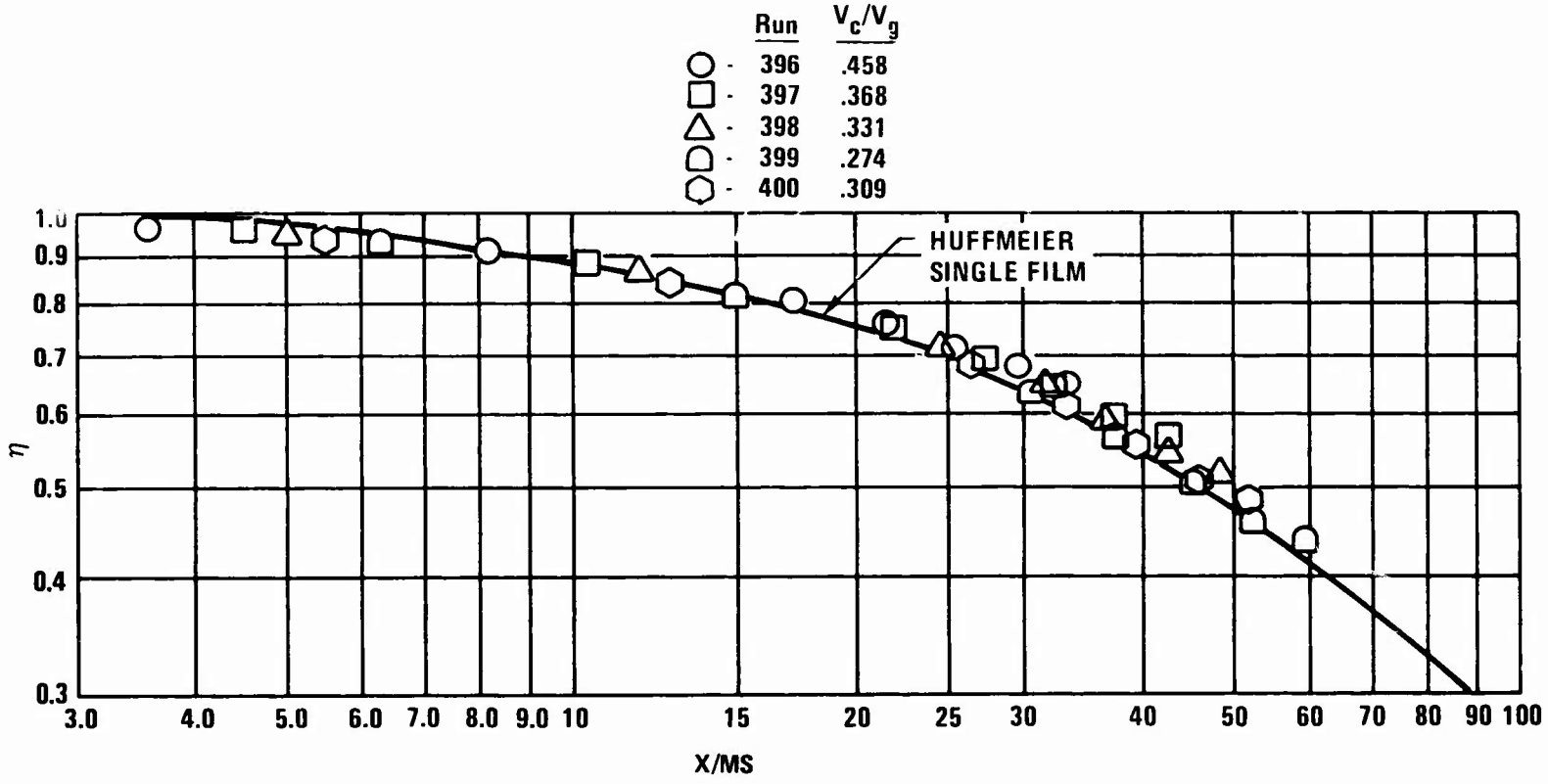


Figure 38. Film Effectiveness Distribution - Single Film at $M_g$ = .4, S = .100 In.

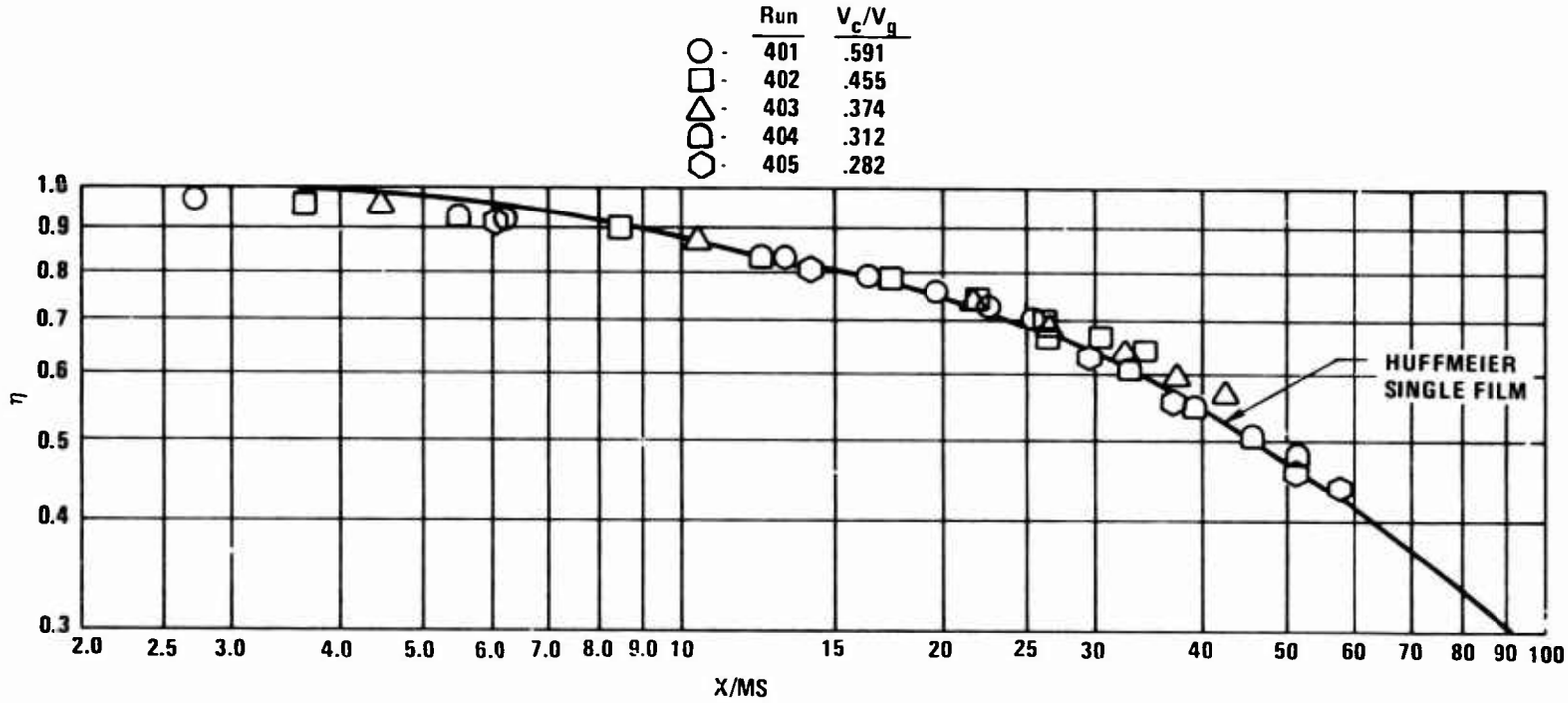


Figure 39. Film Effectiveness Distribution - Single Film at $M_g$ = .3, S = .100 In.

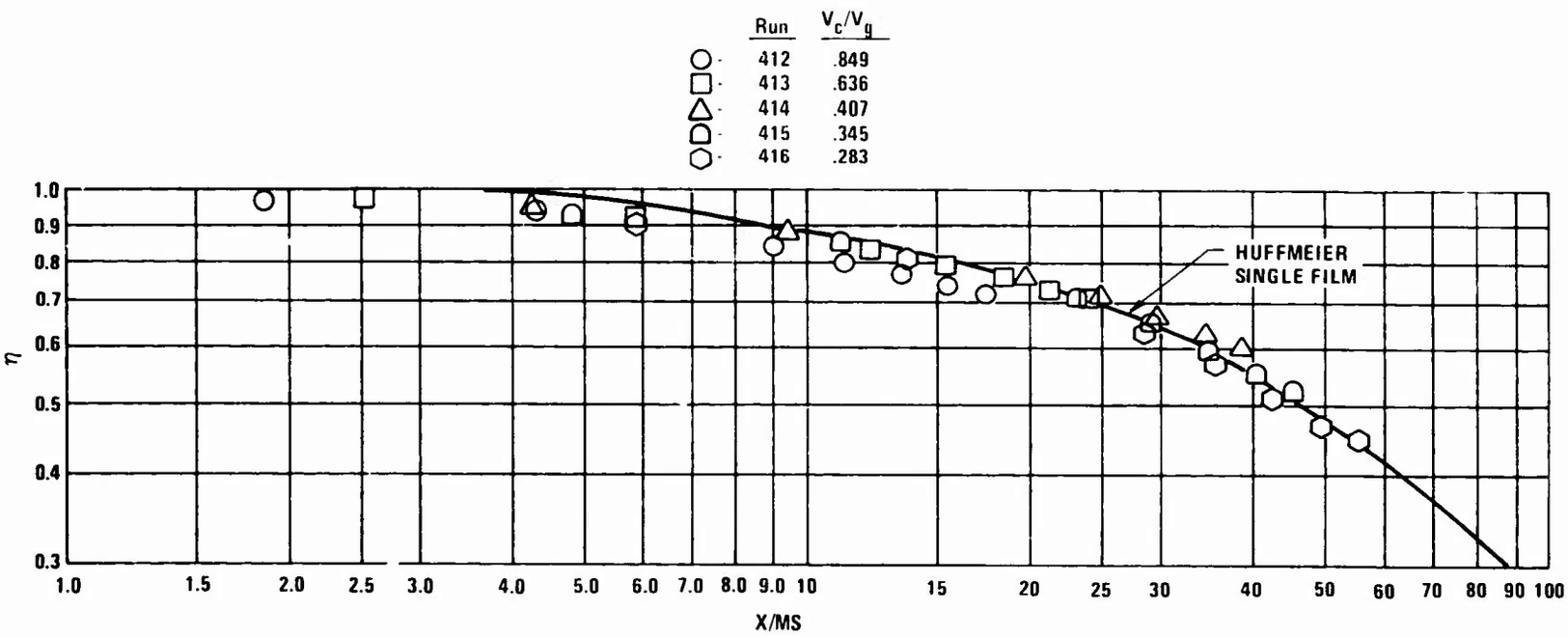


**Figure 40. Film Effectiveness Distribution - Single Film at $M_g$ = .2, S = .100 In.**

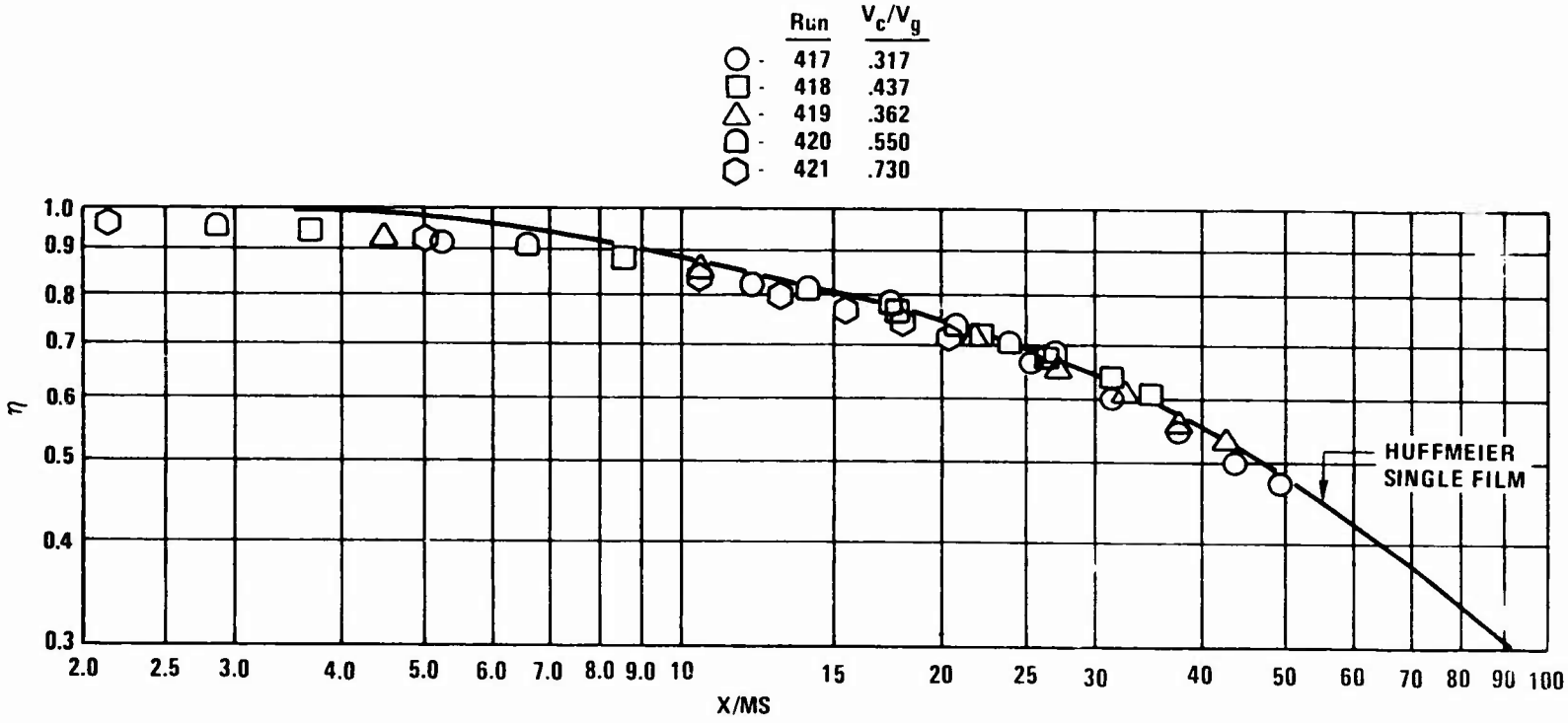


Figure 41. Film Effectiveness Distribution - Single Film Without Duct Cooling at $M_g$ = .2 , S = .100 In.

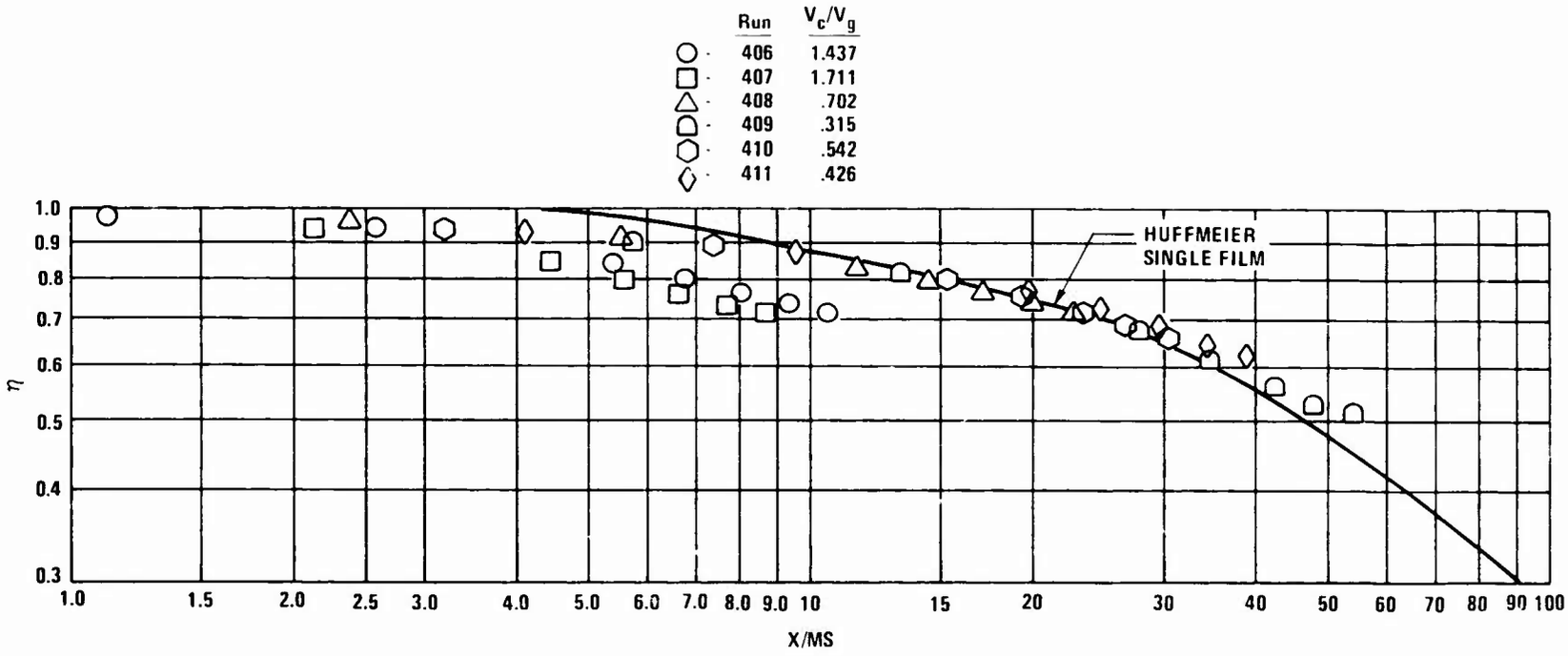


Figure 42. Film Effectiveness Distribution - Single Film at $M_g$ = .1, S = .100 in.

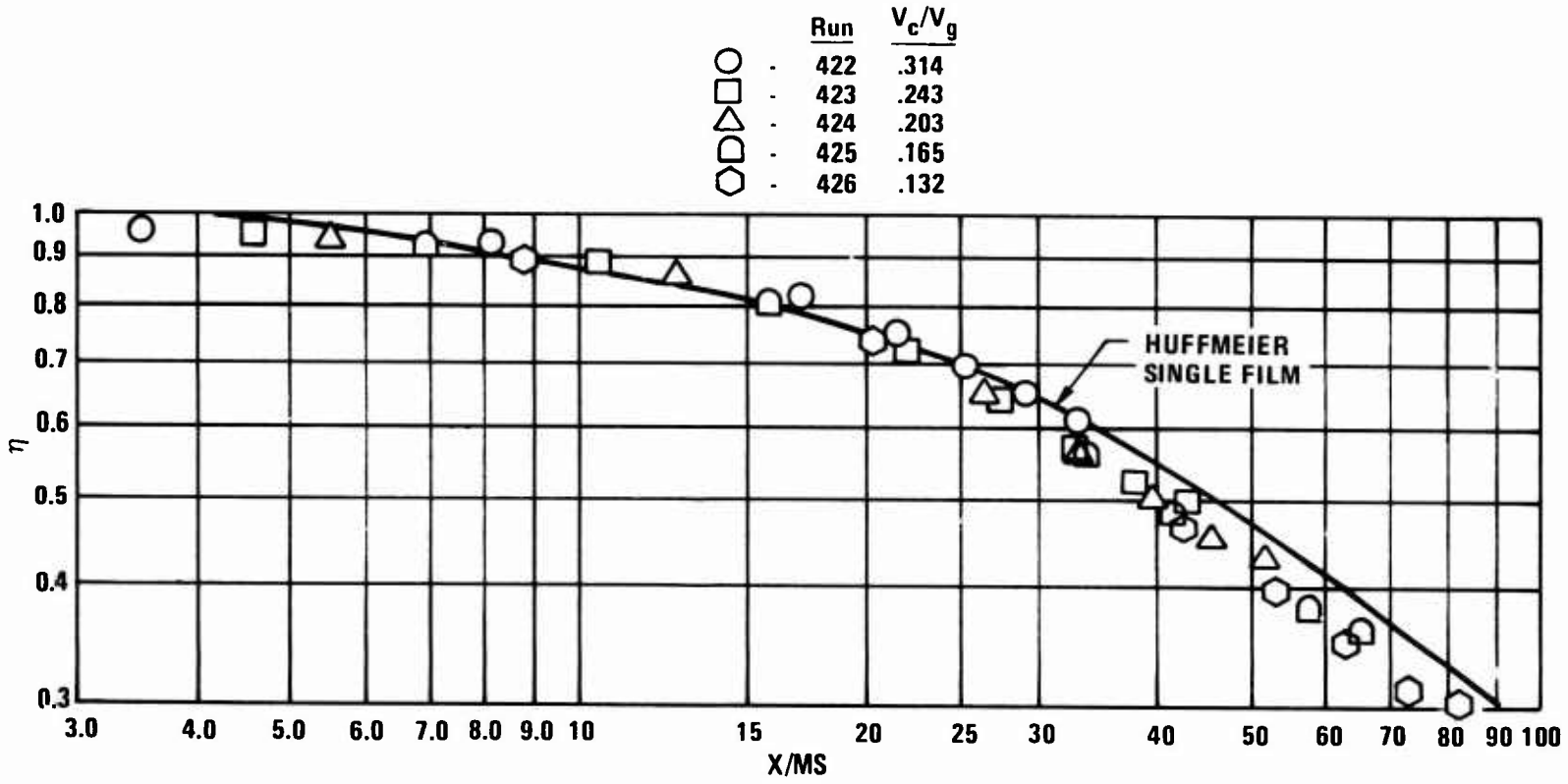


Figure 43. Film Effectiveness Distribution - Single Film at $M_g$ = .4, S = .145 In.

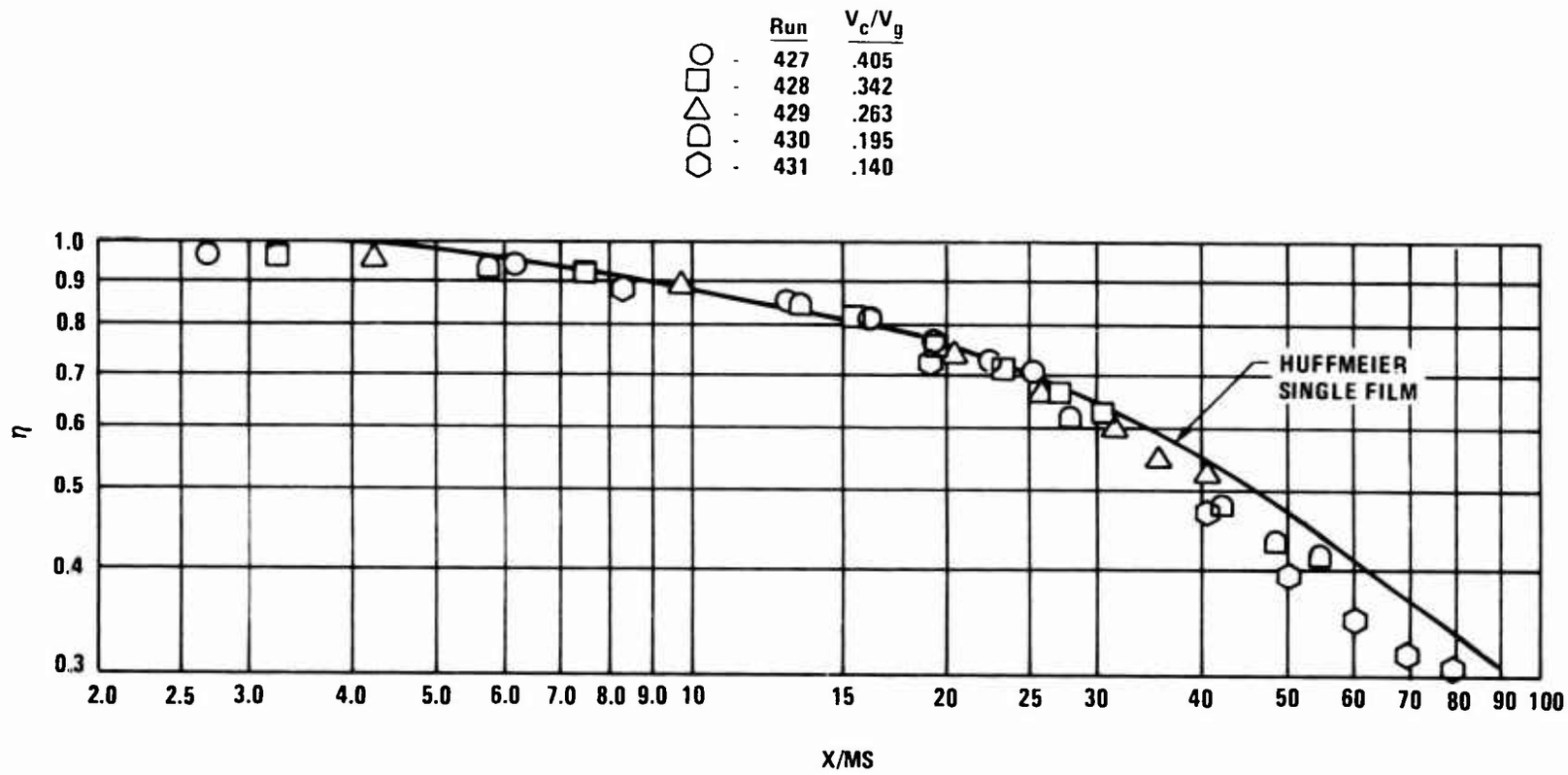


Figure 44. Film Effectiveness Distribution - Single Film at $M_g$ = .3, S = .145 In.

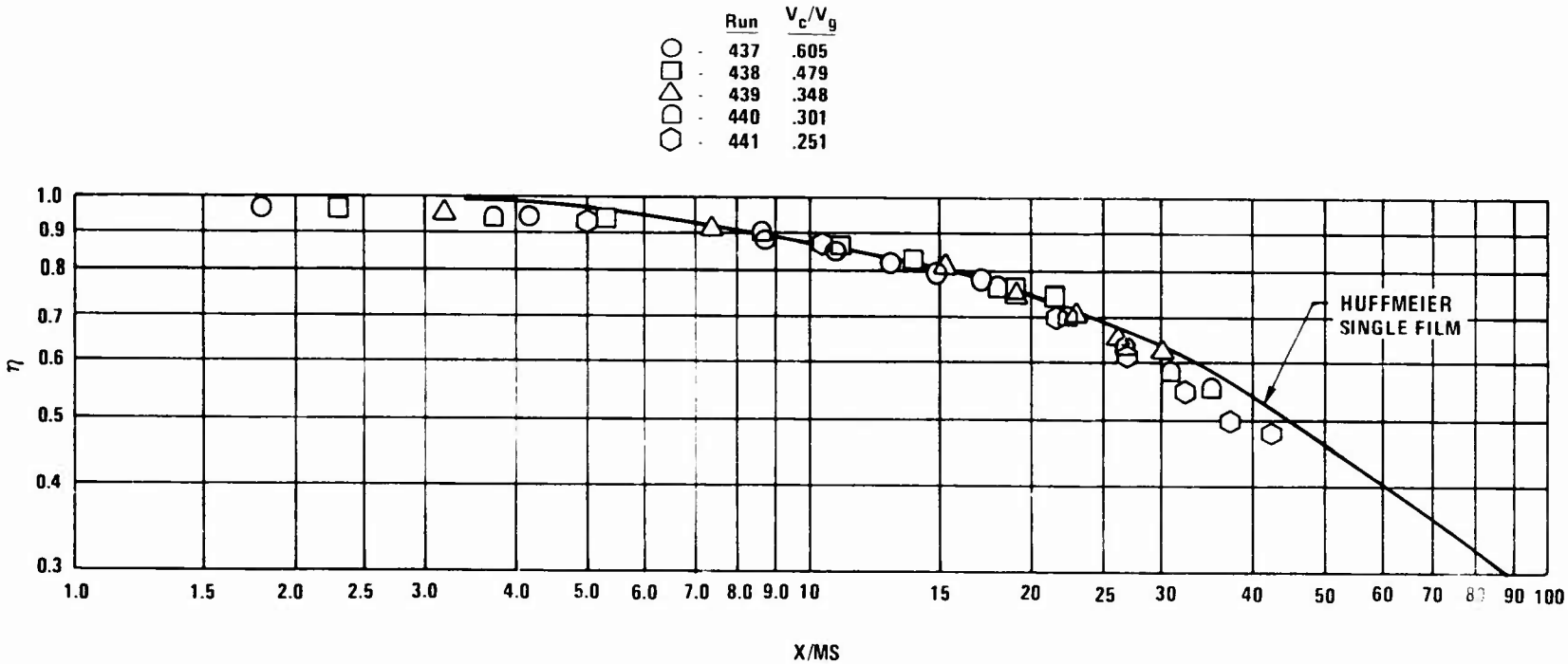


Figure 45. Film Effectiveness Distribution - Single Film at $M_g$ = .2, S = .145 In.

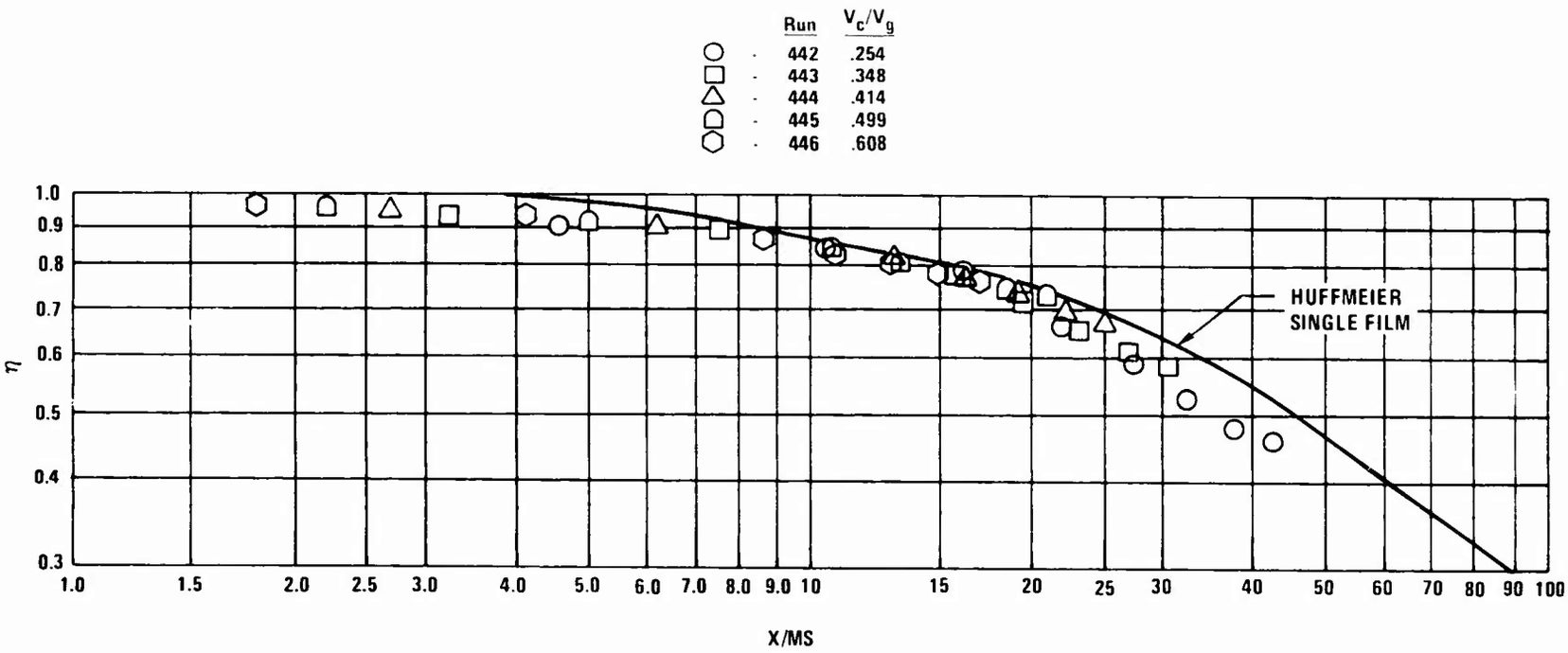


Figure 46. Film Effectiveness Distribution - Single Film Without Duct Cooling at $M_g$ = .2, S = .145 In.

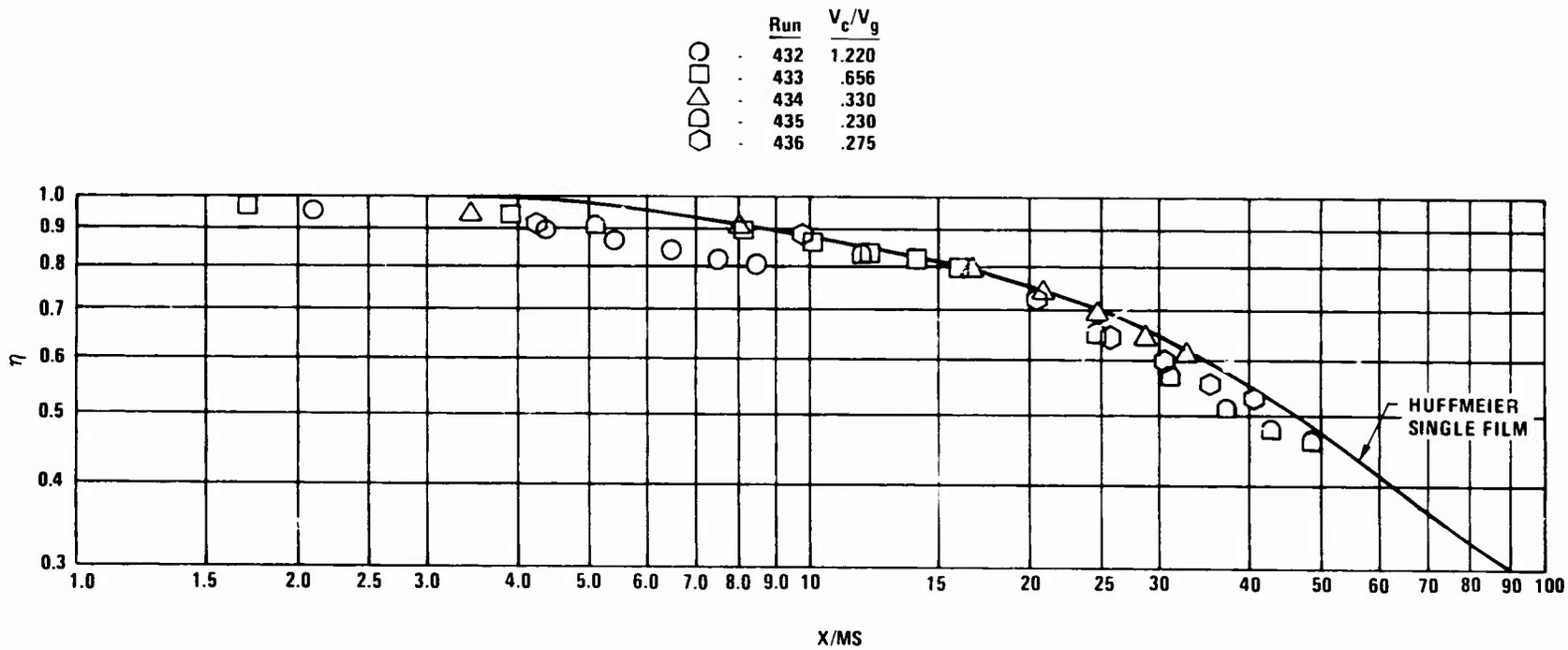


Figure 47. Film Effectiveness Distribution - Single Film at $M_g$ = .10, S = .145 In.

## OVERLAPPED-FILM COOLING

The results presented in Figures 48 through 57 show the effects of overlapped film cooling (i.e., both inlet and test panel film cooling flows over the test panel) on film cooling effectiveness.

On each of these figures, two curves are shown: the lower curve represents Huffmeier's results for single-film cooling effectiveness, while the upper curve represents the combined effectiveness of the upstream and downstream films. The combined cooling effectiveness was based on Huffmeier's single-film effectiveness. It is defined in the following manner:

$$\eta_C = \eta_1 + \eta_2 (1 - \eta_1) \tag{3}$$

where $\eta_1$ = upstream film effectiveness at a given location on the test panel

$\eta_2$ = test panel film effectiveness at the same location as $\eta_1$

$\eta_C$ = combined cooling effectiveness

At the higher hot gas Mach numbers, film effectiveness over the forward portion of the test panel for both 0.100- and 0.145-in. slot heights falls between the curves representing the single and overlapped films. Further downstream on the test panel, the results correlate well within Huffmeier's single-film cooling effectiveness curve. This indicates that for these flow conditions, the film from the inlet panel exists only over the upstream portion of the test panel. At the lower Mach numbers, for both slot heights, the cooling effectiveness falls between the single and overlapped film curves along the entire length of the test panel. This indicates that the inlet panel film exists over the entire length of the test panel.

## FILM COOLING PRESSURE DROP

During the film cooling tests, the pressure drop across metering holes and slot for the 0.100-in. and 0.145-in. slots was measured. The results are shown in Figures 58 and 59 for the single-film tests and in Figures 60 and 61 for the overlapped film. The flow in each of these four cases is practically proportional to the square root of the pressure drop. Therefore, a dimensional flow coefficient could be developed in the form

$$C_F = \frac{W_c}{A_m \sqrt{2 \rho_g (P_{10} - P_{14})}} \tag{4}$$

The flow coefficients corresponding to Figures 58, 59, 60, and 61 were calculated from Equation 4 at specific test points which were located centrally within the data scatter. They may also be calculated directly from the four figures by using $A_s = 41.26$ in.$^2$, which is the total surface area of one panel, $A_m = 0.713$ in.$^2$, and standard sea level air density $\rho_0$, which corresponds to test conditions. On this basis,

$$C_F = \frac{A_s}{A_m \sqrt{2g\rho_0} \times 12} \times \left[ \begin{array}{l} (W_c/A_s) \text{ read from the} \\ \text{figure at } \Delta P = 1 \text{ psi} \end{array} \right]$$

The single-film flow coefficients for S = 0.10 in. and 0.14 in. were 0.477 and 0.667 respectively. For the overlapped film, they were 0.612 and 0.773 respectively. The differences between flow coefficients are probably due to differences in slot height since the total metering hole area, 0.683 in.$^2$, was close to the slot area, 0.702 in.$^2$ for S = 0.100 in. and 1.017 in.$^2$ for S = 0.145 in. The slot lip, which determined the slot height, warped somewhat during the initial overlapped-film cooling tests because of thermal effects, and it had to be reset. This could be expected to affect the smaller slot height more as the results indicate. The single film pressure drop taken toward the end of the program is more consistent and more reliable since the slot height did not change after the initial test.

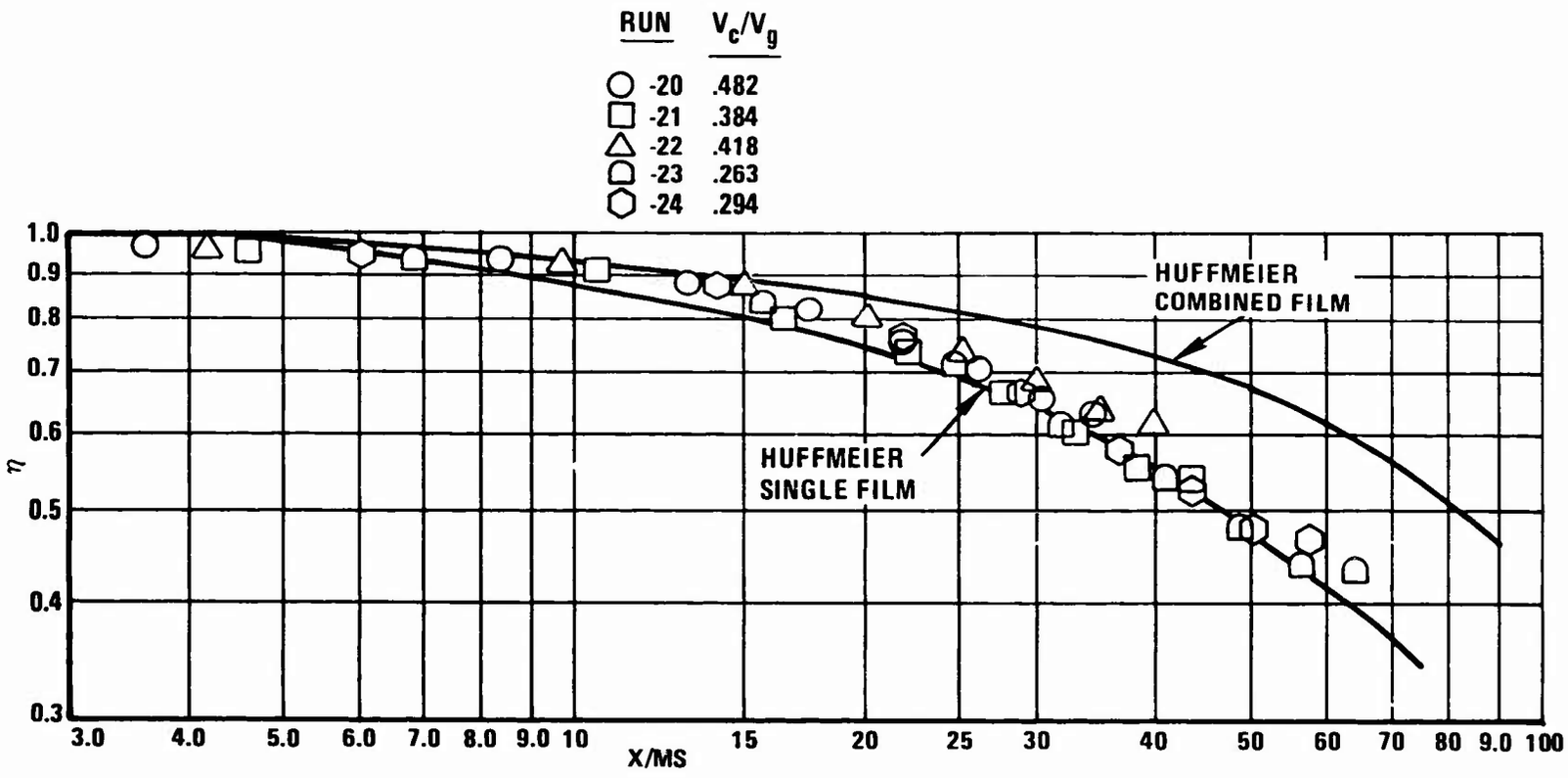


Figure 48. Film Effectiveness Distribution - Overlapped Film at $M_g$ = .40, S = .100 In.

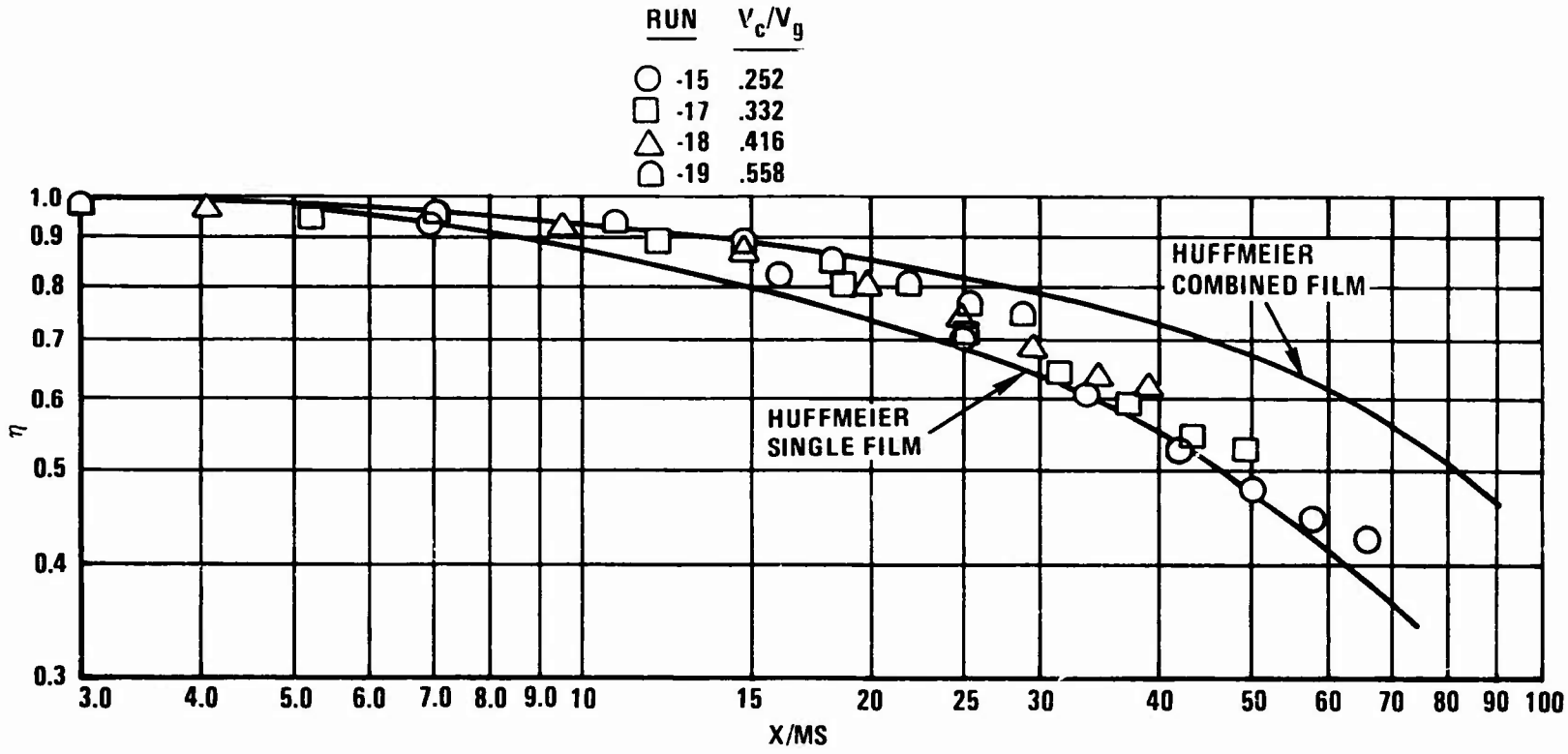


Figure 49. Film Effectiveness Distribution - Overlapped Film at $M_g$ = .30, S = .100 In.

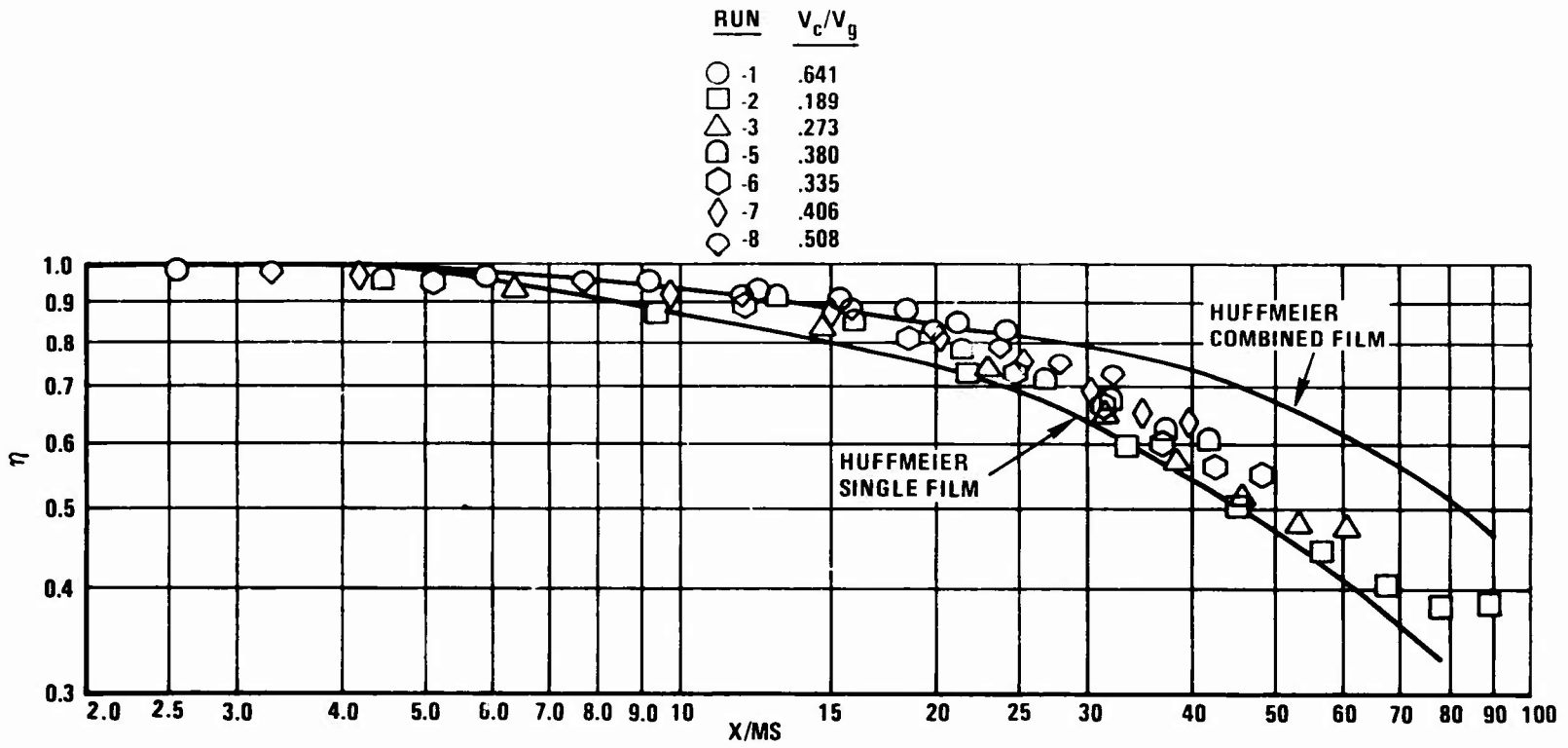


Figure 50. Film Effectiveness Distribution - Overlapped Film at $M_g$ = .20, S = .100 In.

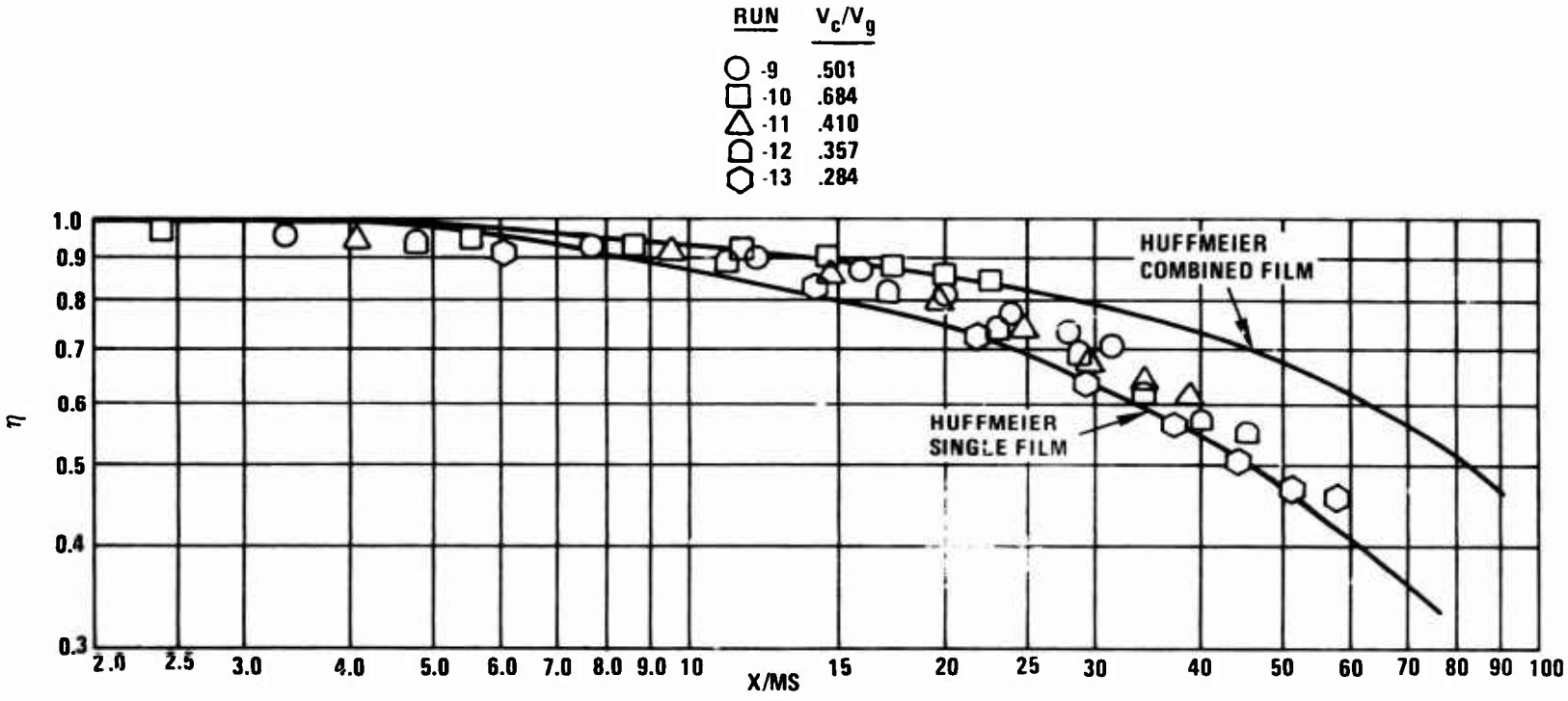


**Figure 51.** Film Effectiveness Distribution - Overlapped Film Without Duct Cooling at $M_g$ = .2, S = .100 In.

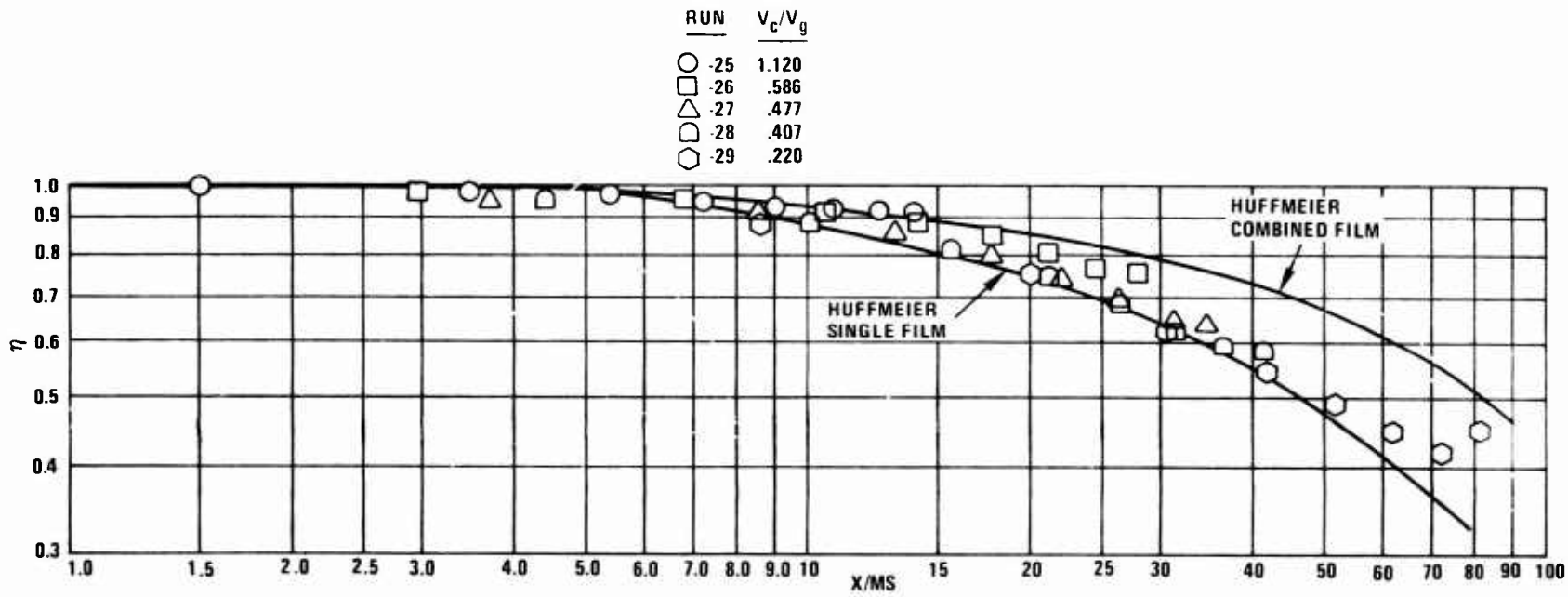


Figure 52. Film Effectiveness Distribution - Overlapped Film at $M_g$ = .10, S = .100 In.

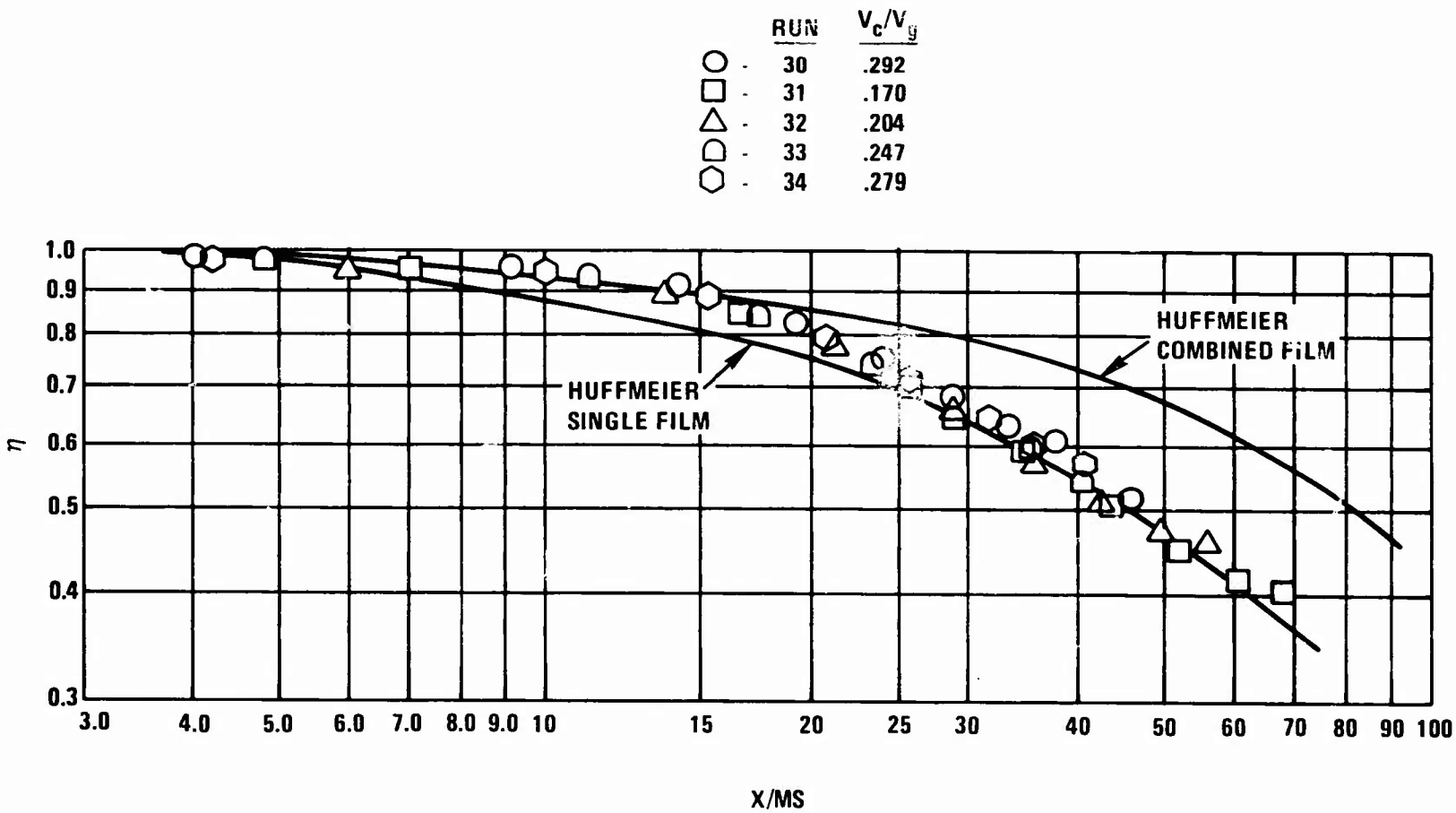


Figure 53. Film Effectiveness Distribution - Overlapped Film at $M_g$ = .40, S = .145 In.

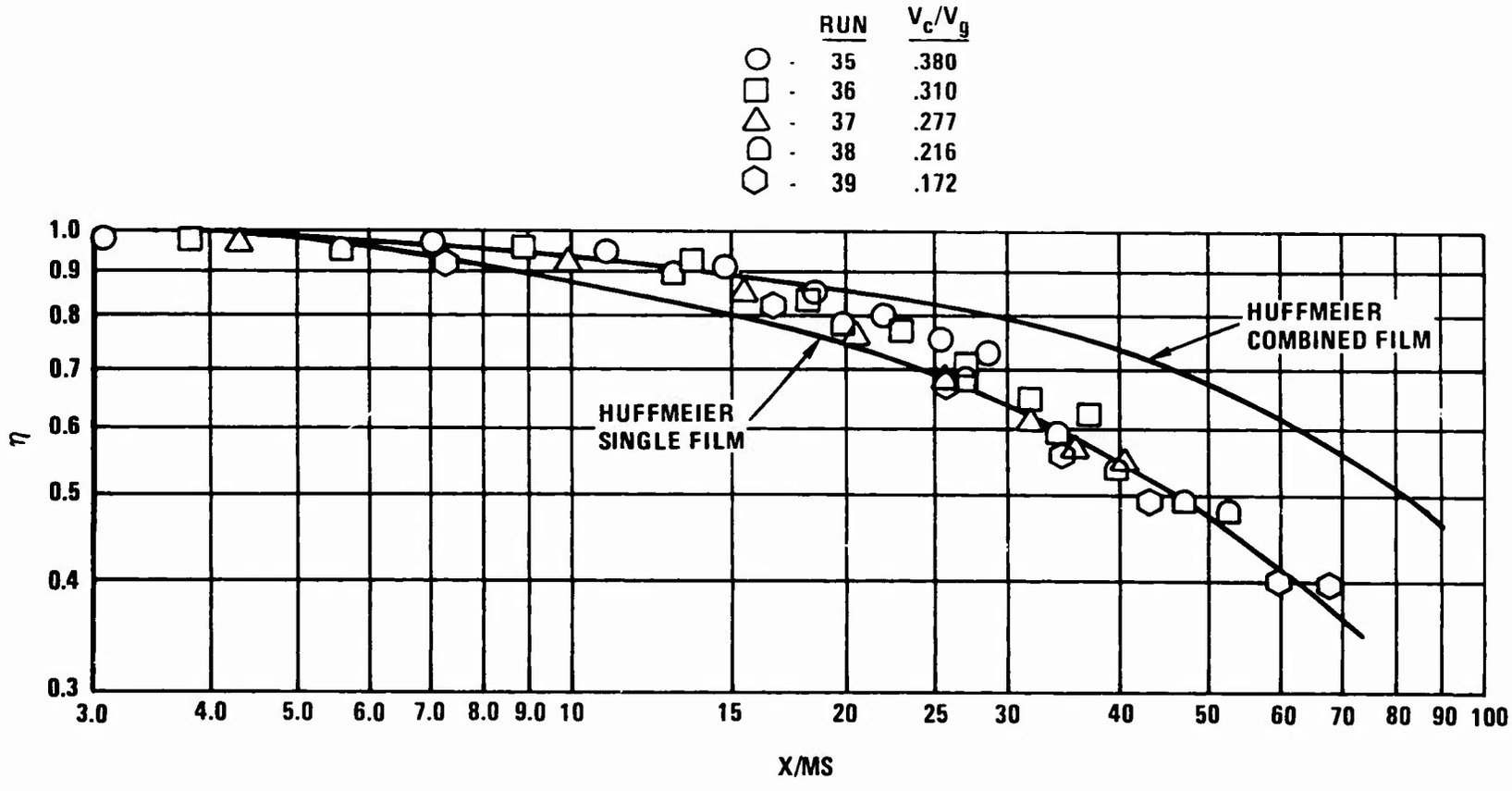


Figure 54. Film Effectiveness Distribution - Overlapped Film at $M_g$ = .30, S = .145 In.

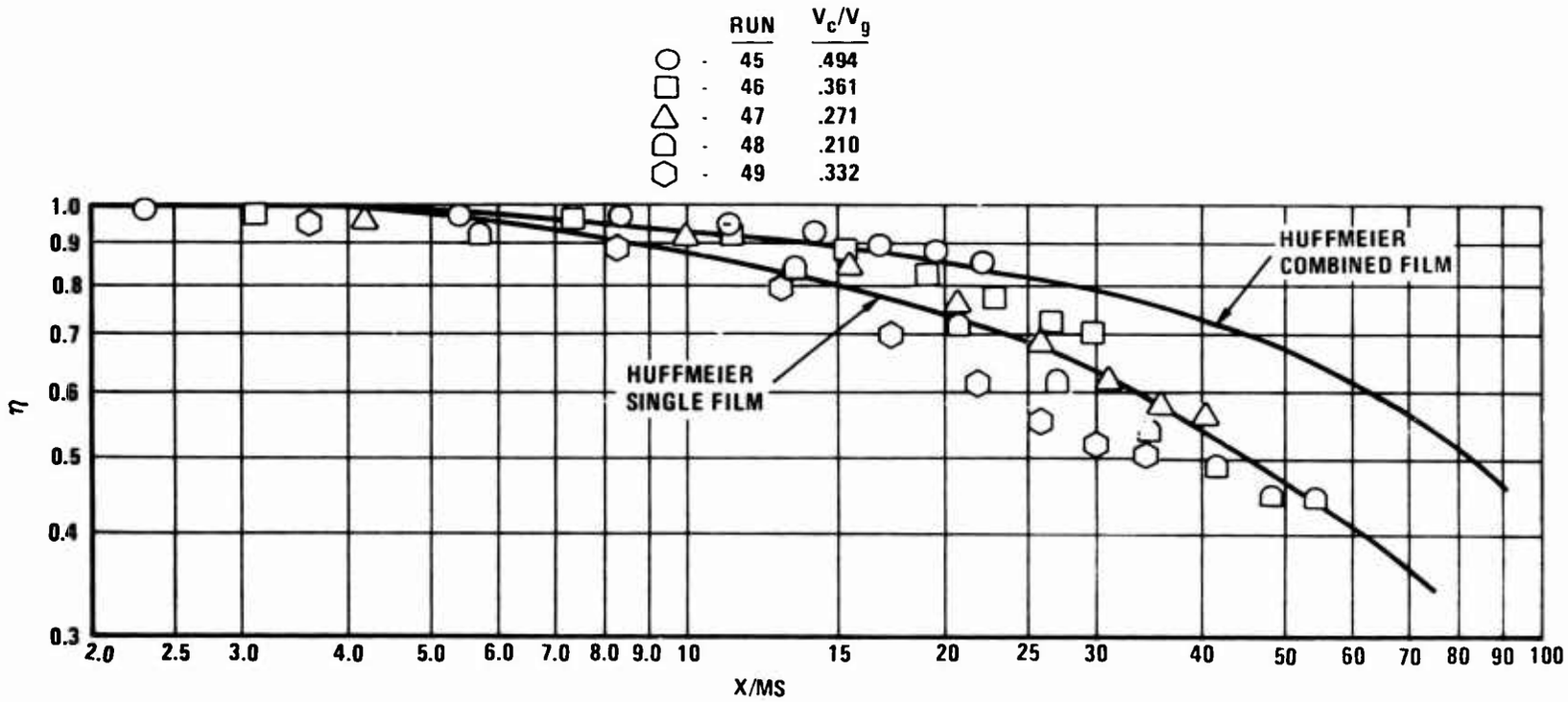


Figure 55. Film Effectiveness Distribution - Overlapped Film at $M_g$ = .20, S = .145 In.

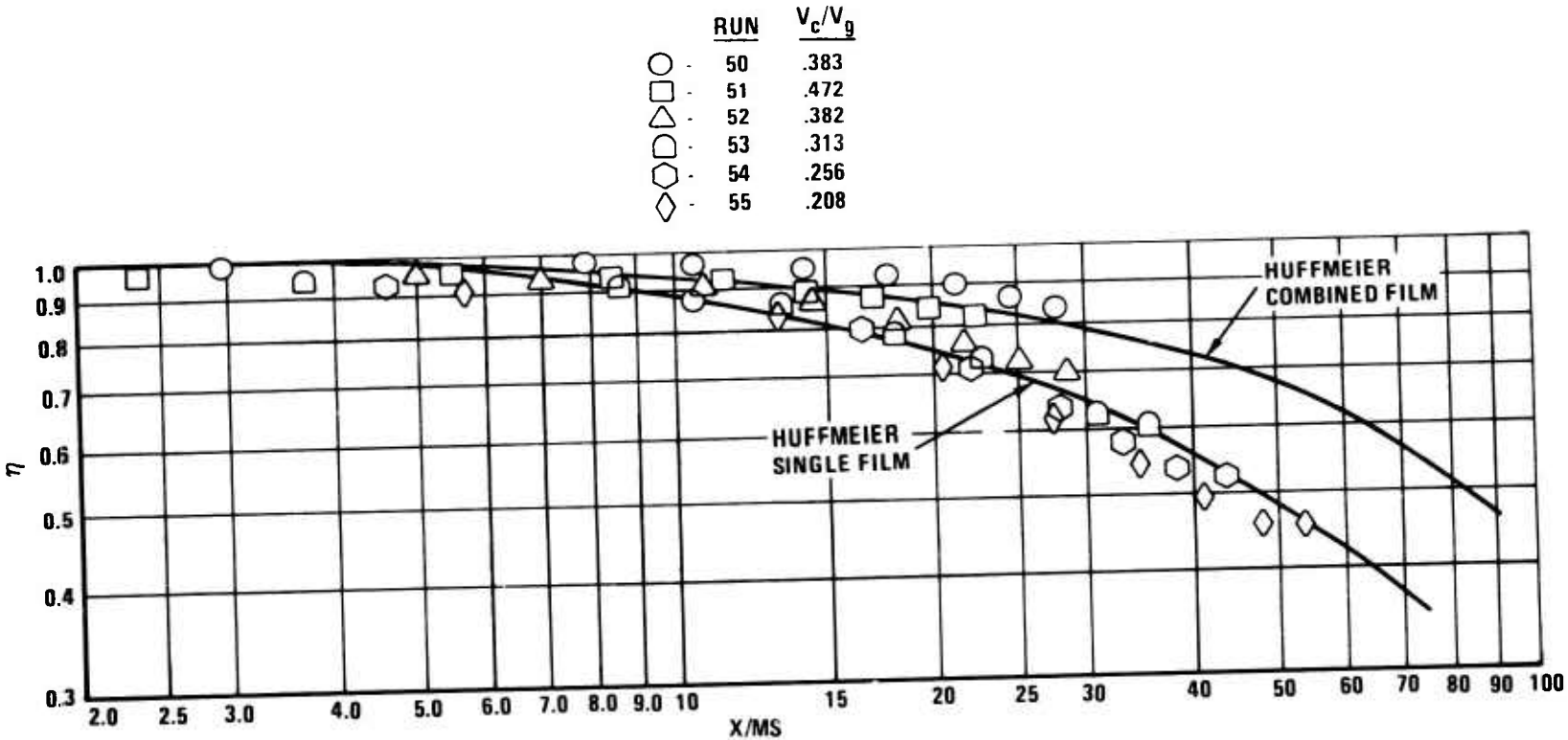


Figure 56. Film Effectiveness Distribution - Overlapped Film Without Duct Cooling at $M_g$ = .2, S = .145 In.

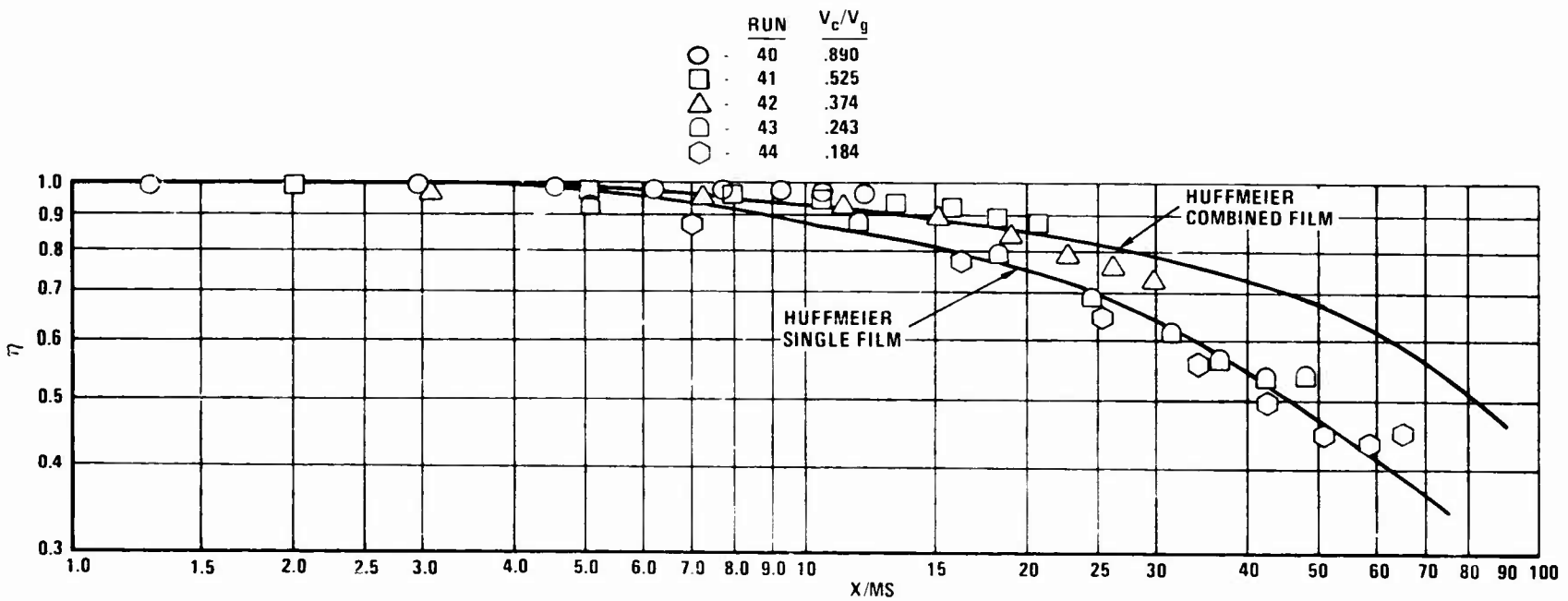


Figure 57. Film Effectiveness Distribution - Overlapped Film at $M_g$ = .10, S = .145 In.

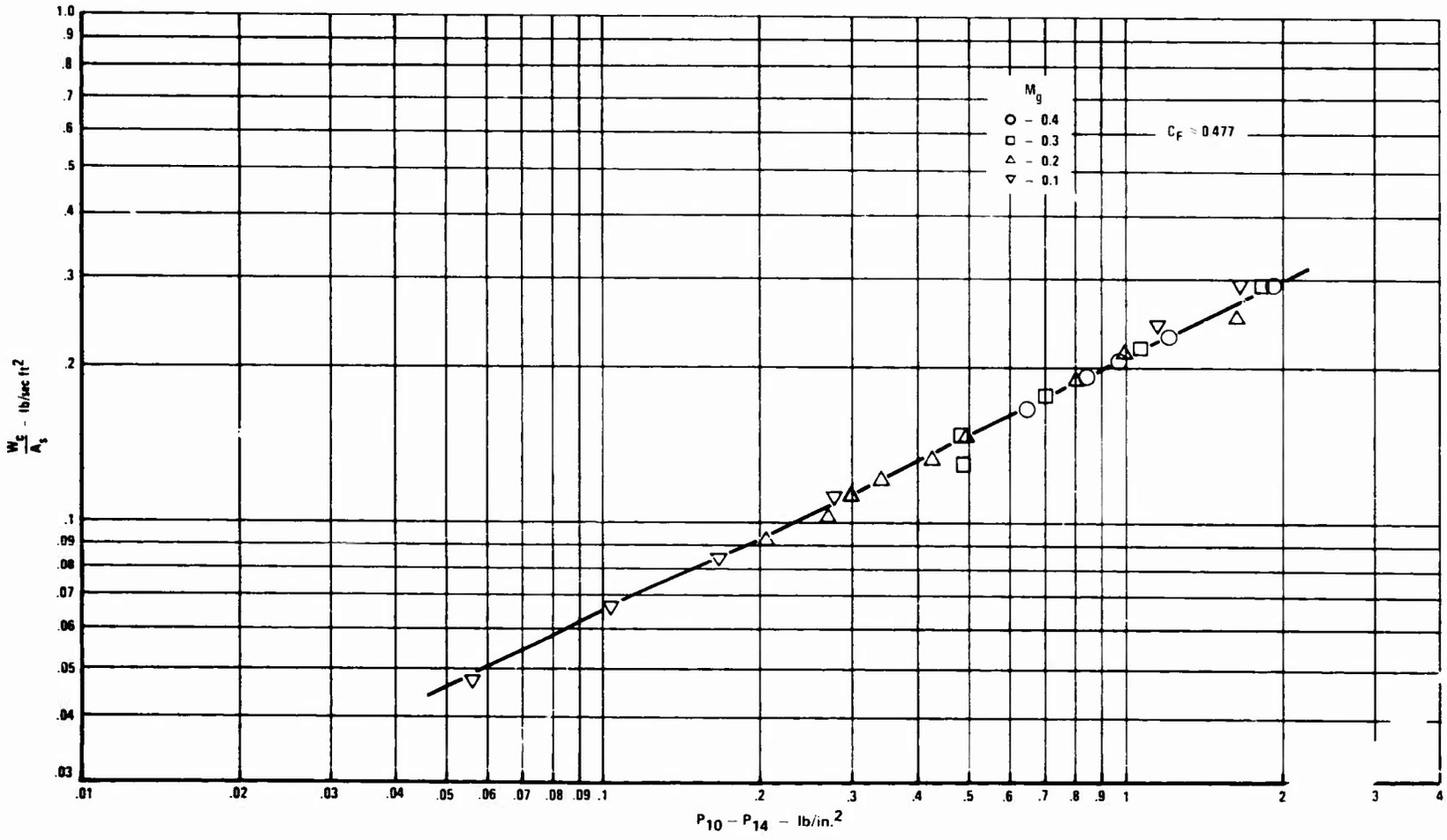


**Figure 58. Pressure Drop Across Metering Holes and Slot - Single Film With 0.100-In. Slot.**

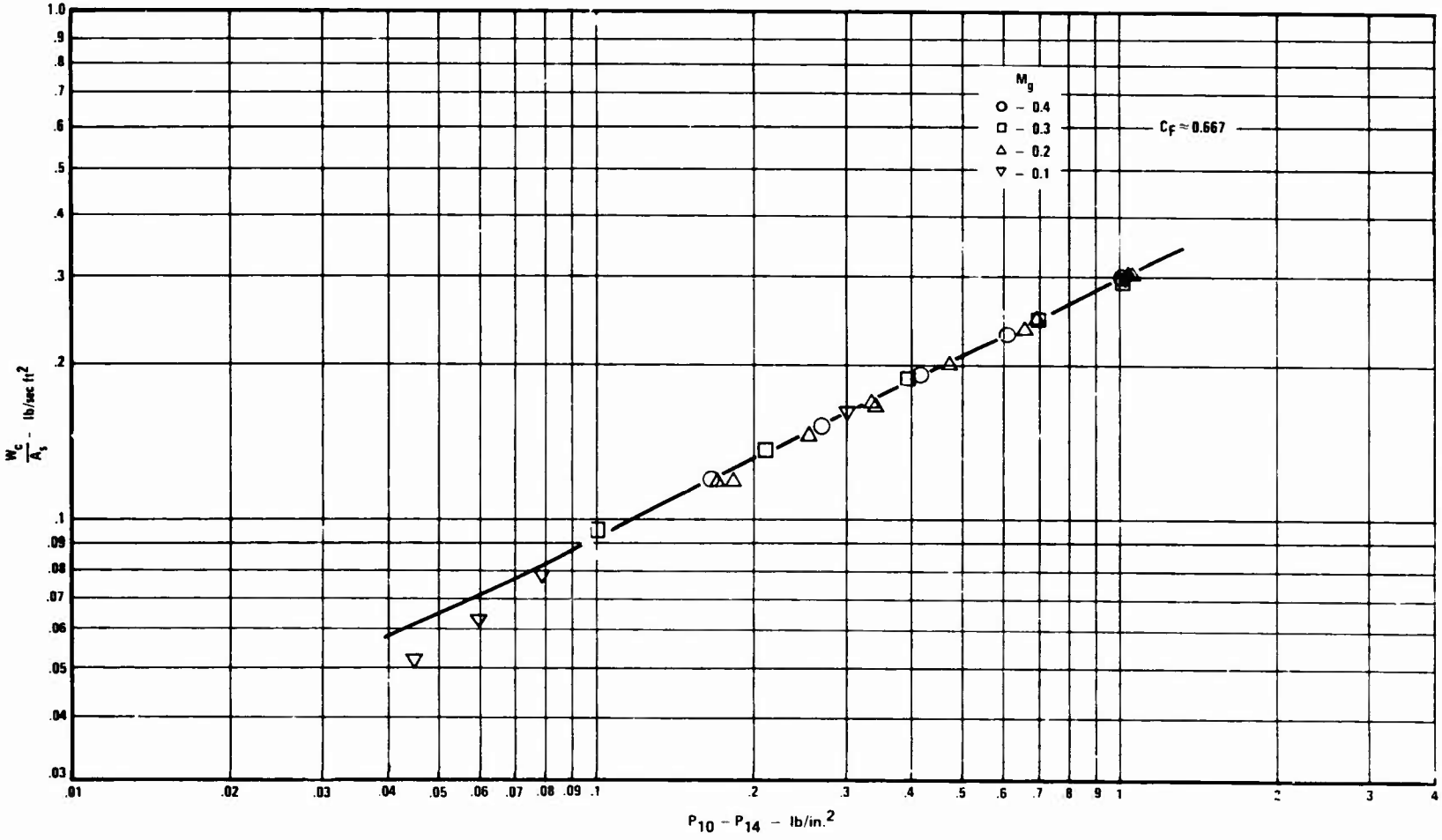


Figure 59. Pressure Drop Across Metering Holes and Slot - Single Film With 0.145-In. Slot.

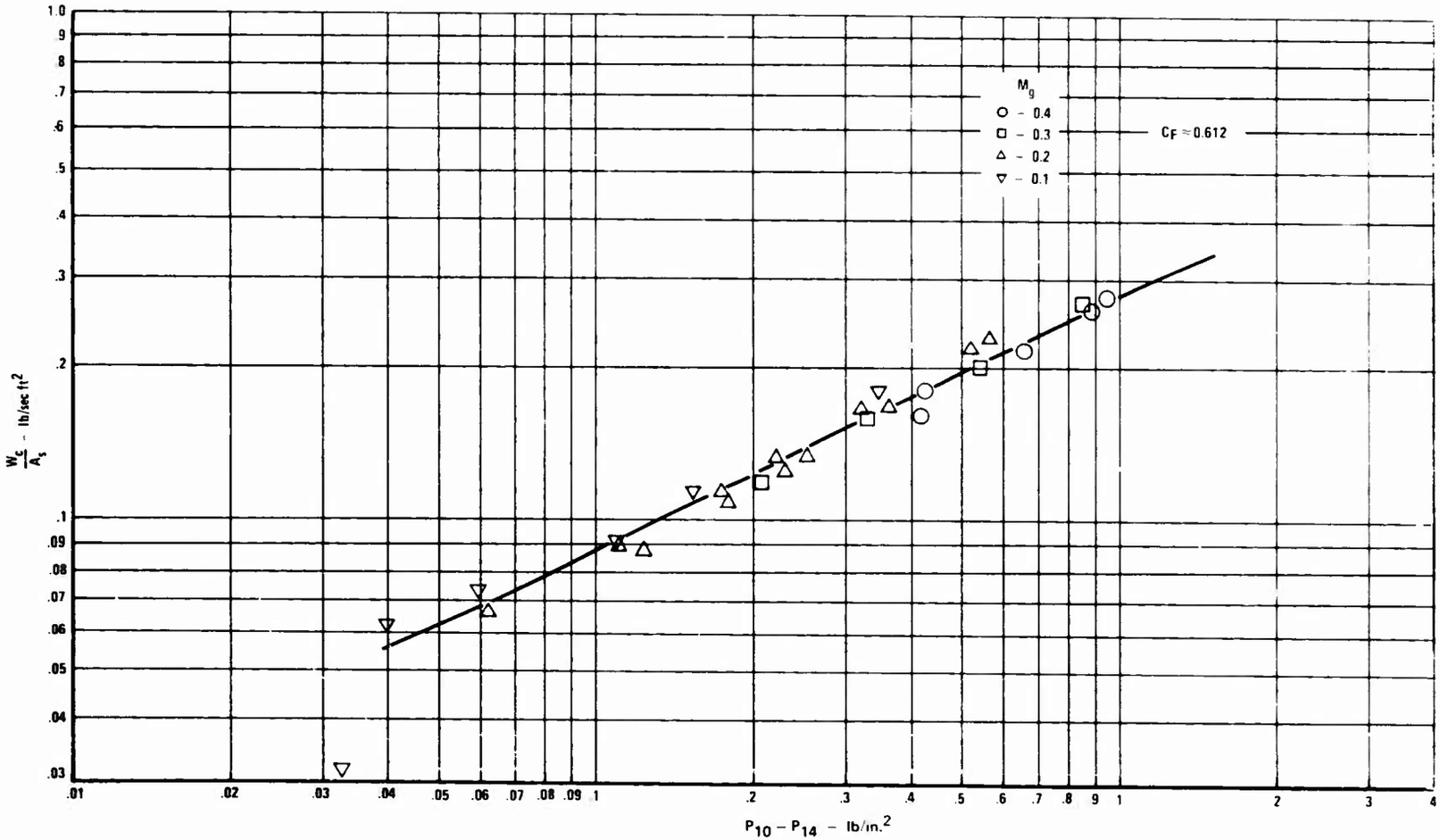


Figure 60. Pressure Drop Across Metering Holes and Slot - Overlapped Film With 0.100-In. Slot.

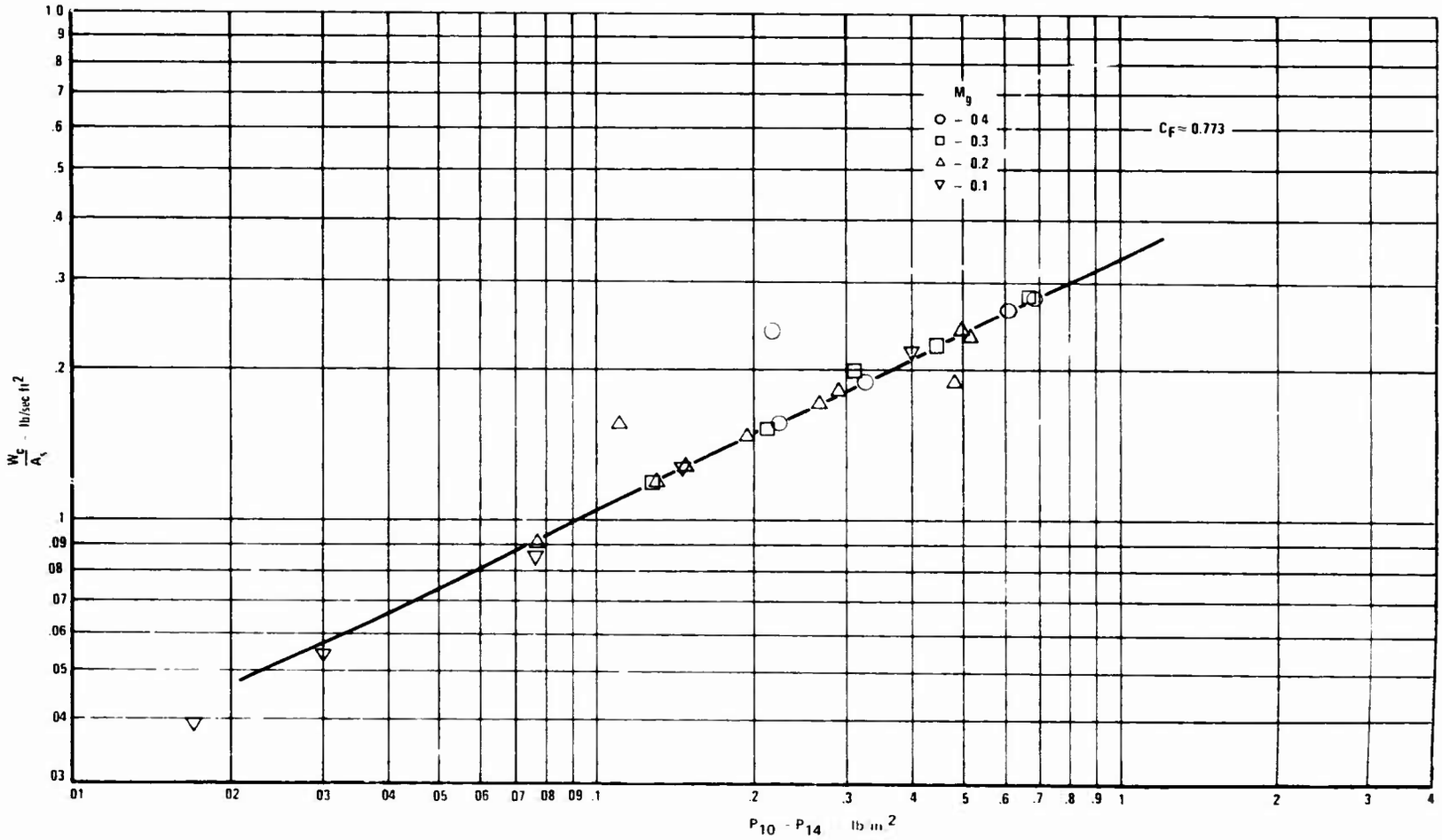


**Figure 61. Pressure Drop Across Metering Holes and Slot - Overlapped Film With 0.145-In. Slot.**

## COMPARISON OF IMPINGEMENT-FILM AND FILM COOLING

Figures 62 through 69 show comparisons between single-film, overlapped-film and impingement-film cooling for a slot height of 0.100 in. The impingement-film results shown in these figures are for an impingement plate hole diameter of 0.070 in., impingement distance ($Z_n/D$) of 4, and impingement hole spacings ($X_n/D$) of 4, 8, and 12.

Cooling effectiveness for the three modes of cooling is presented in these figures as a function of flow per unit panel surface area. The cooling effectiveness shown in Figures 62, 64, 66, and 68 is based on radiation-averaged panel temperatures which include the two temperatures located on the slot lip. Figures 63, 65, 67 and 69 show the same parameters with the two slot lip temperatures eliminated from the radiation average.

Mechanical features built into the test rig to permit variations in the film slot height left a portion of the upstream panel just ahead of the slot lip uncooled. Since this feature is not representative of engine hardware, it was decided to eliminate the slot lip temperature from the radiation-averaged temperature in the remaining data.

The results presented in Figures 62 through 69 show that the cooling effectiveness for impingement-film cooled panels was significantly better than for film-cooled panels. The reduction in radiation-averaged panel temperatures that can be achieved with an impingement-film cooling system as opposed to a film-only system can be calculated from the results shown in those figures since $\eta$ is defined

$$\eta = \frac{T_g - T_w}{T_g - T_c} \tag{5}$$

This equation can also be written

$$T_w = T_g - \eta (T_g - T_c) \tag{6}$$

If systems 1 and 2 are compared at the same hot gas temperature $T_g$ and coolant temperature $T_c$, Equation (6) leads to

$$T_{w2} - T_{w1} = (\eta_1 - \eta_2) (T_g - T_c) \tag{7}$$

For example, when inlet Mach number = 0.4, impingement hole diameter = 0.070 in., slot height = 0.10 in., $X_n/D = 12$, and $Z_n/D = 4$, Figure 69 is used. When the flow per unit surface area is 0.20 lb/sec ft$^2$, cooling effectiveness is about 0.90. Under the same conditions with film cooling only, $\eta$ is about 0.67.

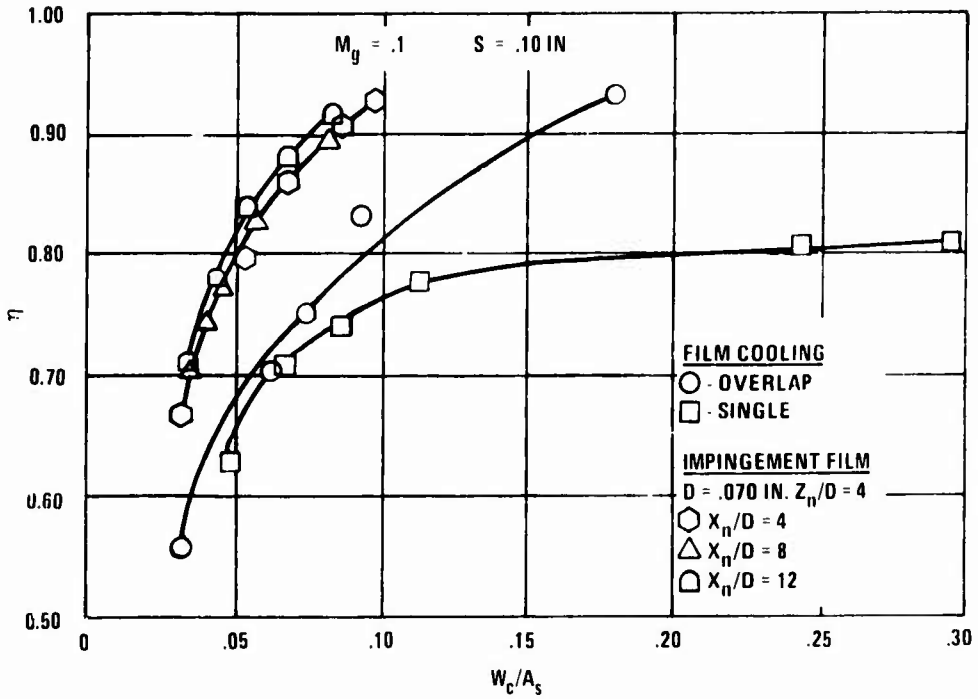


Figure 62. Results Comparing Film Cooling Effectiveness With Impingement-Film Cooling Effectiveness for Various Hole Spacings - $X_n/D$ at $M_g$ = .10.

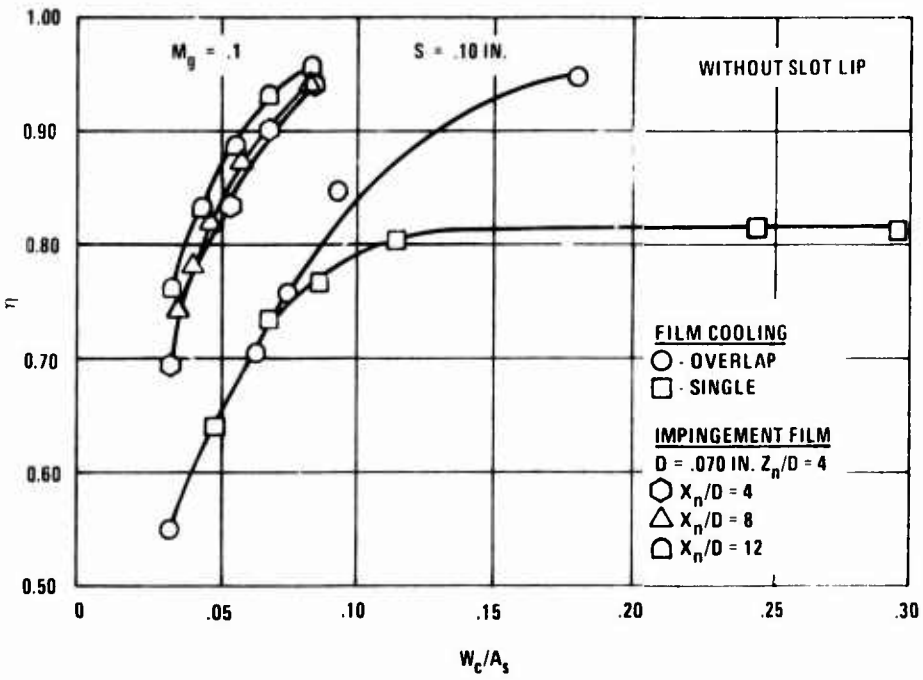


Figure 63. Results Comparing Film Cooling Effectiveness With Impingement-Film Cooling Effectiveness for Various Hole Spacings Without Slot Lip Temperatures at $M_g$ = .10.

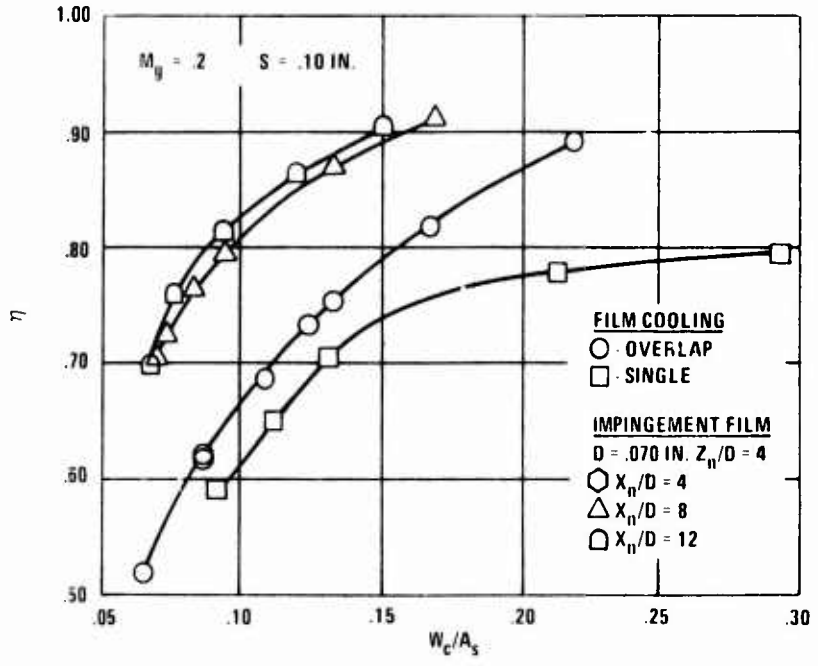


Figure 64. Results Comparing Film Cooling Effectiveness With Impingement-Film Cooling Effectiveness for Various Hole Spacings - $X_n/D$ at $M_g$ = .20.

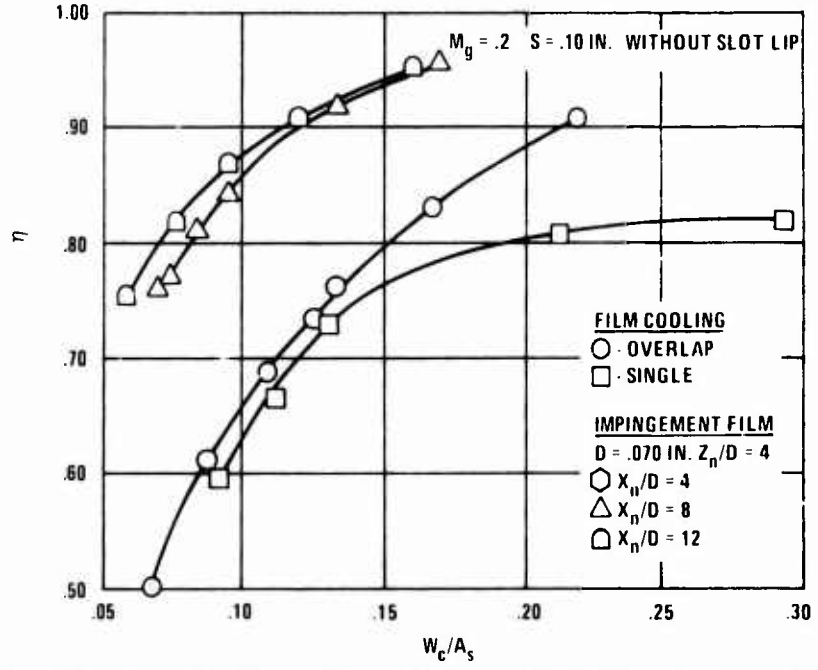


Figure 65. Results Comparing Film Cooling Effectiveness With Impingement-Film Cooling Effectiveness for Various Hole Spacings - $X_n/D$ at $M_g$ = .20.

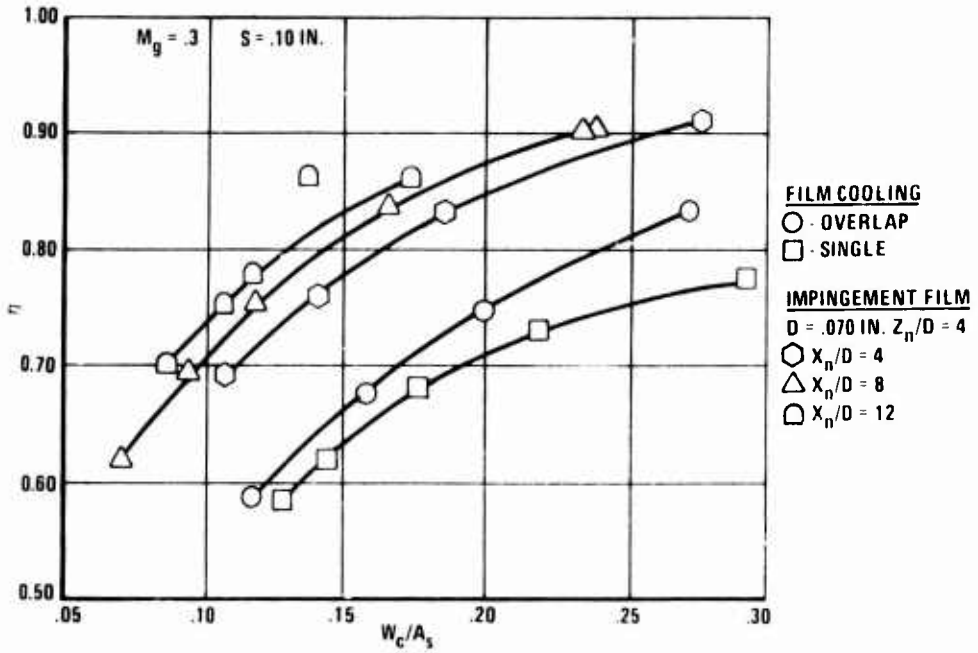


Figure 66. Results Comparing Film Cooling Effectiveness With Impingement-Film Cooling Effectiveness for Various Hole Spacings - $X_n/D$ at $M_g$ = .30.

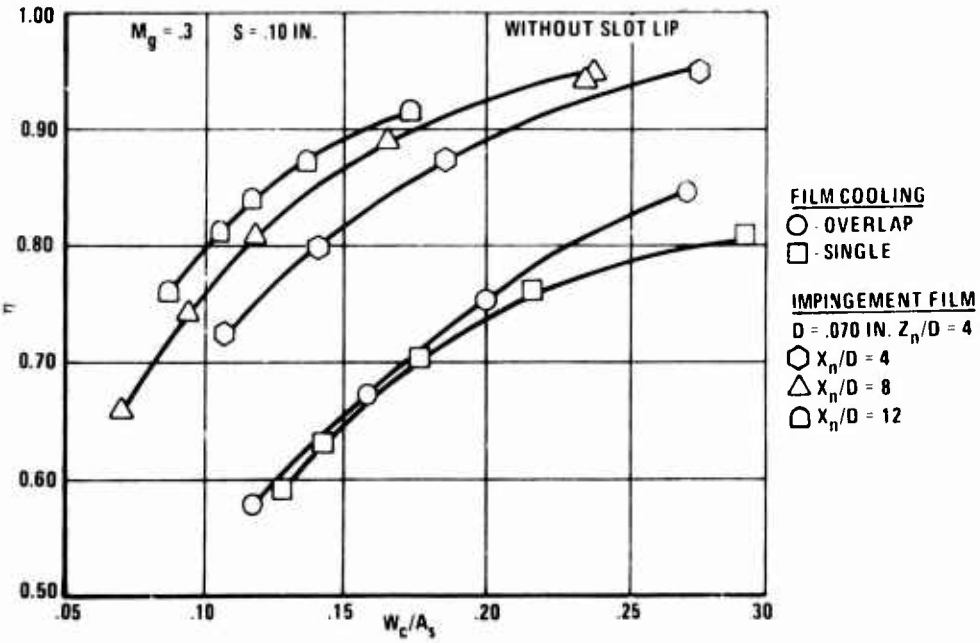


Figure 67. Results Comparing Film Cooling Effectiveness With Impingement-Film Cooling Effectiveness for Various Hole Spacings Without Slot Lip Temperatures at $M_g$ = .30.

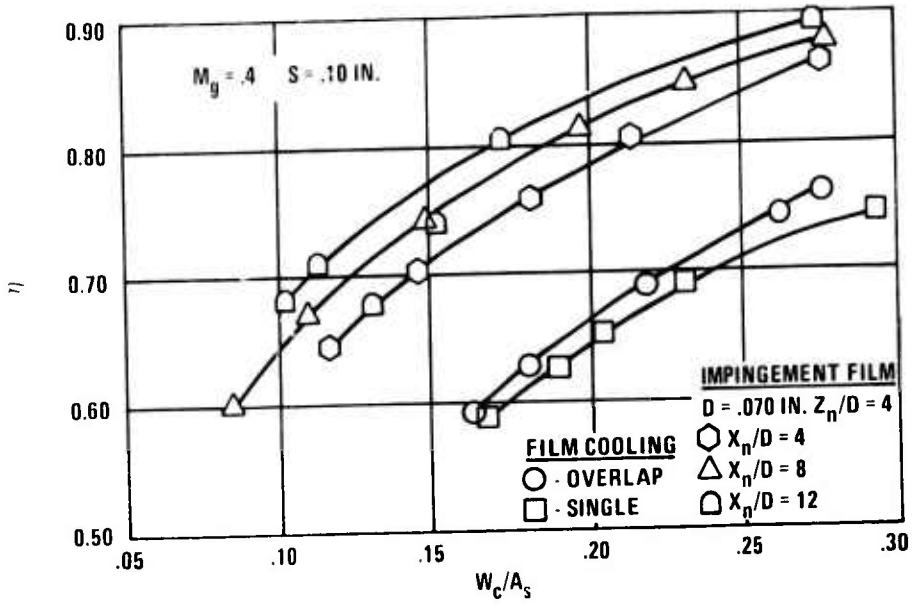


Figure 68. Results Comparing Film Cooling Effectiveness With Impingement-Film Cooling Effectiveness for Various Hole Spacings - $X_n/D$ at $M_g$ = .40.

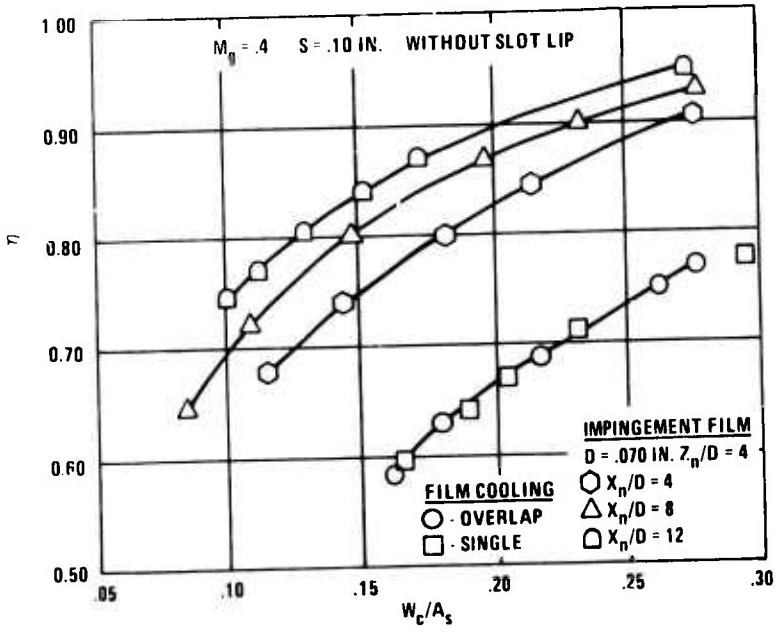


Figure 69. Results Comparing Film Cooling Effectiveness With Impingement-Film Cooling Effectiveness for Various Hole Spacings Without Slot Lip Temperatures at $M_g$ = .40.

Under those conditions, when the hot gas temperature is 1100°F and coolant temperature is 80°F, the difference in wall temperature between system 2, film cooling, and system 1, impingement-film cooling, is found from Equation (7) to be

$$T_{w2} - T_{w1} = (0.90 - 0.67)\ (1100^{\circ}F - 80^{\circ}F) = 235^{\circ}F$$

The results also show the high cooling effectiveness occurring at the largest hole spacing ($X_n/D = 12$). However, associated with the large hole spacing is the requirement for a large pressure drop across the impingement plate. Therefore, for a low pressure drop system, the required amount of cooling airflow may not be attainable at the larger spacings.

## EFFECT OF IMPINGEMENT HOLE DIAMETER ON COOLING EFFECTIVENESS

Figures 70 through 81 show the effects of impingement hole diameter on cooling effectiveness for the series of impingement hole spacings ($X_n/D$) and inlet Mach numbers tested. The results are summarized in the following paragraphs.

### Results Using Impingement Spacing of 4

At an $X_n/D = 4$, the cooling effectiveness increased with increasing impingement hole diameter for all Mach numbers.

### Results Using Impingement Spacing of 8

1. At Mach numbers of 0.4, 0.3, and 0.2, impingement baffles with hole diameters of 0.070 in. and 0.052 in. yield higher cooling effectiveness than a baffle with 0.031-in.-diameter holes at Mach numbers of 0.4, 0.3, and 0.2.

2. At an inlet Mach number of 0.1 and at the lower cooling flows, the baffle with 0.031-in.-diameter holes had higher cooling effectiveness than the baffle with 0.052-in. holes and equalled the performance of the baffle with 0.070-in. holes.

3. The baffle with 0.070-in. holes produced higher cooling effectiveness than the other two baffles at the higher cooling flows.

4. At lower cooling flows, there was not much difference between the cooling effectiveness of baffles with 0.070-in. holes and 0.052-in. holes.

Results Using an Impingement Spacing of 12

1. The 0.070-in. holes yielded the highest effectiveness at an inlet Mach number of 0.2.

2. For Mach numbers of 0.1 and 0.3, at the higher cooling flows, the 0.070-in. holes produced higher cooling effectiveness.

3. At a Mach number of 0.4, there was no apparent difference in cooling effectiveness with changes in diameter.

In general, the larger the impingement hole diameter, the higher the cooling effectiveness. This result contradicts the previously correlated data of Kercher[1] and Tabakoff and Clevenger[3]. The reason for the discrepancy is probably that their cross flow velocities were small since they were associated with relatively few, four or less, rows of impingement holes (see the Impingement Baffle Pressure Differential section). The impingement-film tests on the other hand were conducted on geometry characterized by a large number of rows of holes. There were 33 rows of 0.031-in. holes, 20 rows of 0.052-in. holes and 15 rows of 0.070-in. holes at $X_n/D = 4$. These tests, and also the correlation expressed by Equation (1), indicate that the rate of change of heat flow with impingement hole diameter is negative at small cross-flow velocities and increases steadily passing through zero and then becoming positive as cross-flow velocities increase.

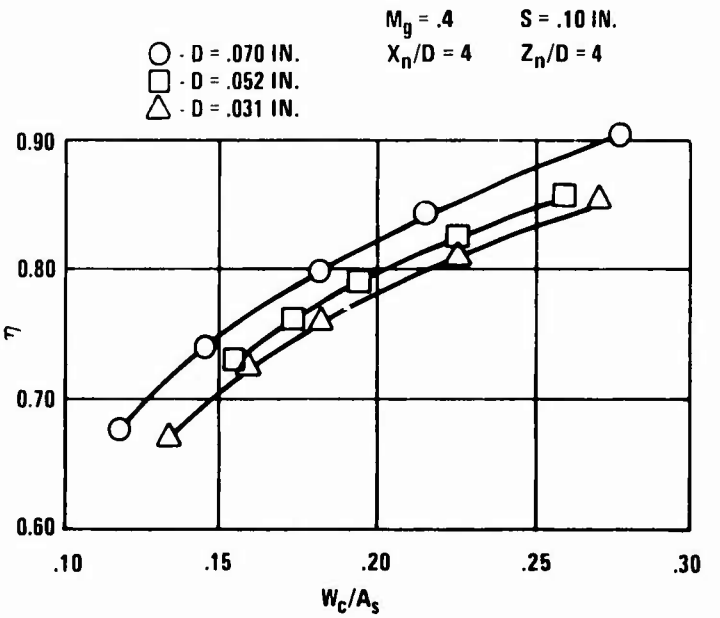


Figure 70. Effect of Impingement Hole Diameter on Cooling Effectiveness at $M_g$ = .4, $X_n/D$ = 4.

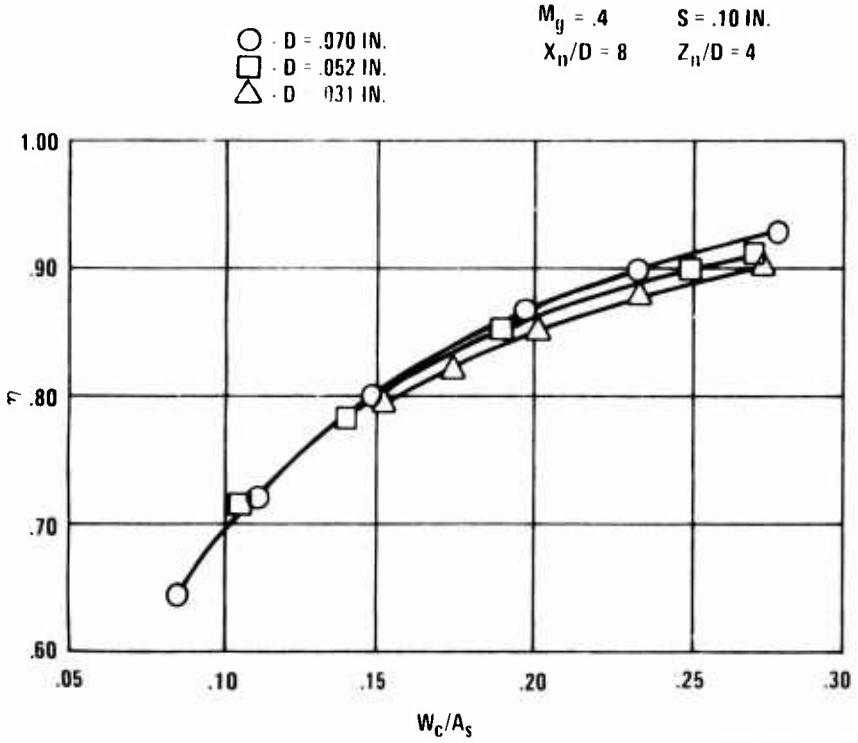


Figure 71. Effect of Impingement Hole Diameter on Cooling Effectiveness at $M_g$ = .4, $X_n/D$ = 8

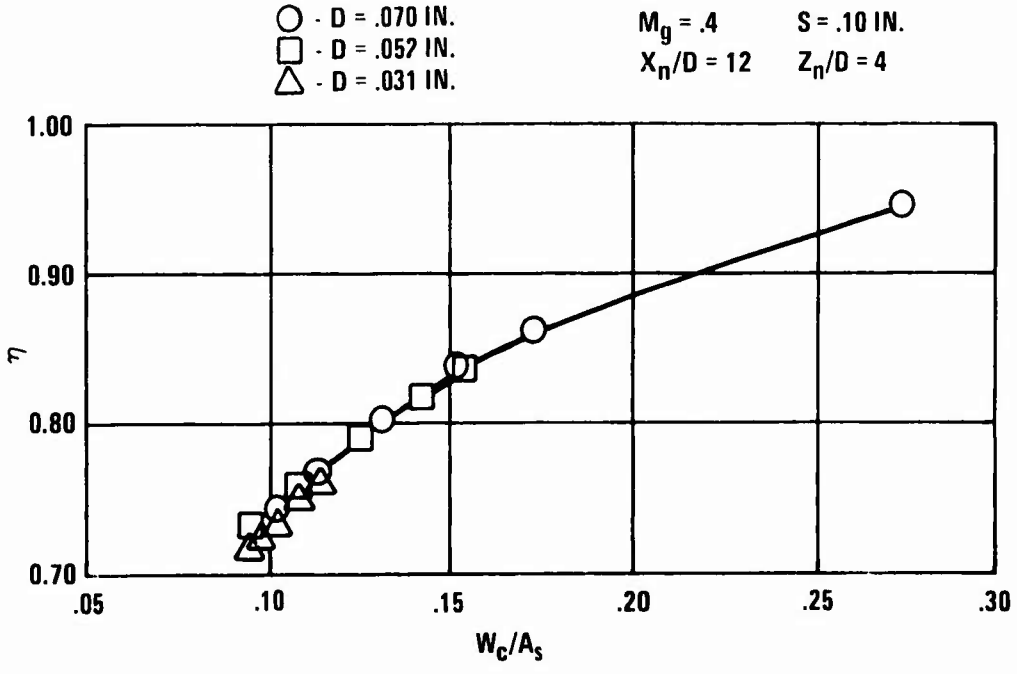


Figure 72. Effect of Impingement Hole Diameter on Cooling Effectiveness at $M_g$ = .4, $X_n/D$ = 12.

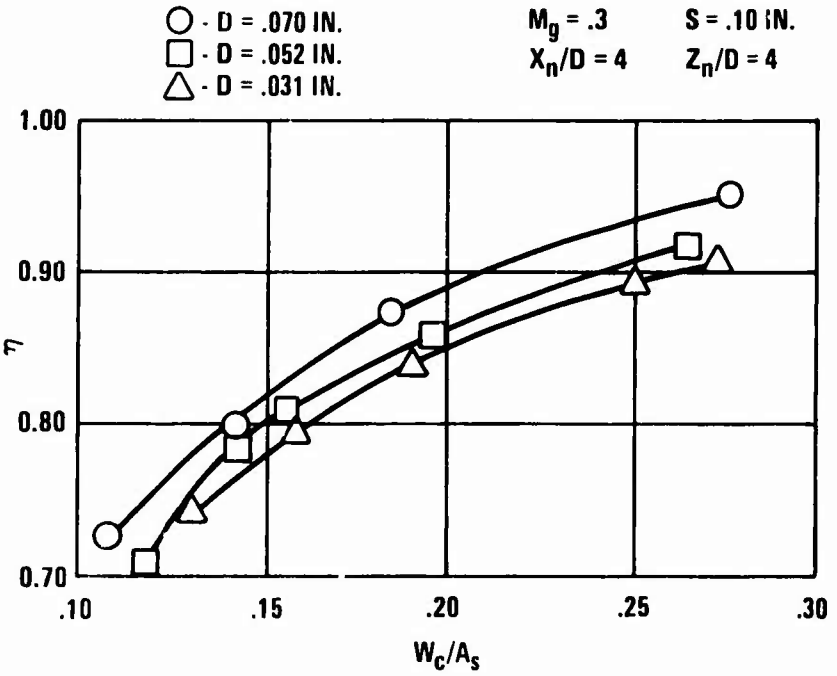


Figure 73. Effect of Impingement Hole Diameter on Cooling Effectiveness at $M_g = .3$, $X_n/D = 4$.

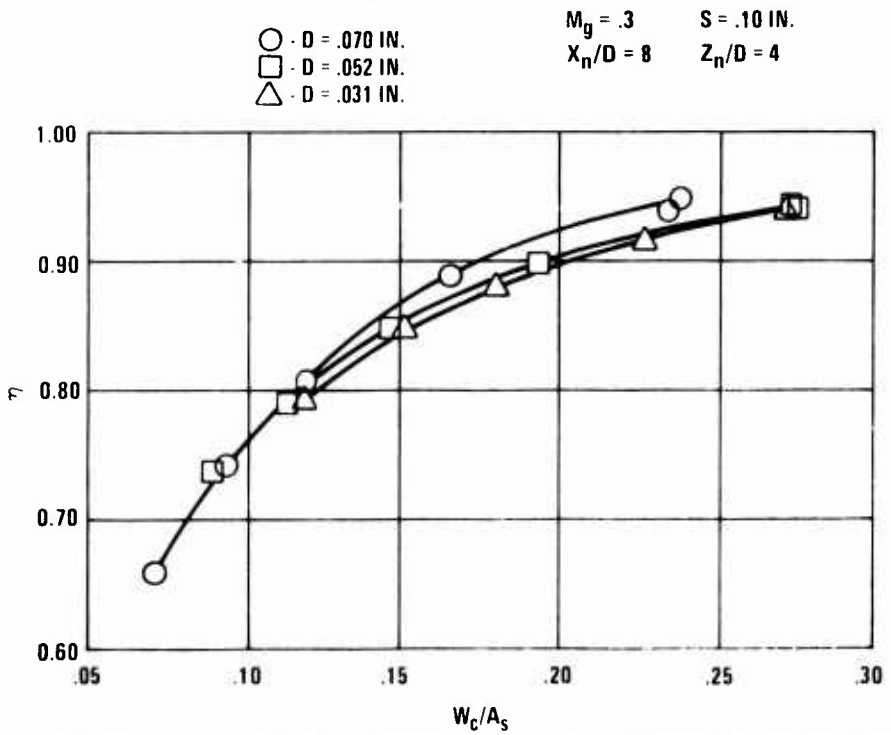


Figure 74. Effect of Impingement Hole Diameter on Cooling Effectiveness at $M_g = .3$, $X_n/D = 8$.

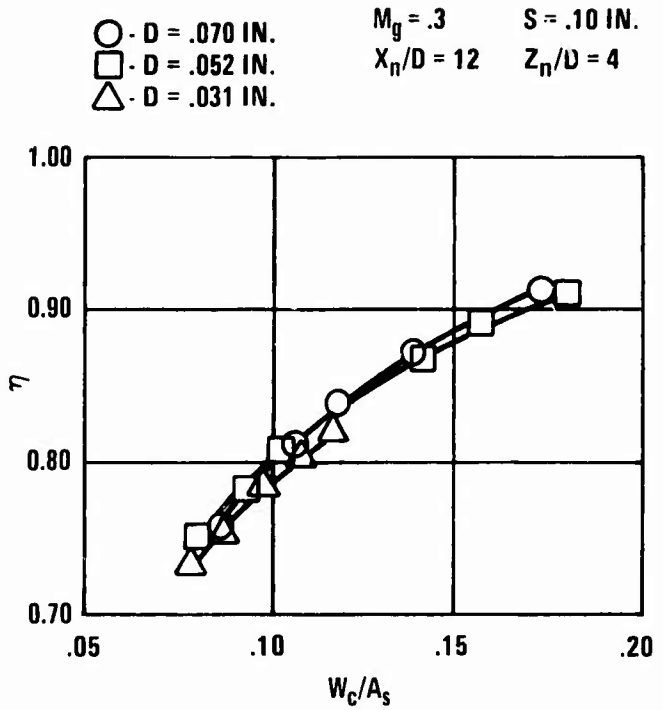


Figure 75. Effect of Impingement Hole Diameter on Cooling Effectiveness at $M_g = .3$, $X_n/D = 12$.

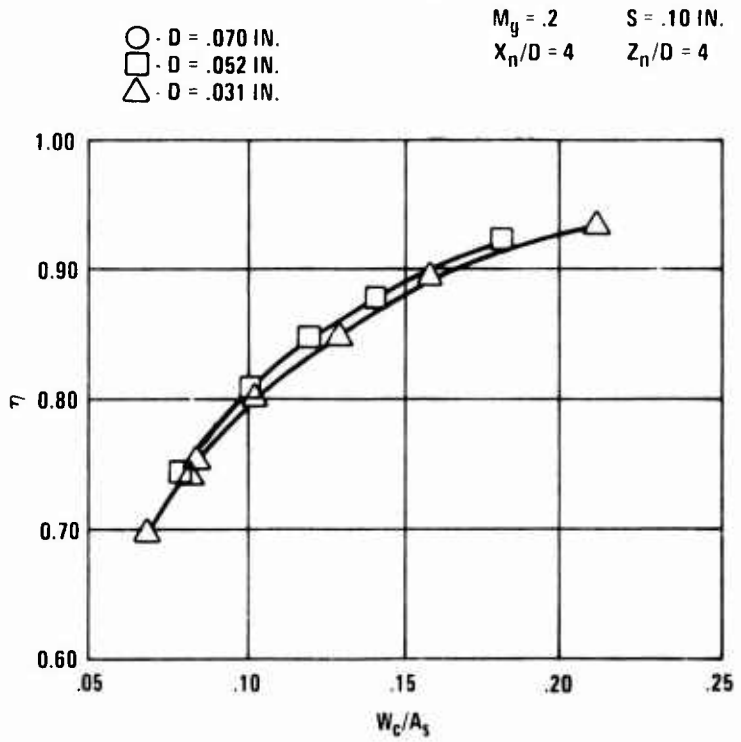


Figure 76. Effect of Impingement Hole Diameter on Cooling Effectiveness of $M_g = .2$, $X_n/D = 4$ .

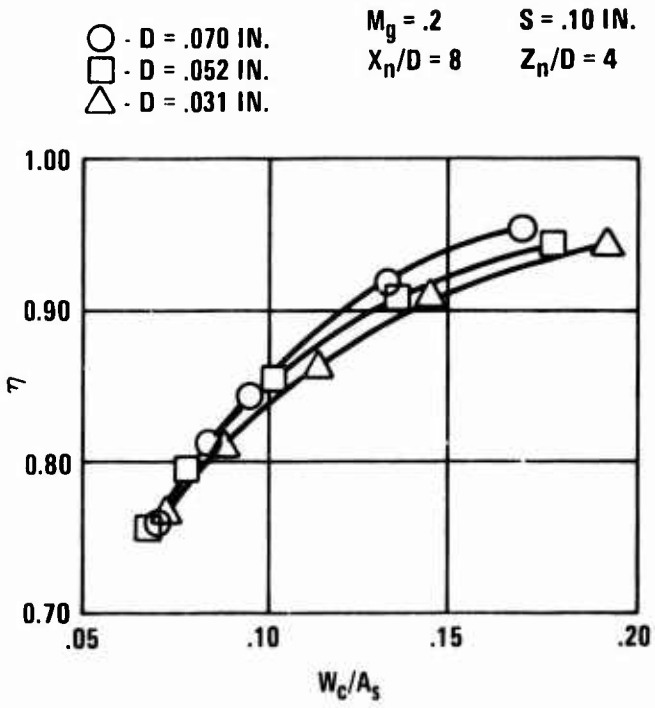


Figure 77. Effect of Impingement Hole Diameter on Cooling Effectiveness at $M_g = .2$, $X_n/D = 8$.

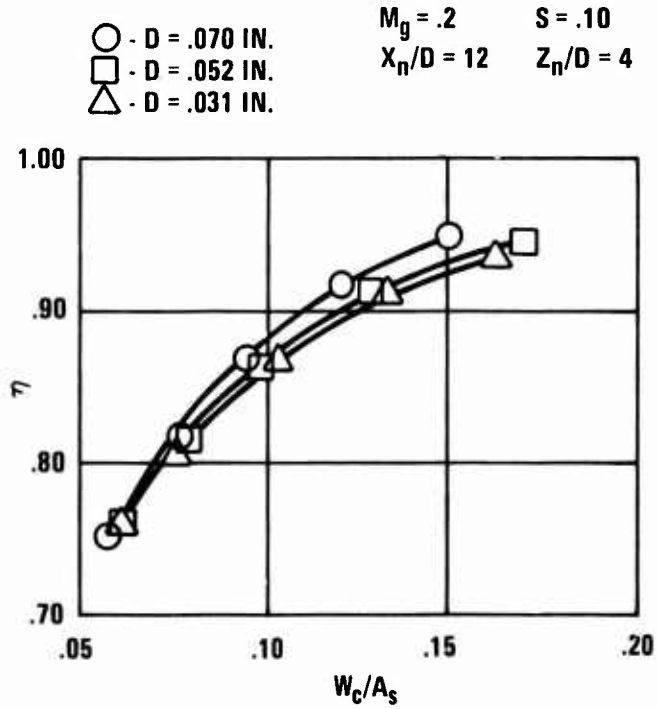


Figure 78. Effect of Impingement Hole Diameter on Cooling Effectiveness at $M_g = .2$, $X_n/D = 12$.

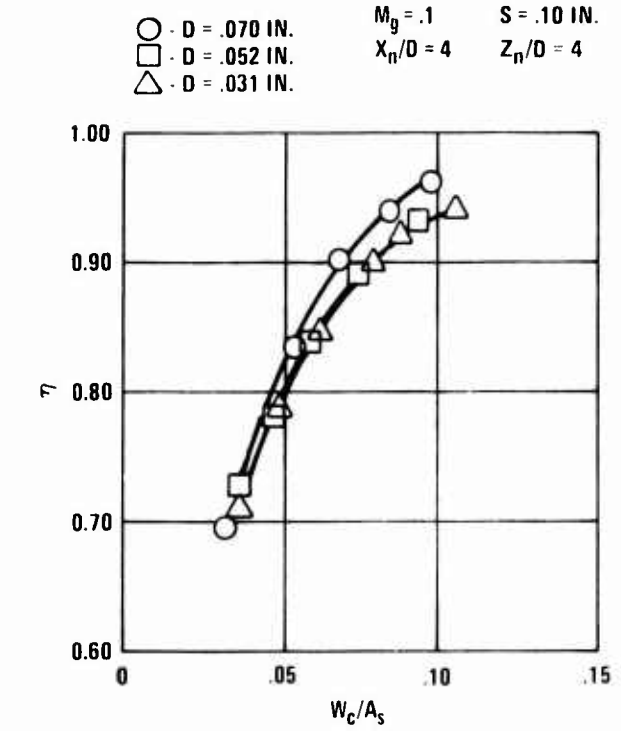


Figure 79. Effect of Impingement Hole Diameter on Cooling Effectiveness at $M_g = .1$, $X_n/D = 4$.

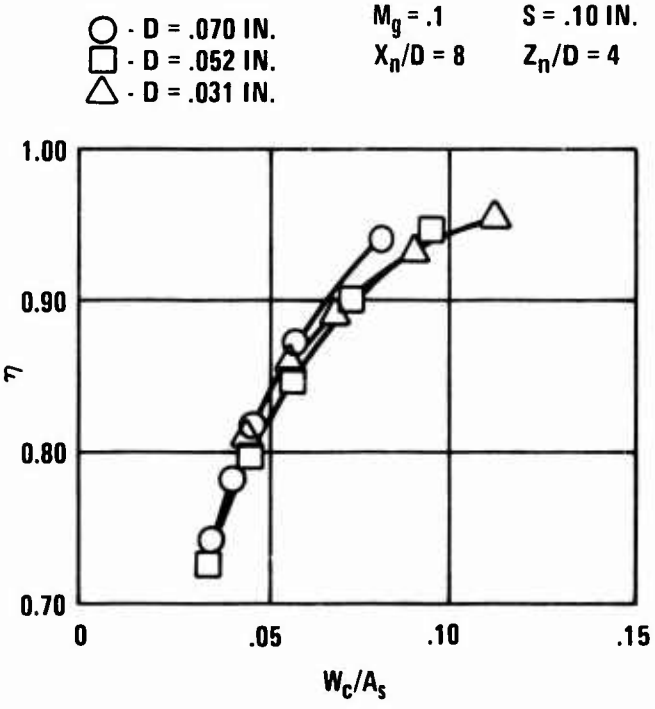


Figure 80. Effect of Impingement Hole Diameter on Cooling Effectiveness at $M_g = .1$, $X_n/D = 8$.

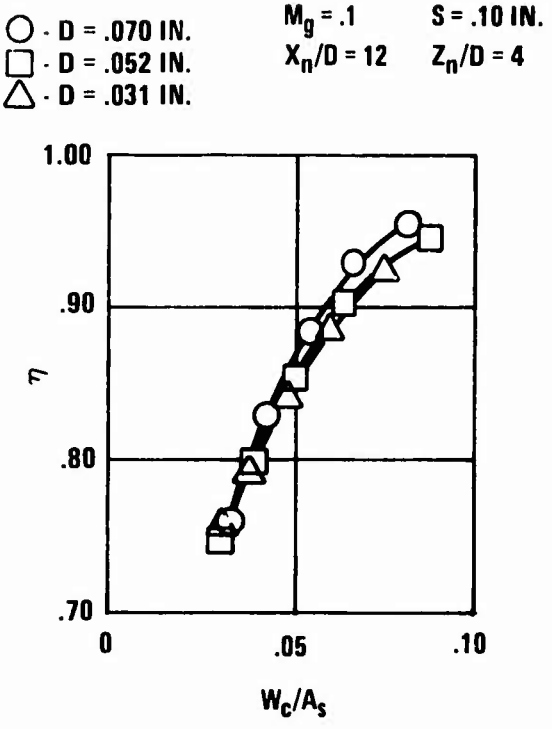


Figure 81. Effect of Impingement Hole Diameter on Cooling Effectiveness at $M_g = .1$, $X_n/D = 12$.

## EFFECT OF IMPINGEMENT PLATE DISTANCE ($Z_n/D$) ON COOLING EFFECTIVENESS

Figures 82 through 89 show the effects of impingement distance ($Z_n/D$) for two hole diameters (0.070 in., 0.052 in.) and one hole spacing ($X_n/D = 8$) for various Mach numbers. The following paragraphs summarize the results:

1. For both hole diameters, the highest cooling effectiveness was achieved with an impingement distance ($Z_n/D$) of four diameters.

2. For both hole diameters, the impingement distance of 2 diameters yielded higher effectiveness than the impingement distance of 6 diameters.

   Two probable reasons for the higher cooling effectiveness at the impingement distance of 4 diameters are:

   a. Increased cross-flow velocity degrades the impingement effectiveness at $Z_n/D = 2$.

   b. Jet velocity decay probably causes a similar effect at $Z_n/D = 6$.

EFFECT OF IMPINGEMENT SPACING ($X_n/D$) ON THE AVERAGE IMPINGEMENT HEAT TRANSFER COEFFICIENT

Figures 90 through 92 show the average impingement heat transfer coefficients (h) plotted as a function of flow per unit panel surface area. In each figure, the results are presented with impingement spacing ($X_n/D$) as the parameter, holding hole diameter and impingement spacing ($Z_n/D$) constant. The figures confirm that the impingement spacing of 12 diameters yields the highest heat transfer characteristics. The average impingement heat transfer coefficients (h) obtained at impingement spacings of 8 and 12 diameters are significantly better than those obtained at 4 diameters. Figure 92 shows that for an impingement spacing of 8 and a hole diameter of 0.031 in., the data appears questionable due to its scatter and abnormal characteristics relative to the results of the other 2 diameters. Closer examination of the results (tests 292 through 316) indicated a clear dependence of heat transfer coefficient on duct inlet Mach number which should not exist. Therefore, this set of data was disregarded in summarizing the above results.

Figures 90 to 92 also show scatter. This scatter occurs at low duct inlet Mach numbers ($M_g = 0.2$ and 0.1), and the possible cause may be the low heat pickup in the air which results in small differences in the cooling air temperature used in calculating the average impingement heat transfer coefficient (i.e., temperature measurement tolerances). Also, as the convective heat transfer decreases, conduction effects become more pronounced.

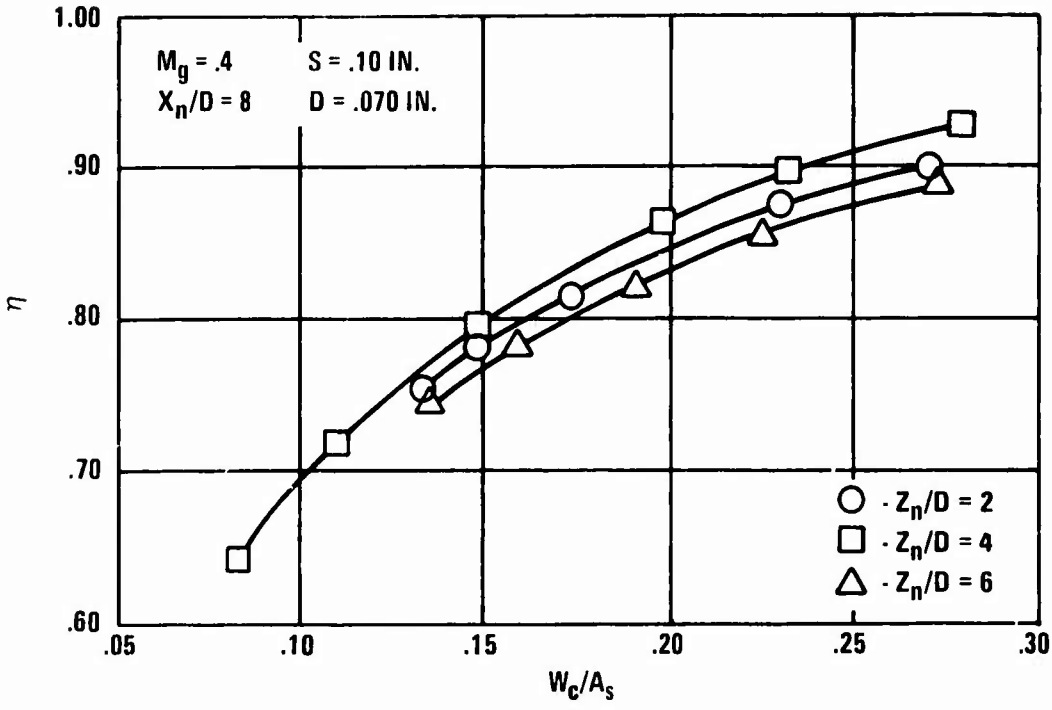


Figure 82. Effect of Impingement Distance on Cooling Effectiveness for D = .070 In. at $M_g$ = .4.

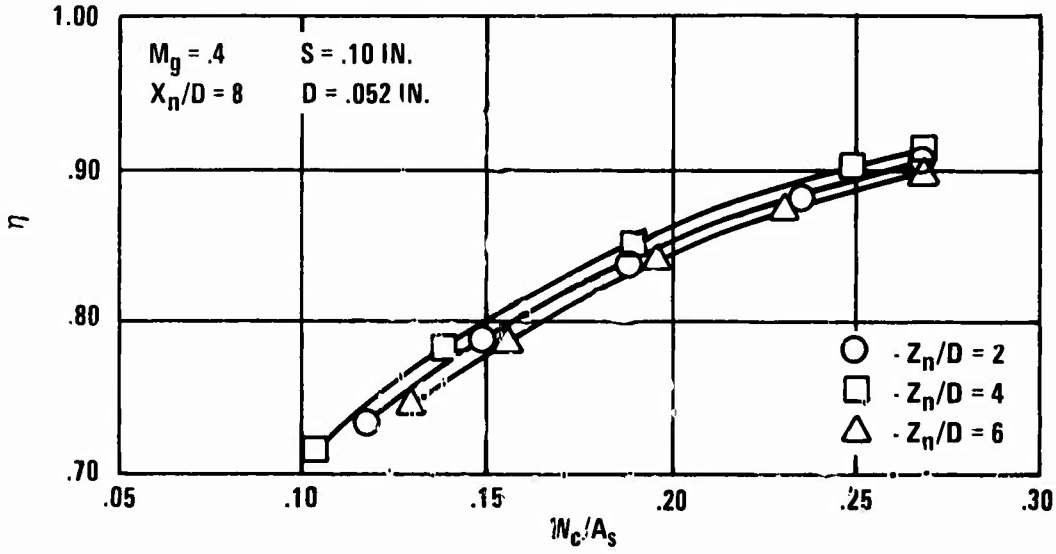


Figure 83. Effect of Impingement Distance on Cooling Effectiveness for D = .052 In. at $M_g$ = .4.

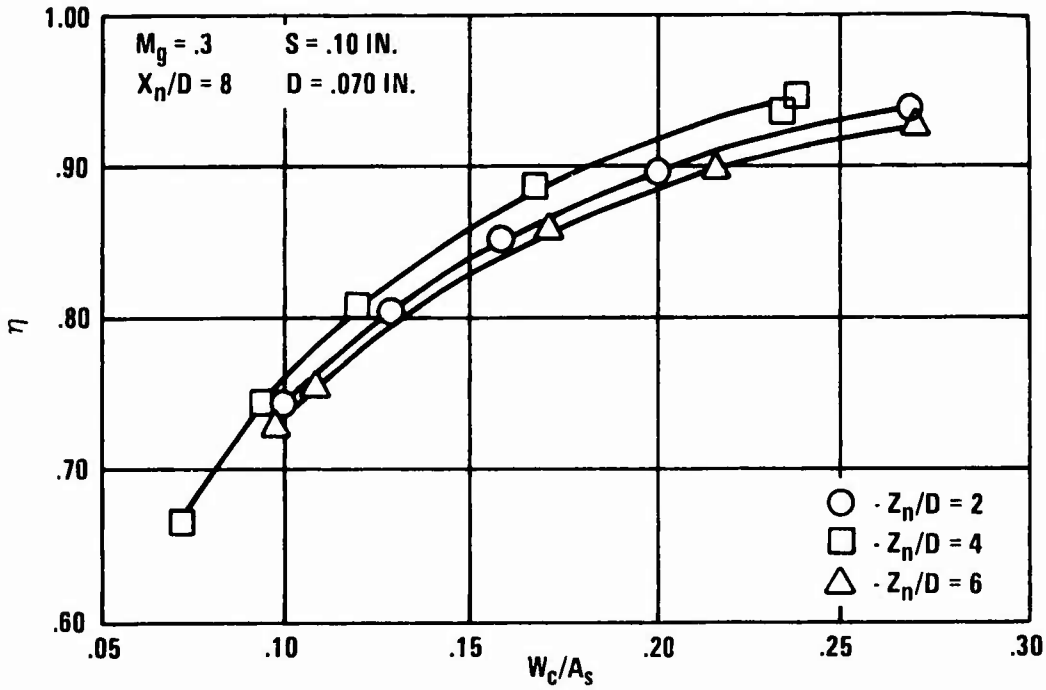


Figure 84. Effect of Impingement Distance on Cooling Effectiveness for D = .070 In. at $M_g$ = .3.

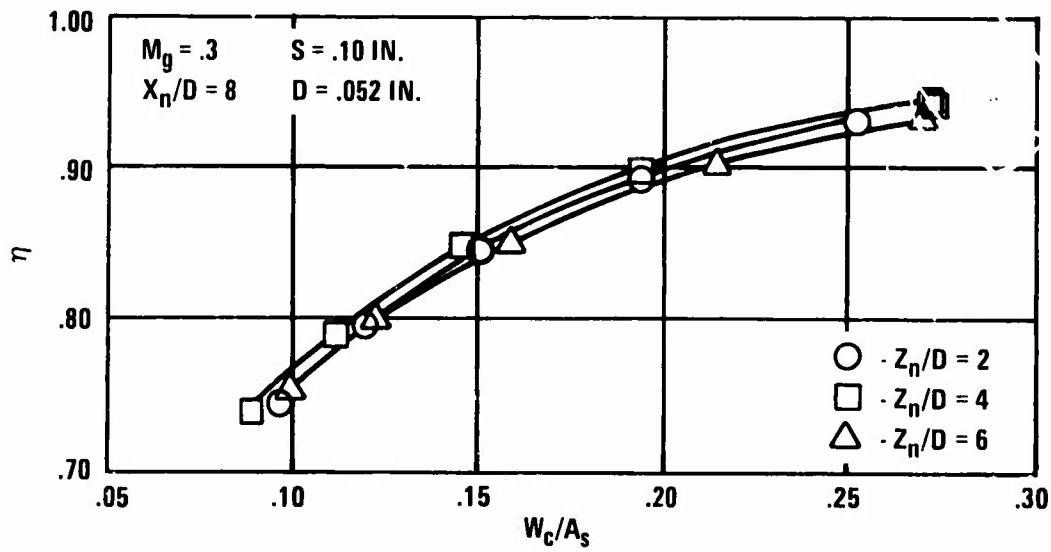


Figure 85. Effect of Impingement Distance on Cooling Effectiveness for D = .052 In. at $M_g$ = .3.

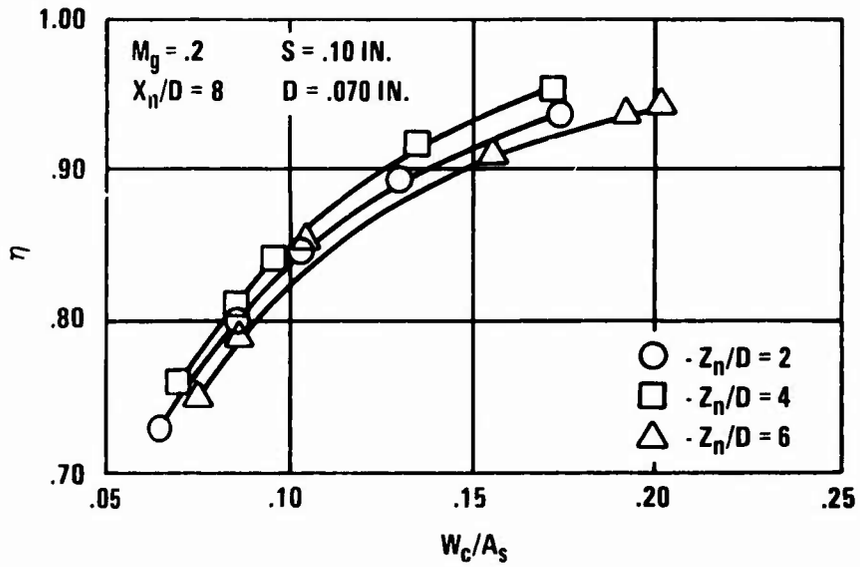


Figure 86. Effect of Impingement Distance on Cooling Effectiveness for D = .070 In. at $M_g$ = .2.

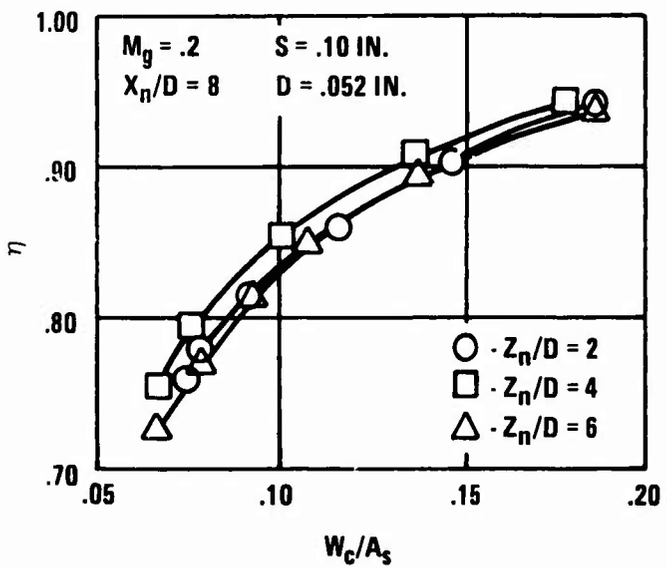


Figure 87. Effect of Impingement Distance on Cooling Effectiveness for D = .052 In. at $M_g$ = .2.

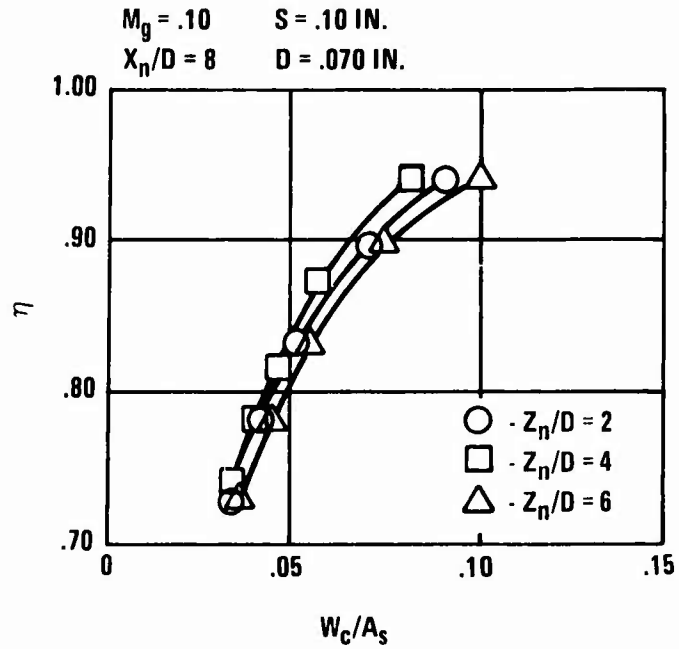


Figure 88. Effect of Impingement Distance on Cooling Effectiveness for D = .070 In. at $M_g$ = .1.

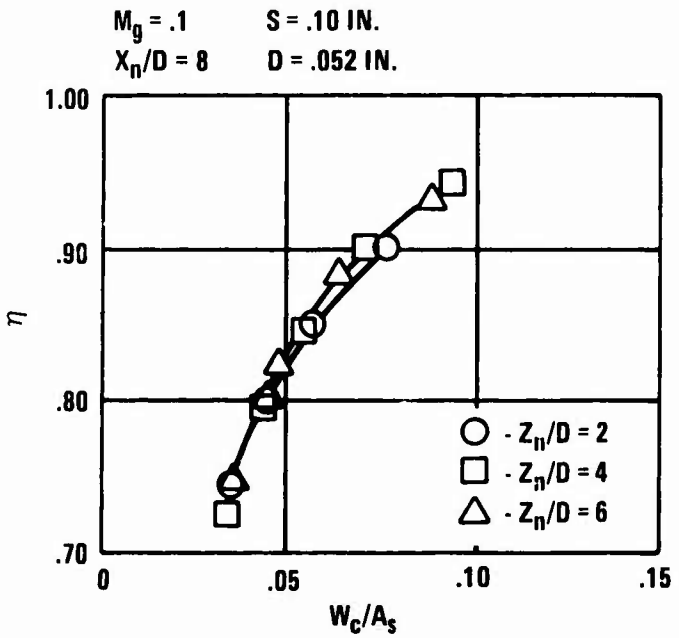


Figure 89. Effect of Impingement Distance on Cooling Effectiveness for D = .052 In. at $M_g$ = .1.

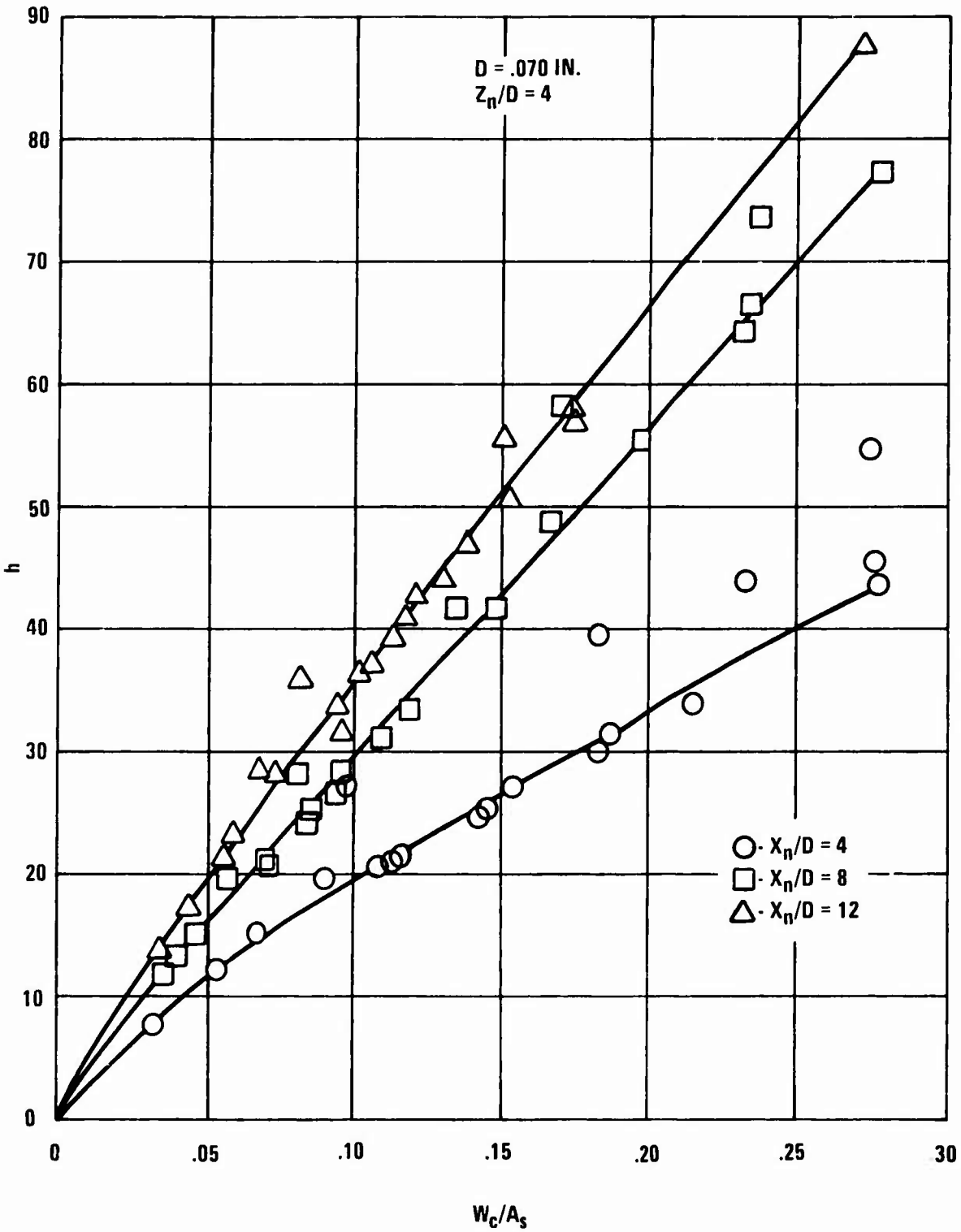


Figure 90. Effect of Impingement Spacing on Average Impingement Heat Transfer Coefficient for D = .070 In.

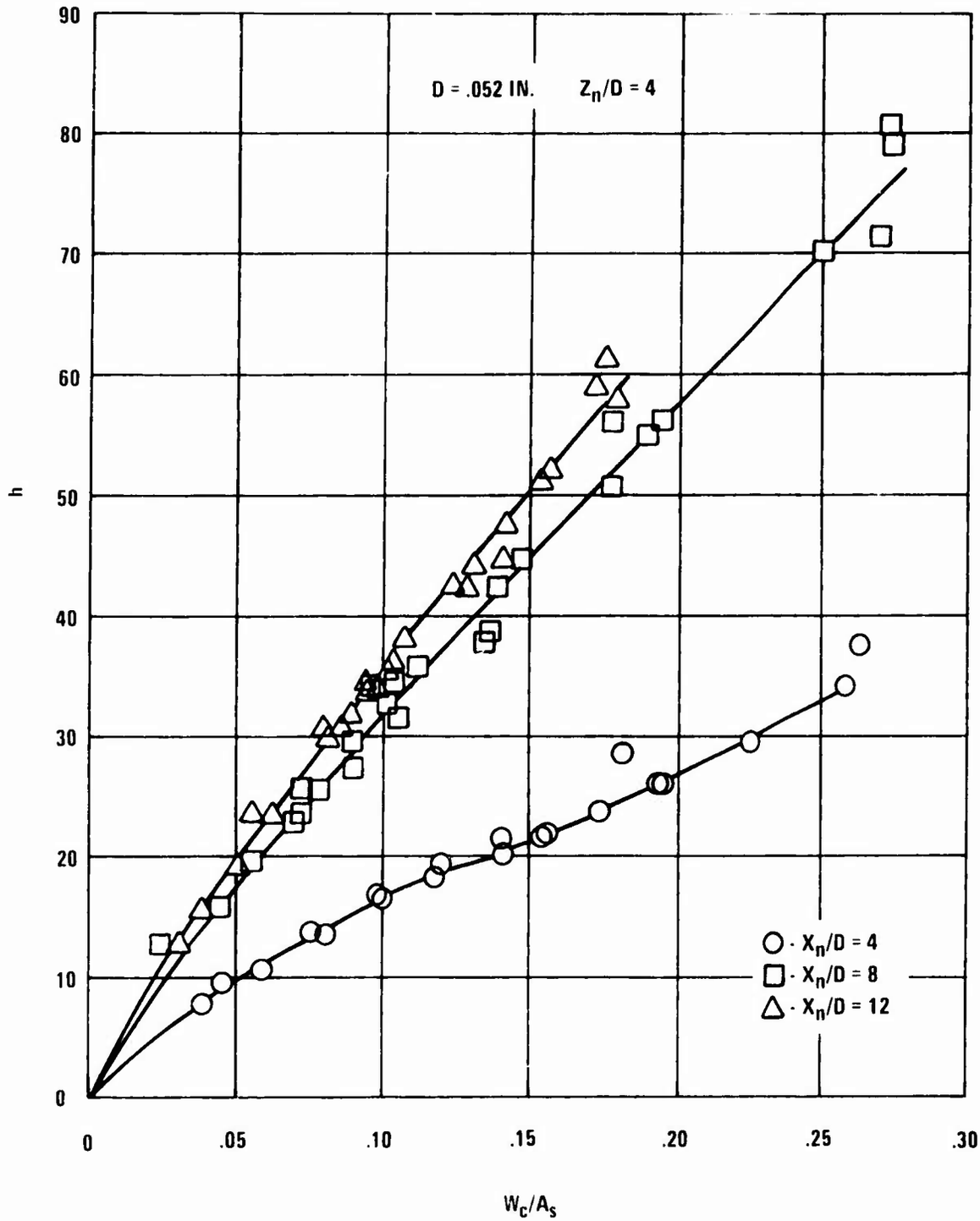


Figure 91. Effect of Impingement Spacing on Average Impingement Heat Transfer Coefficient for D = .052 In.

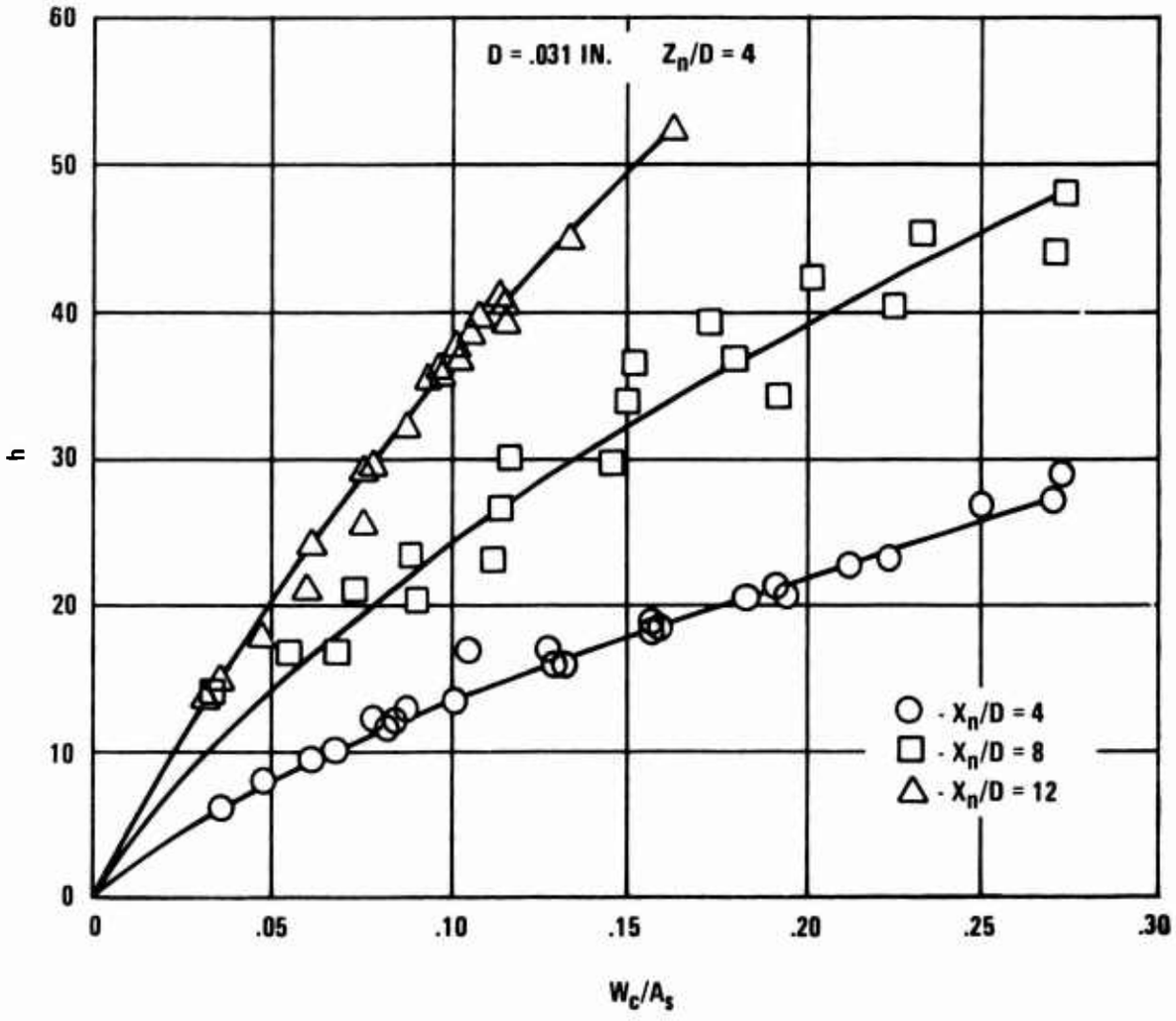


Figure 92. Effect of Impingement Spacing on Average Impingement Heat Transfer Coefficient for D = .031 In.

## EFFECT OF IMPINGEMENT DISTANCE ($Z_n/D$) ON THE AVERAGE IMPINGEMENT HEAT TRANSFER COEFFICIENT

Figures 93 and 94 present additional average impingement heat transfer coefficients which show the effects of impingement distance for fixed impingement hole spacing ($X_n/D$) = 8 and hole diameter. The highest heat transfer coefficients occur at an impingement distance of 4 diameters, while the values obtained at an impingement distance of 2 diameters are higher than those at 6 diameters. These results are similar to those noted in the cooling effectiveness data.

## IMPINGEMENT BAFFLE PRESSURE DIFFERENTIAL

During the impingement-film portion of the test program, the pressure differential from cooling air inlet pressure to metering hole inlet pressure was measured. This pressure differential across the impingement baffle is shown in Figures 95, 96 and 97, as a function of cooling flow per unit of cooled panel surface area. Figure 95 includes all the data for 0.031-in. impingement holes. The data was taken at $M_g$ = 0.1, 0.2, 0.3, 0.4; $X_n/D$ = 4, 8, 12; and $Z_n/D$ = 4. Figures 96 and 97 include test results obtained at the same conditions but with impingement hole diameters = 0.052 in. and 0.070 in. respectively. Figures 96 and 97 also include results for $Z_n/D$ = 2 and 6.

As was the case with the slot pressure differentials shown on Figures 58, 59, 60 and 61, the cooling flow was practically proportional to the square root of the impingement baffle pressure differential. Therefore, a dimensionless flow function for the impingement baffle could be defined

$$C_{FI} = \frac{W_c}{A_D \sqrt{2\, \rho_g\ (DP8)}} \qquad (8)$$

The flow coefficients appearing in Figure 98 were calculated from Equation 8 at specific test points located centrally in the data scatter. They may also be calculated directly from Figures 95, 96 and 97 by using $A_S$ = 41.26 in.$^2$; $A_D$ = 1.183, 0.292, 0.1259 at X/D = 4, 8, 12 in Figure 95; $A_D$ = 1.380, 0.357, 0.162 at X/D = 4, 8, 12 in Figure 96; $A_D$ = 1.500, 0.411, 0.181 at X/D = 4, 8, 12 in Figure 97; and standard sea level air density $\rho_0$. On this basis

$$C_{FI} = \frac{A_S}{A_D \sqrt{2\, g\, \rho_0} \times 12} \times \left[\begin{array}{l}(W_c/A_S) \text{ read from the} \\ \text{Figure at } \Delta P = 1 \text{ psi}\end{array}\right]$$

When the flow coefficient was computed, it appeared to depend on the cross-flow velocity ratio. Therefore, an overall cross-flow velocity ratio was defined as the total cooling flow per unit area of channel between impingement baffle and cooled panel, divided by the total cooling flow per unit of impingement hole area. This ratio, determined by the ratio of total impingement hole area to channel area for a single column of impingement holes, is

$$\frac{A_D}{A_I} = \frac{N_r \frac{\pi}{4} D^2}{(X_n)(Z_n)} = \frac{\frac{\pi}{4} N_r}{\left(\frac{X_n}{D}\right)\left(\frac{Z_n}{D}\right)} \qquad (9)$$

when $N_r$ is the number of rows of holes running across the main stream.

The flow function $C_{FI}$ is shown as a function of $A_D/A_1$ on Figure 98. The figure shows that the combination of small holes, which leads to large $N_r$, and small $X_n/D$ results in relatively large cross-flow velocities. They cause small flow functions because of the relatively large impingement baffle pressure differentials. The relatively large cross-flow velocities found under these conditions are also the probable reason that the heat flow from the cooled panel was less than that found at larger $X_n/D$ and impingement hole diameter. This indicates that the cross-flow velocities which are large enough to reduce the impingement baffle flow coefficient tend to break up the individual jets formed by the baffle in such a way that the local Reynolds numbers on the cooled panel due to the jets are reduced and with them the heat flow from the panel is reduced.

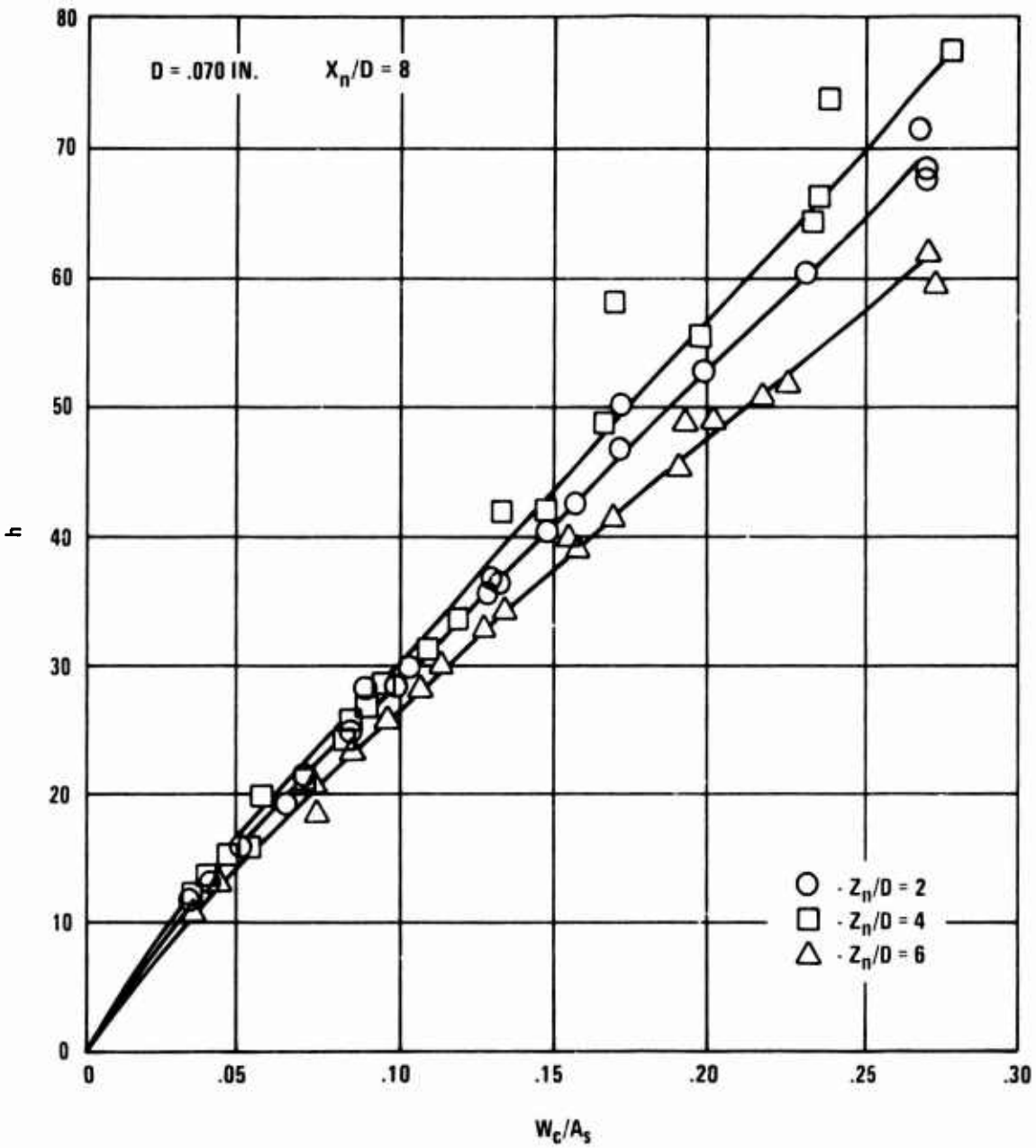


Figure 93. Effect of Impingement Distance on Average Impingement Heat Transfer Coefficient for D = .070 In.

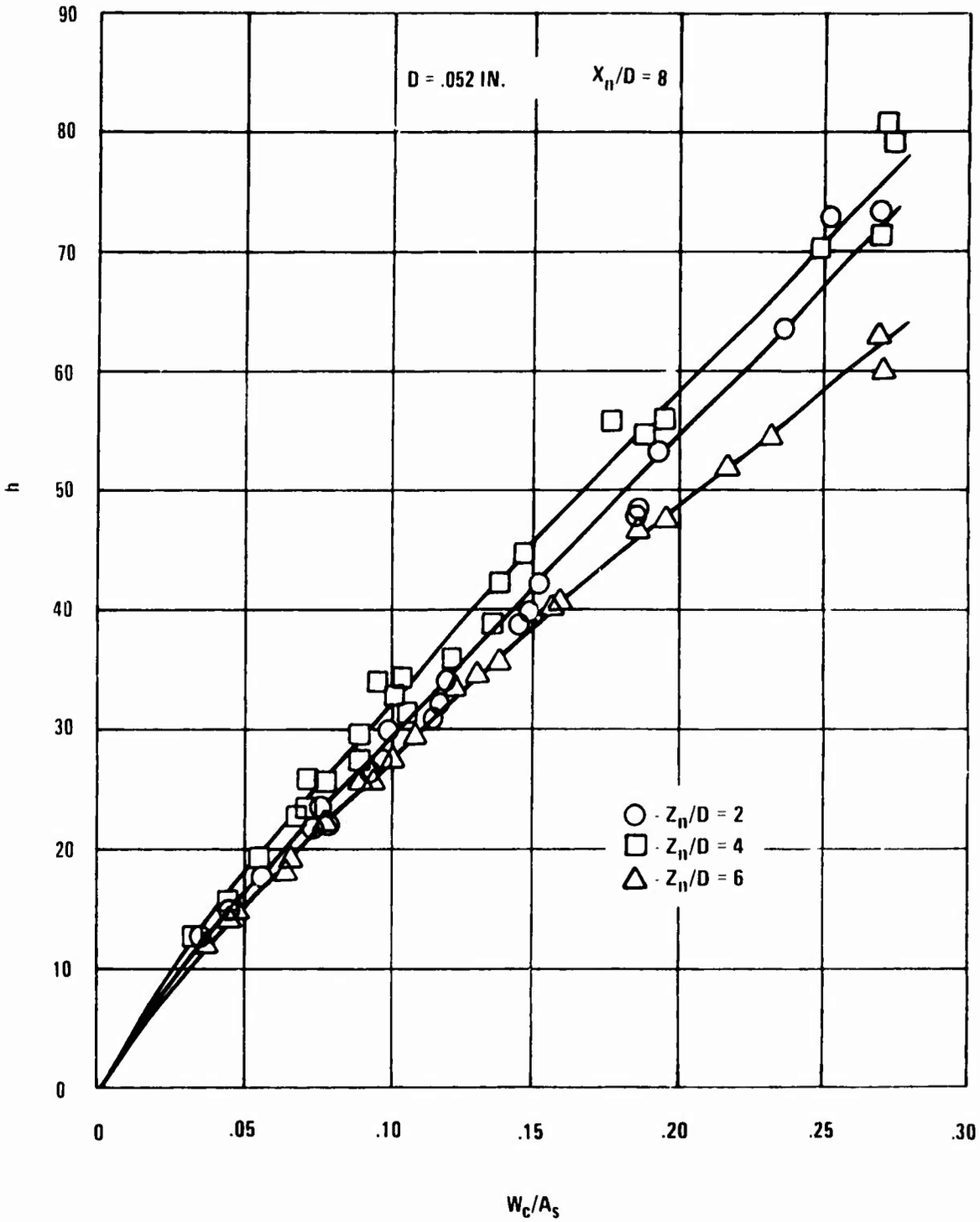


Figure 94. Effect of Impingement Distance on Average Impingement Heat Transfer Coefficient for D = .052 In.

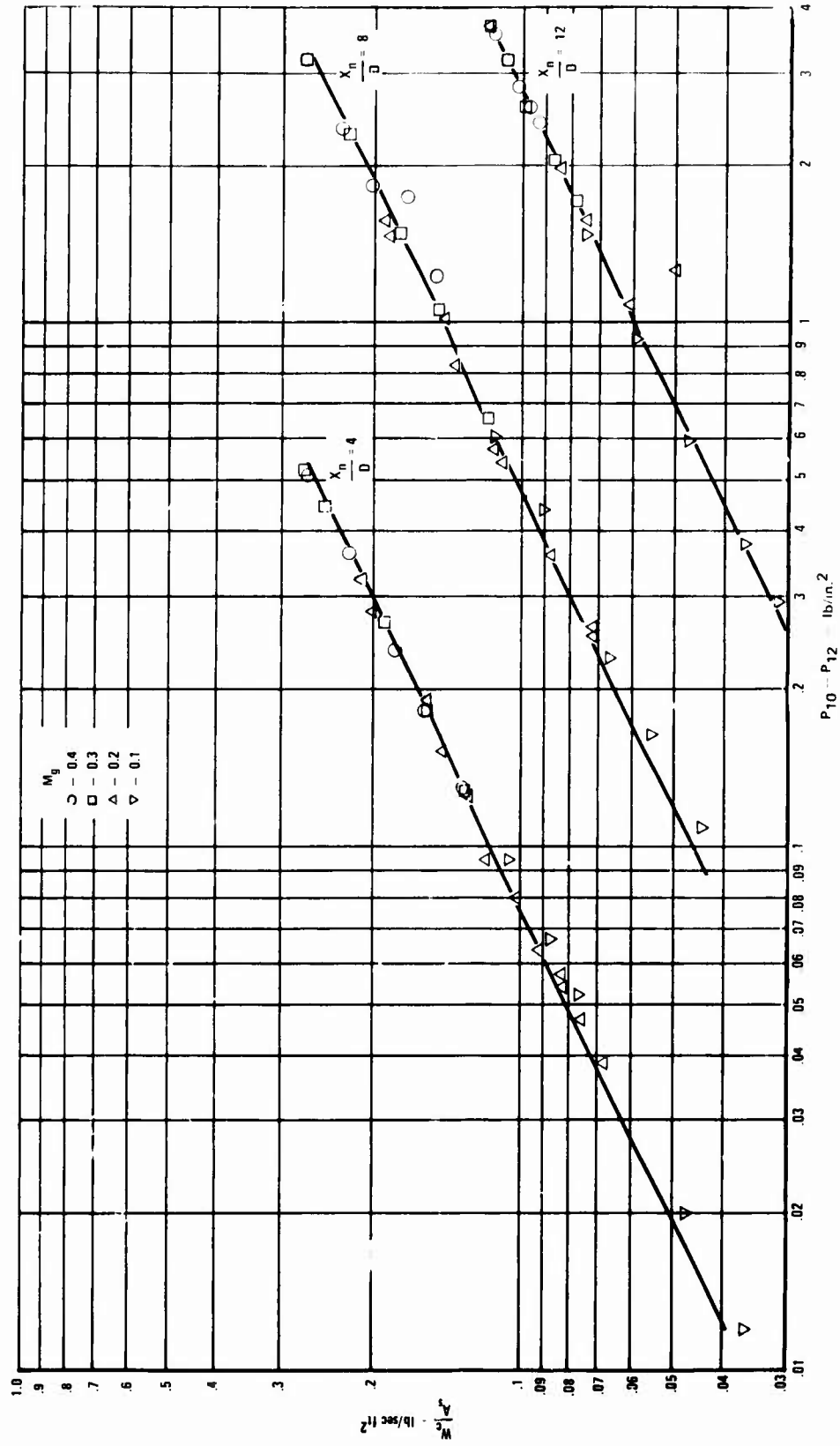


Figure 95. Cooling Air Pressure Impingement Baffle Pressure Drop – 0.031-In. Impingement Holes.

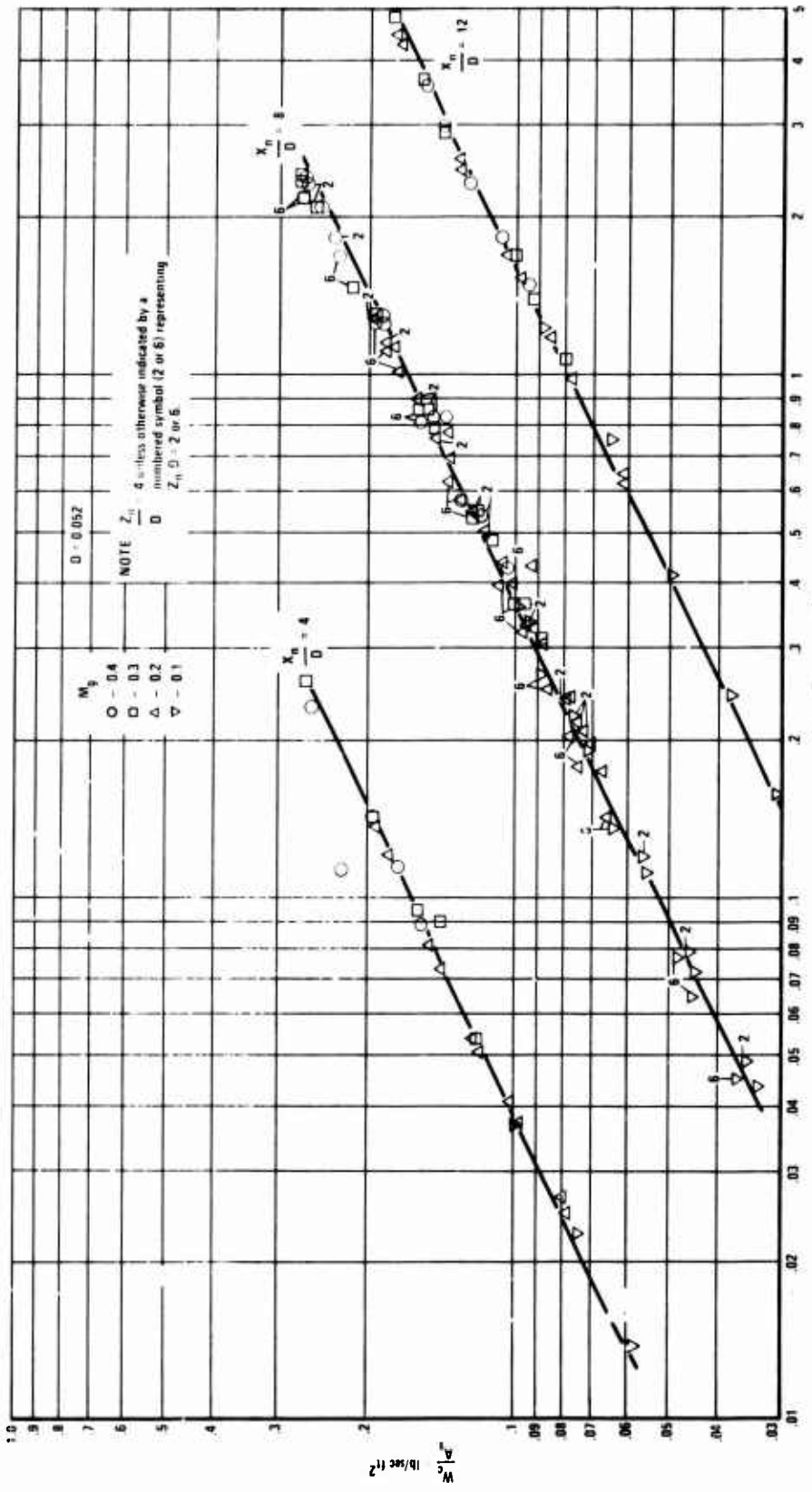


Figure 96. Cooling Air Pressure Impingement Pressure Drop - 0.052-In. Impingement Holes.

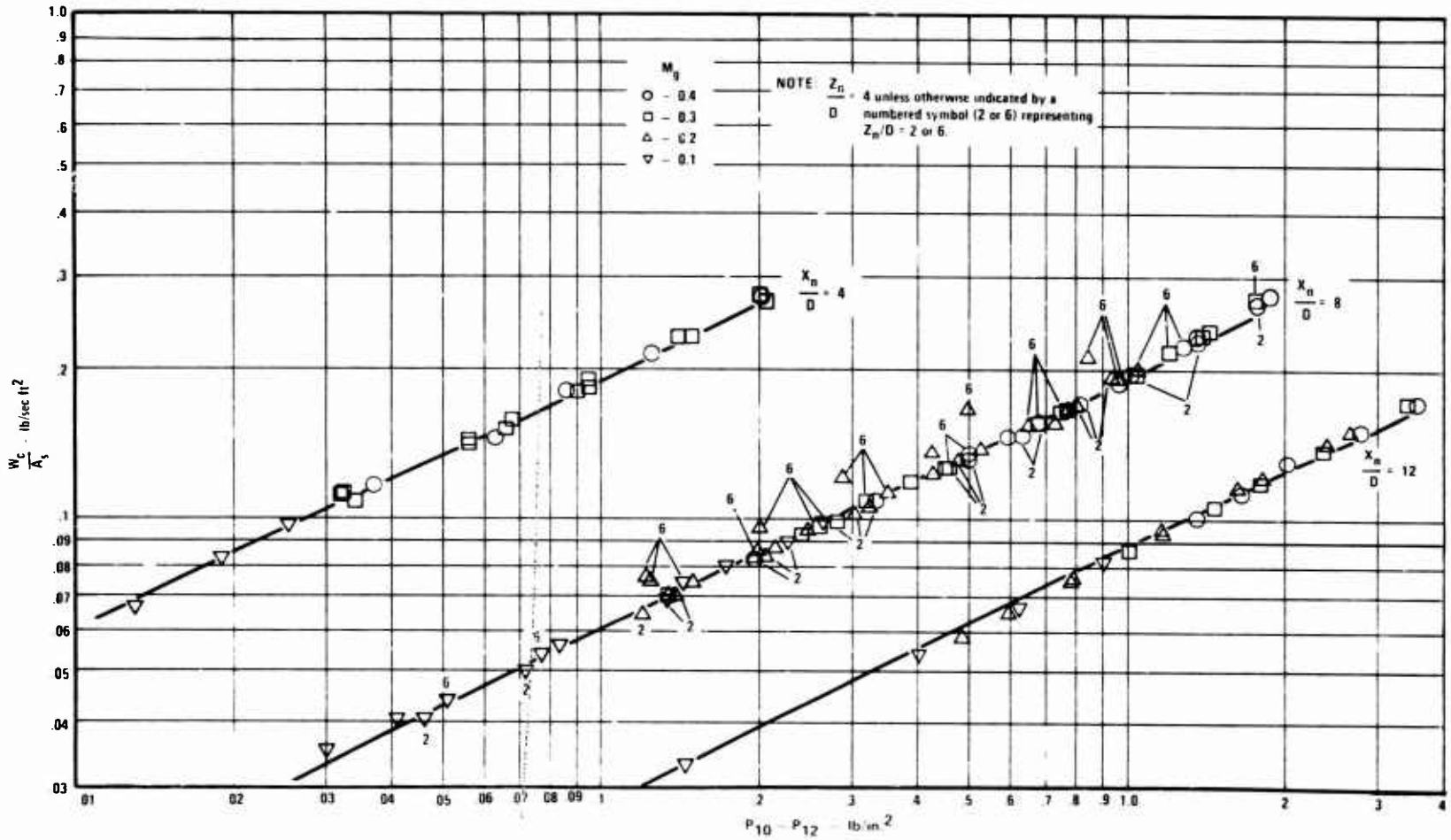


Figure 97. Cooling Air Pressure Impingement Baffle Pressure Drop - 0.070-In. Impingement Holes.

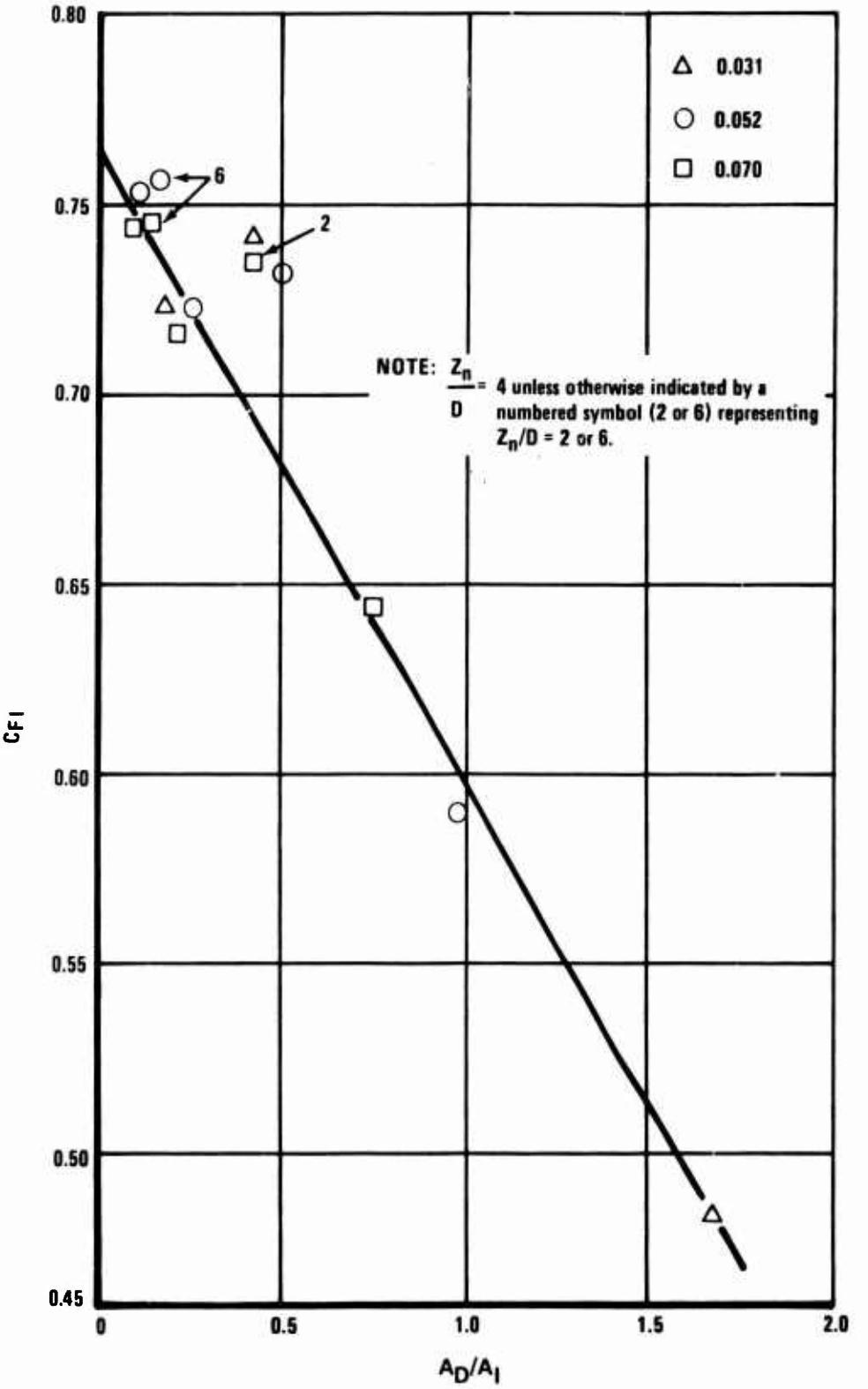


Figure 98. Effect of Crossflow on Flow Coefficient.

## CONCLUSIONS

Impingement-film cooling is significantly better than single-film and overlapped-film cooling within a pressure limitation requirement of 100 in. of water.

The heat transfer characteristic behavior obtained by varying the impingement hole spacing ($X_n/D$) is in agreement with previous experimental studies (i.e., the larger the hole spacing, the higher the cooling effectiveness).

The heat transfer characteristic behavior obtained for the effects of impingement hole diameter, with total hole area constant, was the reverse of that expected. At the smaller spacings ($X_n/D$) tested, cooling effectiveness improved with increased hole diameter, and at the largest impingement hole spacing tested ($X_n/D$) = 12), the effect of hole diameter disappeared.

The optimum impingement distance ($Z_n/D$) for the array tested occurred between 3.5 and 4.0 diameters.

The single-film cooling effectiveness data was in good agreement with the data which Huffmeier obtained with a similar geometry.

At the higher Mach numbers and for panels of the length tested, the upstream panel film is practically destroyed at the beginning of the downstream test panel.

In designing a low-pressure impingement-film cooling system, the impingement hole spacing should be tailored to correspond to the available total cooling pressure. For a system requiring a pressure difference limit of 100 in. of water, an impingement spacing ($X_n/D$) of 8 diameters would produce a good design.

In design calculations for systems with multiple-film cooled panels of the length tested or longer, the effect of the upstream film on the downstream panels should be neglected.

For systems similar to the one tested, with impingement spacing ($X_n/D$) between 8 and 12 diameters, the selection of hole diameter may not be a critical parameter for cooling performance. Its choice should depend on other considerations, such as cost, manufacturing ease, and sensitivity to plugging.

## LITERATURE CITED


1. Kercher, D.M., HEAT TRANSFER BY A MULTIPLE ARRAY OF ROUND AIR JETS IMPINGING PERPENDICULAR TO A FLAT SURFACE INCLUDING EFFECTS OF SPENT AIR, M.S. Thesis, University of Cincinnati; 1967.

2. Kercher, D.M., and Tabakoff, W., HEAT TRANSFER BY A SQUARE ARRAY OF ROUND AIR JETS IMPINGING PERPENDICULAR TO A FLAT SURFACE INCLUDING THE EFFECT OF SPENT AIR, ASME Paper No. 69-GT-4.

3. Tabakoff, W., and Clevenger, W., GAS TURBINE BLADE HEAT TRANSFER AUGMENTATION BY IMPINGEMENT OF AIR JETS HAVING VARIOUS CONFIGURATIONS, ASME Paper No. 71-GT-9.

4. Metzger, D.E., and Korstad, R.J., EFFECTS OF CROSSFLOW ON IMPINGEMENT HEAT TRANSFER, ASME Paper No. 71-GT-1.

5. Heat Transfer Design Data Book, JETS OF AIR IMPINGING ON A SURFACE, Section G503.6, General Electric Company.

6. Gauntner, J.W., Livingood, J.N.B., and Hrycak, P., SURVEY OF LITERATURE ON FLOW CHARACTERISTICS OF A SINGLE TURBULENT JET IMPINGING ON A FLAT PLATE, NASA TN D-5652, February 1970.

7. Snedeker, R.S., Donaldson, C., and Margolis, D.P., A STUDY OF THE MEAN AND TURBULENT STRUCTURE OF A FREE JET AND JET IMPINGEMENT HEAT TRANSFER, ARAP Report No. 96 (AD 656592), December 1966.

8. Keeble, T.S., IMPINGEMENT COOLING, Aus ARL/ME 308 (N 70-25107), August 1969.

9. FILM COOLING IMPINGEMENT COOLING, DDC Report Bibliography, Search Control No. 085834, July 1972.

10. Gordon, R., and Cobonque, J., HEAT TRANSFER BETWEEN A FLAT PLATE AND JETS OF AIR IMPINGING ON IT, Proceedings of International Heat Transfer Conference; Part II, 1961, p. 454.

11. Taylor, J.F., Grimmett, H.L., and Comings, E.W., ISOTHERMAL FREE JETS OF AIR MIXING WITH AIR, CHEMICAL ENGINEERING PROCESS, Vol. 47, 1951, pp. 175-180.

12. Perry, K.P., HEAT TRANSFER BY CONVECTION FROM A HOT GAS JET TO A PLANE SURFACE, Proceedings of the Institute of Mechanical Engineers, Vol. 168, 1954, p. 778.

13. Nina, M.N.R., and Whitelaw, J.H., THE EFFECTIVENESS OF FILM COOLING WITH THREE-DIMENSIONAL SLOT GEOMETRIES, ASME Paper No. 71-GT-11.

14. Proctor, W.L., CF6/TF39 COMBUSTOR FILM COOLING EFFECTIVENESS, General Electric Co.; GER72AEG143, December, 1971.

15. Proctor, W.L., CF6/TF39 COMBUSTOR SHORT OVERHANG FILM COOLING EFFECTIVENESS, General Electric Co.; GER72AEG132, February, 1972.

16. Huffmeier, R.W., FILM COOLING AND HEAT TRANSFER DOWNSTREAM OF A METERED INJECTION SLOT, General Electric Co.; GER67FPD380, November 1967.

17. Elovic, E., COMBUSTOR FILM COOLING DATA CORRELATION STATUS REPORT, General Electric Co.; TM70-674, August 1970.

18. Sturgess, G.J., AN INVESTIGATION OF THE INTERNAL AERODYNAMIC MIXING CHARACTERISTICS FROM A TF34 FILM COOLING SLOT, Part II, EFFECTS OF SLOT HEIGHT, General Electric Co.; TM70AEG1993, November 1970.

19. Sivasegaram, S., and Whitelaw, J.H., FILM COOLING SLOTS: THE IMPORTANCE OF LIP THICKNESS AND INJECTION ANGLE, Journal Mechanical Engineering Science, Vol. 11, No. 1, 1969, pp. 22-27.

20. Sturgess, G.J., FILM COOLING OF COMBUSTION CHAMBERS PART III, A PARAMETRIC STUDY OF POTENTIAL CORE LENGTH IN THE FILM COOLING OF COMBUSTION CHAMBERS, General Electric Co.; TM69AEG1931, July 1969.

21. Pai, B.R., and Whitelaw, J.H., THE INFLUENCE OF DENSITY GRADIENTS ON THE EFFECTIVENESS OF FILM COOLING, ARC 29928 (AD 670300),HMT182, February 1968.

22. Pai, B.R., and Whitelaw, J.H., THE INFLUENCE OF STRONG PRESSURE GRADIENTS ON FILM COOLING EFFECTIVENESS, Fourth International Heat Transfer Conference, Paris-Versailles, Vol. II, FC1.11, 1970.

23. Akfirat, J.C., TRANSFER OF HEAT FROM AN ISOTHERMAL FLAT PLATE TO A TWO-DIMENSIONAL WALL JET, Third International Heat Transfer Conference, Chicago, 1966.

24. Koffel, W.K., AN ANALYSIS OF COMBUSTOR FILM SLOT DESIGN PARAMETERS, General Electric Co.; GER71AEG144, March 1971.

25. Sturgess, G.J., FILM COOLING OF COMBUSTION CHAMBERS. PART IV, ADDITIONAL POTENTIAL CORE INFORMATION FROM INJECTION GEOMETRIES OF A PRACTICAL NATURE, General Electric Co.; GE TM69AEG2149, October, 1969.

26. FILM COOLING OF JET ENGINES, DDC Report Bibliography, Search Control No. 085048, June 1972.

27. Goldstein, R.J., FILM COOLING ADVANCES IN HEAT TRANSFER, Volume 7, 1971.

28. Haering, G.W., A PROPOSED CORRELATION SCHEME FOR GAS-FILM COOLING DATA, Technical Report AFAPL-TR-66-56, August 1966.

## APPENDIX

## TEST CONFIGURATION DESCRIPTION TABLES

TABLE II. TEST CONFIGURATION DESCRIPTION AND TEST POINTS KEY

| Config. No. | Impingement Baffles | | | | Inlet Panel Cooling Air | | Test Run Nos. | |
|---|---|---|---|---|---|---|---|---|
| | Slot Ht (in.) | Hole Dia (in.) | $Z_n/D$ | $X_n/D$ | Match | None | First | Last |
| 1 | .100 | | None | | X | | 1 | 29 |
| 2 | .145 | | None | | X | | 30 | 55 |
| 3 | .100 | .070 | 4 | 4 | X | | 56 | 80 |
| 4 | | | | 8 | X | | 81 | 107 |
| 5 | | | | 12 | X | | 108 | 133 |
| 6 | .100 | .052 | 4 | 4 | X | | 134 | 158 |
| 7 | | | | 8 | X | | 159 | 184 |
| 8 | | | | 12 | X | | 185 | 210 |
| 9 | .100 | .031 | 4 | 4 | X | | 264 | 291 |
| 10 | | | | 8 | X | | 292 | 316 |
| 11 | | | | 12 | X | | 317 | 342 |
| 12 | .100 | .052 | 6 | 8 | X | | 211 | 237 |
| 13 | | .070 | 6 | 8 | X | | 369 | 395 |
| 14 | .100 | .052 | 2 | 8 | X | | 238 | 263 |
| 15 | | .070 | 2 | 8 | X | | 343 | 368 |
| 16 | .100 | | None | | | X | 396 | 421 |
| 17 | .145 | | None | | | X | 422 | 446 |

TABLE III. MEASURED IMPINGEMENT BAFFLE HOLE DIMENSIONS

| Design Intent Hole Dia (in.) | $X_n/D$ | Actual* Hole Dia (in.) | Number of Columns | Number of Rows | Actual** No. of Holes |
|---|---|---|---|---|---|
| .031 | 4 | .0291 | 56 | 33 | 1838 |
| | 8 | | 28 | 17 | 468 |
| | 12 | | 19 | 11 | 209 |
| .052 | 4 | .0517 | 33 | 20 | 658 |
| | 8 | | 17 | 10 | 170 |
| | 12 | | 11 | 7 | 77 |
| .070 | 4 | .0717 | 25 | 15 | 373 |
| | 8 | | 13 | 8 | 102 |
| | 12 | | 9 | 5 | 45 |

*Based on a 5% sample of the holes on each plate with $X_n/D = 4$.

**Each plate has some missing holes due to the standoffs to hold a constant $Z_n/D$.

TABLE IV. MEASURED TEST APPARATUS DIMENSIONS

**Diffuser Duct**

| | |
|---|---|
| Inlet | 2.048 x 7.022 |
| Exit | 3.018 x 6.960 |

**Metering Holes**

| | |
|---|---|
| Inlet Panel | 63 holes @ D = .1179 |
| Test Panel | 63 holes @ D = .1174 |

**Slots**

| | | Slot Height (in.) | |
|---|---|---|---|
| | Length (in.) | .100 | .140 |
| Inlet Panel | 7.024 | .085 | .130 |
| Test Panel | 7.026 | .100 | .145 |

NOTE: All dimensions in inches.

## DISTRIBUTION

| | |
|---|---|
| Director of Defense Research & Engineering | 1 |
| Assistant Secretary of the Army (R&D) | 1 |
| Assistant Chief of Staff for Logistics, DA | 1 |
| Chief of Research & Development, DA | 1 |
| Army Materiel Command | 1 |
| Army Aviation Systems Command | 2 |
| AEWSPS USAMC Project Manager | 5 |
| Hq, Army Air Mobility R&D Laboratory | 2 |
| Systems Research Integration Office, AMRDL | 1 |
| Ames Directorate, Army Air Mobility R&D Laboratory | 1 |
| Eustis Directorate, Army Air Mobility R&D Laboratory | 13 |
| Langley Directorate, Army Air Mobility R&D Laboratory | 2 |
| Lewis Directorate, Army Air Mobility R&D Laboratory | 2 |
| Army Aviation Systems Test Activity | 2 |
| Army Advanced Materiel Concepts Agency | 1 |
| Army Mobility Equipment R&D Center | 1 |
| Army Materiel Systems Analysis Agency | 1 |
| Army Electronics Command | 1 |
| Army Tank-Automotive Command | 1 |
| Air Force Materials Laboratory | 1 |
| Aeronautical Systems Division, AFSC | 1 |
| Air Force Avionics Laboratory | 1 |
| Naval Air Systems Command | 4 |
| Chief of Naval Research | 1 |
| Naval Research Laboratory | 1 |
| Naval Ship Research & Development Center | 1 |
| Hq, U. S. Marine Corps | 1 |
| Ames Research Center, NASA | 1 |
| Langley Research Center, NASA | 1 |
| Lewis Research Center, NASA | 1 |
| Scientific & Technical Information Facility, NASA | 2 |
| National Aviation Facilities Experimental Center, FAA | 1 |
| Government Printing Office | 1 |
| Defense Documentation Center | 2 |

Unclassified

Security Classification

**DOCUMENT CONTROL DATA - R & D**

*(Security classification of title, body of abstract and indexing annotation must be entered when the overall report is classified)*

| | |
|---|---|
| 1. ORIGINATING ACTIVITY (Corporate author)<br>General Electric Company<br>Aircraft Engine Group<br>Lynn, Massachusetts | 2a. REPORT SECURITY CLASSIFICATION<br>Unclassified<br>2b. GROUP |

3. REPORT TITLE

IMPINGEMENT-FILM HEAT TRANSFER PROGRAM

4. DESCRIPTIVE NOTES (Type of report and inclusive dates)

FINAL REPORT

5. AUTHOR(S) (First name, middle initial, last name)

T. Chew B. F. Shattuck
R. S. Fatyol

| 6. REPORT DATE | 7a. TOTAL NO. OF PAGES | 7b. NO. OF REFS |
|---|---|---|
| December 1973 | 129 | 28 |

| 8a. CONTRACT OR GRANT NO. | 9a. ORIGINATOR'S REPORT NUMBER(S) |
|---|---|
| DAAJ02-72-C-0094<br>b. PROJECT NO.<br>c.<br>Task 1F162205AA5202<br>d. | USAAMRDL Technical Report 73-31<br>9b. OTHER REPORT NO(S) (Any other numbers that may be assigned this report) |

10. DISTRIBUTION STATEMENT

Distribution limited to U. S. Government agencies only; test and evaluation; December 1973. Other requests for this document must be referred to the Eustis Directorate, U. S. Army Air Mobility Research and Development Laboratory, Fort Eustis, Virginia 23604.

| 11. SUPPLEMENTARY NOTES | 12. SPONSORING MILITARY ACTIVITY |
|---|---|
| | Eustis Directorate, U.S. Army Air Mobility Research and Development Laboratory, Fort Eustis, Virginia |

13. ABSTRACT

This report covers the investigation of an impingement-film cooling system designed to cool the exhaust ducts of turboshaft engines thereby reducing infrared radiation levels. The program was initiated with a literature search which indicated the useful range of impingement hole size, spacing, and distance from impingement hole to cooled panel. It provided similar information for the cooling slot design. Test hardware incorporating these features was fabricated for testing. Seventeen configurations, four of which had no impingement (film cooling only), were tested. The remaining 13 configurations were tested with different combinations of impingement hole size, spacing, and distance to cooled panel.

Film cooling test results were in good agreement with the correlations and results quoted in the literature. The cooling effectiveness with impingement-film cooling was consistently superior to that with film cooling only. The highest effectiveness was achieved with the configuration having the largest impingement hole diameter, D = 0.070 in. and spacing $X_n/D = 12$. The optimum impingement distance $Z_n$ was in the neighborhood of 4 impingement hole diameters. While the largest hole spacing tested gave the highest cooling effectiveness it also required a relatively large pressure drop across the cooling system. Under the most difficult cooling conditions of hot gas Mach number equal to 0.4, the highest cooling effectiveness ($\eta$) achieved within a specified impingement system pressure drop of 100 in. of water was 0.93.

DD FORM 1 NOV 68 1473 REPLACES DD FORM 1473, 1 JAN 64, WHICH IS OBSOLETE FOR ARMY USE.

Unclassified

Security Classification

Unclassified

Security Classification

| 14. KEY WORDS | LINK A | | LINK B | | LINK C | |
|---|---|---|---|---|---|---|
| | ROLE | WT | ROLE | WT | ROLE | WT |
| Impingement Cooling | | | | | | |
| Film Cooling | | | | | | |
| Heat Transfer | | | | | | |
| Diffuser Test | | | | | | |
| Literature Survey | | | | | | |
| Simulated Exhaust System | | | | | | |
| Parametric Test | | | | | | |

Unclassified

Security Classification